Density-Functional Theory and Quantum Chemistry Studies on "dry" and "wet" NaCl(001)

vorgelegt von
M. Sc.
Bo Li

der Fakultät II of Mathematik und Naturwissenschaften
der Technischen Universität Berlin
zur Erlangung des akademischen Grades
DOCTOR RERUM NATURALIUM

genehmigte Dissertation

Promotionsausschuss:

Vorsitzender: Prof. Dr. Mario Dähne
Berichter: Prof. Dr. Eckehard Schöll
Berichter: Prof. Dr. Matthias Scheffler

Tag der wissenschaftlichen Aussprache: 17.12.2008

Berlin 2009

D 83

Abstract

Common salt, NaCl, is a everyday material that we are all familiar with. It has been of fascination and played a central role in society since at least the middle ages, when it was known as "white gold" because of its essential role as a food preservative. However, many fundamental physical and chemical properties of NaCl and in particular NaCl surfaces remain unanswered. Given the relevance of NaCl surfaces to physical processes in the upper atmosphere or the importance of NaCl/water in biophysics, there is an increasing need to better understand salt surfaces. This thesis tackles the issue of the properties of salt surfaces with the application of a variety of electronic structure techniques.

To begin, the properties of bulk NaCl, NaCl(001), and defects on NaCl(001) surfaces have been examined with density-functional theory within the plane-wave pseudopotential approach. Aiming to remedy the lack of quantitative energetic and structural knowledge of such surfaces, several DFT exchange-correlation functionals are employed to determine the surface energy and surface structure. A range of 9–15 meV/Å^2 is obtained for the surface energy of NaCl(001), and the surface is predicted to undergo only small relaxations of the top layer atoms.

The isolated step formation energy of monoatomic (100)-like steps on NaCl(001) is estimated to be about 40–60 meV/Å^2 and the interaction energy between adjacent steps is weak. The *ab initio* atomistic thermodynamics has been employed to determine the relative stabilities of stoichiometric (100)-like and non-stoichiometric (111)-like steps on NaCl(001), revealing that (100)-like steps are significantly more stable than (111)-like steps at all accessible values of the chlorine chemical potential.

In addition to these DFT studies, we have used Møller-Plesset perturbation theory to examine the adsorption of halogen atoms on several alkali halides surfaces. To some surprise, these studies indicate that the halogen atoms bind preferentially to halide substrate atoms on a series of alkali halide surfaces, rather than to the alkali atoms as might be anticipated. An analysis of the electronic structures in each system reveals that this novel adsorption mode is stabilized by the formation of a textbook two-center three-electron covalent bond.

Finally, water adsorption on NaCl(001) is examined. It is shown that the adsorption energy is very sensitive to the exchange-correlation functionals employed yielding values that range from 280 meV to 640 meV. Considerable effort is then employed with MP2 and CCSD(T) to arrive at a reliable estimate of the adsorption energy of 517 meV. This represents one of the most reliable theoretical estimates of an adsorption energy on a solid surface obtained so far. In the end, a careful analysis of the electronic structure of the water/NaCl(001) adsorption system reveals the nature of the adsorption bond.

Zusammenfassung

Gewöhnliches Kochsalz, Natriumchlorid (NaCl), ist ein aus dem Alltag bekannter Stoff, mit dem wir alle vertraut sind. Mindestens seit dem Mittelalter, als (Koch-)Salz auf Grund seiner Verwendung als Konservierungsstoff als "weißes Gold" bekannt war, hat es eine Faszination auf Menschen ausgeübt und eine zentrale Rolle in der Gesellschaft gespielt. Viele fundamentale physikalische und chemische Eigenschaften von NaCl und insbesondere Oberflächen von Kochsalzkristallen sind jedoch noch immer unbekannt. Berücksichtigt man jedoch die Bedeutung von NaCl-Oberflächen für physikalische Prozesse in höheren Regionen der Erdatmosphäre oder die Bedeutung von in Wasser gelöstem NaCl in der Biophysik, so gibt es ein zunehmendes Interesse daran, Kochsalzoberflächen besser zu verstehen. Diese Dissertation beschäftigt sich daher mit den Eigenschaften von Kochsalzoberflächen durch Anwendung von einer Vielzahl von Methoden aus dem Bereich der Elektronenstrukturtheorie.

Zunächst wurden Eigenschaften von NaCl-Volumenkristallen und NaCl(001)-Oberflächen einschließlich Defekten im Rahmen von Dichtefunktionaltheorie (DFT) mit ebenen Wellen und Pseudopotentialen untersucht. Um den Mangel an quantitativen Kenntnissen über Energetik und Struktur von diesen Oberflächen zu beseitigen, werden verschiedene DFT-Austauschkorrelationsfunktionale zur Bestimmung von Oberflächenenergien und -strukturen eingesetzt. Für die Oberflächenenergie wird ein Wert von 9–15 meV/Å^2 ermittelt, und es wird vorhergesagt, dass nur die Atome in der obersten Schicht geringfügig relaxieren.

Die Energie zur Bildung von monoatomaren (100)-artigen Stufen auf NaCl(001) wird mit 40–60 meV/Å^2 angegeben, wobei die Wechselwirkungsenergie zwischen benachbarten Stufen schwach ist. Die "*ab initio* atomistic thermodynamics"-Methode wurde verwendet, um die relative Stabilität von stöchiometrischen (100)-artigen und nicht-stöchiometrischen (111)-artigen Stufen auf NaCl(001) zu bestimmen, mit dem Ergebnis, dass für alle erreichbaren Werte des chemischen Potentials für Chlorine (100)-artige Stufen deutlich stabiler als (111)-artige Stufen sind.

Zusätzlich zu diesen DFT-Studien haben wir die Møller-Plesset-Störungstheorie benutzt, um die Adsorption von Halogenatomen auf Alkalihalogenid-Oberflächen zu untersuchen. Ein wenig überraschend haben diese Untersuchungen ergeben, dass das Halogenatom auf einer Reihe von Alkalihalogeniden bevorzugt an Halogenatomen des Substrats bindet, anstatt, wie zunächst erwartet, an den Alkaliatomen. Eine Analyse der elektronischen Struktur in jedem System enthüllt, dass dieser neu entdeckte Adsorptionsmechanismus durch die Ausbildung einer aus den Lehrbüchern bekannten kovalenten Zweizentren-Dreielektronenbindung stabilisiert wird.

Abschließend wurde die Adsorption von Wasser auf NaCl(001) untersucht. Es hat sich herausgestellt, dass die Adsorptionsenergie sehr stark vom verwendeten Austauschkorrelationsfunktional abhängt, so dass sich Werte zwischen 280 und 640 meV ergeben. Mit beträchtlichem Aufwand sind dann MP2- und CCSD(T)-Rechnungen durchgeführt worden, um eine verlässliche Abschätzung für den Wert

der Adsorptionsenergie von 517 meV zu erhalten. Dies ist einer der besten theoretischen Werte, die jemals für eine Adsorptionsenergie auf einer Festkörperoberfläche ermittelt wurden. Zuletzt wurde durch eine sorgfältige Analyse der elektronischen Struktur des Wasser-NaCl(001)-Adsorptionssystems die Natur der Adsorptionsbindung ermittelt.

Contents

List of Figures

List of Tables

Abbreviations

AFM	Atomic Force Microscope
BSSE	Basis Set Superposition Error
CBS	Complete Basis Set
CCSD(T)	Coupled Cluster method with Single and Double and perturbative connected Triple excitations
CI	Configuration Interaction
DFT	Density-Functional Theory
DOS	Density of States
ECP	Effective Core Potential
ELF	Electron Localisation Function
GGA	Generalised Gradient Approximation
HF	Hartree-Fock
HAS	Helium Atom Scattering
LDA	Local Density Approximation
LEED	Low Energy Electron Diffraction
ML	MonoLayer
MP2	Møller Plesset second order Perturbation Theory
PC	Point Charge
PDOS	Partial Density of States
STM	Scanning Tunneling Microscopy
UHV	Ultrahigh Vacuum
xc	exchange-correlation

Chapter 1

Introduction

Atomic-scale computational materials science has become an interdisciplinary subject that straddles physics, chemistry, biology, and geophysics. This field can also be considered as the art of the computer experiment and certainly computational materials science or computer experiments have enlarged and deepened the scope of understanding from traditional laboratory experiments. Generally one might say that for the experiment in the laboratory, it will tell us *what* happens in most cases, while in principle, computational materials science should allow us to find out *why* something happens and hopefully also to predict what will happen under certain circumstances. Furthermore, computer experiments can readily access conditions which laboratory experiments can not easily reach. For example, geophysical pressures of thousands of GPa representative of the earth's core require considerable effort to reach in a laboratory experiment, yet for theory can be computed without any particular difficulty [1, 2].

The key point with all simulations is how reliable they are and whether they accurately model reality. Traditionally, pre-parameterised empirical potentials were used to model the interaction between collections of atoms. These have achieved considerable success in many areas. Increasingly popular although, computationally much more expensive, are so-called first principles approaches. In this thesis a variety of first principles approaches have been applied, often with the goal of describing the system with the highest possible accuracy.

The central task in first principles simulations is to solve the many-body Schrödinger equation and obtain the total energy and wave function of the system which are the starting point for the most physical properties of the materials. There are many and varied first principles approaches. Often it is useful to categorize them as wave function based methods, e.g., quantum chemistry methods and quantum Monte Carlo, or electron-density based (density-functional theory (DFT)) methods[1]. Both have gained great success and particularly in condensed matter electronic structure calculations, DFT predominates. One reason for this is that calculations can be done for large systems (hundreds or even thousands of atoms) at modest computational costs.

[1]The Nobel Prize in Chemistry 1998 was awarded to J. A. Pople and W. Kohn for their contributions to computational methods in quantum chemistry and density-functional theory, respectively.

There is no doubt that DFT is exact in principle, however DFT relies on approximations to the exchange-correlation functional in practice. Although DFT has proved to be very successful, the deficiencies of DFT are also well documented. One prominent example in surface physics is that DFT with the local density approximation (LDA) and generalised gradient approximation (GGA) predict the wrong adsorption site for CO on Pt(111) and other close-packed metal surfaces [3, 4] because of the intrinsic error in these approximations. In addition adsorption energies of atoms and molecules on surfaces can often differ by large amounts (50%) from experiment depending on the choice of approximation for the exchange-correlation functional [5, 6, 7]. Although there exists a useful scheme now for categorising DFT exchange-correlation functionals (so-called Jacob's ladder) [8], systematically improving DFT exchange-correlation functionals is difficult. By contrast quantum chemistry methods which begin with Hartree-Fock as a base and gradually add in increasing accounts of electron correlation provide an alternative when high precision, beyond that available with current exchange-correlation functionals, is required. The difficulty with these wave function approaches is that they are not amenable to very large or periodic systems. Thus applying "quantum chemistry to condensed matter" is not straightforward, but it is something that is becoming increasingly popular. This thesis reports one such story when water adsorption on NaCl is examined (chapter 6). At the other hand, the quantum Monte Carlo method is also readily applied to condensed matter simulations and attracts more and more attention [9]. However it also has its own unfavorable shortcomings such as difficulties with the fermion sign problem and huge computational expense.

The focus of this thesis is sodium chloride, mostly the surface properties of NaCl without and with adsorbed water molecules. NaCl, or simply common salt, has an obvious importance in our daily life. It will occupy a central position in the kitchen forever! In 2002, the worldwide total amount of common salt was 210 million metric tonnes and the main method to get common salt is to evaporate seawater [10]. Aside from its importance in daily life, NaCl has a prominent status in biophysics, environmental science, and catalysis, etc. In addition, NaCl, and more generally alkali halides, are often considered as prototype insulators with large band gaps, with the structure and physical properties of alkali halides having been well tabulated in textbooks [11, 12]. Despite our familiarity with these materials, there remain many unanswered questions about the basic properties of NaCl. In particular many fundamental questions of the properties of NaCl surfaces remain unanswered. Indeed, given the recent interest in utilizing ultra-thin NaCl films as a means to electronically decouple adsorbates from metal surfaces, it has become increasingly important to understand the properties of NaCl surfaces [13, 14, 15, 16].

In this thesis, both "dry" and "wet" NaCl surfaces have been examined. For dry NaCl(001), a detailed DFT study has been performed aimed at understanding the precise details of the surface structure. Because of issues such as surface charging and electron stimulated desorption, traditional electron based surface science probes encounter difficulties in working with alkali halide surfaces. Therefore, theory can make useful contributions. Here, important information about how the atoms relax at the NaCl interface is obtained. One additional aspect of these calculations is

the surface energy. The surface energy, one of the basic thermodynamic properties of any material, remains a challenge to both the current DFT methods and experimental measurements. In particular for the surface energy of NaCl(001)[2], the experimental measurements are old (from the 1960's) and do not agree with each other. By performing a range of well-converged DFT studies with several exchange-correlation functionals, it is hoped that we have moved closer to a reliable estimate of the surface energy of NaCl.

Defects are universally present on solid surfaces. Adatoms, steps, and vacancies are very common types of defects on solid surfaces. They are also known to be chemically reactive sites playing important roles in many surface reactions and specifically for NaCl in the dissolution of the crystal [17]. Thus it is very useful to obtain an accurate description of the energetics of defects on surfaces. However, for defects on NaCl(001), like adatoms and steps, current understanding is in its infancy. Two key contributions concerning defects are made in this thesis. First, for NaCl(001), the formation energy of steps on NaCl is obtained for the first time. Second, the initially surprising suggestion is made that halogen atom adsorbates on alkali halide surfaces prefer to adsorb on halide sites. This unexpected adsorption is attributed to the formation of a classic two-center three-electron chemical bond which was first introduced by Pauling in the 1930's [18].

Although many studies have been performed for water on NaCl [19, 20, 21, 22, 23, 24, 25, 26], one basic and important question about this system is still unclear. That is how large the adsorption energy of a water molecule on NaCl(001) is. Even though reliable adsorption energy measurements of adsorbates on surfaces are somewhat rare, it is quite remarkable that for such an important system as water on NaCl, there is only one measurement of the adsorption energy of isolated water molecules on NaCl(001) [19]. The value, obtained in this helium atom scattering (HAS) study, is 650 meV and it is not clear if it corresponds to adsorption on flat terraces of NaCl(001) but defective sites instead. From DFT values for the adsorption energy of 0.3 to 0.6 eV/H_2O have been obtained. Thus there is no agreement here and it is unclear if this is because of some problem with the exchange-correlation functionals tested or with the experimental measurement. Here, quantum chemistry methods (MP2 and CCSD(T)) are used to address this issue. This is done by following a procedure which involves the use of embedded clusters and basis set extrapolation schemes in order to ensure that a careful understanding of the precise accuracy of the calculations can be obtained. The adsorption energy obtained is likely one of the most reliable theoretical estimates for a molecule on any surface and the "roadmap" developed and followed could hopefully be generalized to the other adsorption calculations on ionic crystal surfaces.

The remainder of this thesis is organized as follows. Chapter 2 will introduce the theoretical background of the electronic structure calculations used. In chapter 3, the properties of bulk NaCl and NaCl(001) will be discussed, focusing in particular on the surface energy of NaCl(001). Chapter 4, will study the properties of stepped NaCl(001). The adsorption of halogen adatoms on alkali halide surfaces is examined

[2]Details are in chapter 3

in chapter 5. Chapter 6 deals with the adsorption of water on NaCl(001). The main focus of this chapter is the sensitivity of the results to the DFT exchange-correlation functionals employed and an attempt to use explicitly correlated methods to obtain a highly accurate value of the adsorption energy. In chapter 7, several other DFT exchange-correlation functionals, including hybrid functionals, are tested for water adsorption and the nature of the adsorption is examined. Finally, a short summary of the whole thesis and the outlook for the future research direction is presented. The convergence tests, the derivation of the ledge energy of non-stoichiometric steps on NaCl(001), and a few other supporting materials are included in the appendices.

Chapter 2

Theoretical Background

This chapter will focus on the theoretical background of methodologies for approximately solving the many electron problem such as the Hartree-Fock, Møller-Plesset perturbation theory, coupled cluster, and density-functional theory methods. Also some of the practicalities necessary to consider in performing such calculations such as basis sets and pseudopotentials will be discussed.

2.1 The Electronic Structure Problem

A major goal of electronic structure calculations is to solve the non-relativistic time-independent Schrödinger equation,

$$\hat{H}\Psi = E\Psi \tag{2.1}$$

where $\hat{H}$ is the Hamiltonian for a system consisting of M nuclei and N electrons which are described by position vector R_A and r_i, respectively. The distance between the i-th electron and A-th nucleus is $r_{iA} = |r_i - R_A|$; the distance between i-th and j-th electron is $r_{ij} = |r_i - r_j|$, and the distance between the A-th nucleus and B-th nucleus is $R_{AB} = |R_A - R_B|$. In atomic units (energy in Hartree and length in Bohr), $\hat{H}$ can be expanded as:

$$\hat{H} = -\sum_{i=1}^{N}\frac{1}{2}\nabla_i^2 - \sum_{A=1}^{M}\frac{1}{2M_A}\nabla_A^2 - \sum_{i=1}^{N}\sum_{A=1}^{M}\frac{Z_A}{r_{iA}} + \sum_{i=1}^{N}\sum_{j>i}^{N}\frac{1}{r_{ij}} + \sum_{A=1}^{M}\sum_{B>A}^{M}\frac{Z_A Z_B}{R_{AB}}. \tag{2.2}$$

In the above equation, M_A is the ratio of the mass of nucleus A to the mass of an electron and Z_A is the atomic number of nucleus A. The ∇_i^2 and ∇_A^2 are the Laplacian operators. The first two terms in Eq. (2.2) are for the kinetic energy of the electrons and nuclei, respectively. The third term represents the Coulomb attraction between electrons and nuclei. The fourth and fifth terms represent the repulsion between electrons and between nuclei, respectively.

The compact form of Eq. (2.2) is as a result of using atomic units and the conversions between atomic units and SI units are listed in Table 2.1. A quantity Q in SI units is related to its value in atomic units $Q^{'}$ by

$$Q = XQ^{'} \quad . \tag{2.3}$$

Throughout this chapter, atomic units will be employed.

Table 2.1: Conversion of atomic units to SI units.

Physical quantity	Symbol	Value of X (SI)
Length	a_0 (Bohr)	5.2919×10^{-11}m
Mass	m_e	9.1095×10^{-31}kg
Charge	e	1.6022×10^{-19}C
Energy	E_h (Hartree)	4.3598×10^{-18}J
Angular Momentum	$\hbar$	1.0546×10^{-34}Js

2.1.1 The Born-Oppenheimer Approximation

The Born-Oppenheimer approximation [27] plays a vital role in electronic structure calculations. The underling rationalization of this approximation is that the mass of nuclei are much heavier than electrons. Even for the lightest nucleus, a proton, its mass is approximately 3000 times larger than the electron. Thus in most cases the nuclei move much more slowly than electrons. Hence, in many cases, one can consider the electrons are moving in a field produced by the fixed nuclei. This is the qualitative rationalization to separate the movement of electrons and nuclei. Under the Born-Oppenheimer approximation the second term in Eq. (2.2) is neglected, and the final term, the repulsion between nuclei, can be treated as a constant for a fixed configuration of the nuclei. The remaining terms in Eq. (2.2) are called the electronic Hamiltonian ($\hat{H}_{elec}$),

$$\hat{H}_{elec} = -\sum_{i=1}^{N}\frac{1}{2}\nabla_i^2 - \sum_{i=1}^{N}\sum_{A=1}^{M}\frac{Z_A}{r_{iA}} + \sum_{i=1}^{N}\sum_{j>i}^{N}\frac{1}{r_{ij}} \quad . \tag{2.4}$$

The solution to a Schrödinger equation involving the electronic Hamiltonian,

$$\hat{H}_{elec}\Psi_{elec} = E_{elec}\Psi_{elec} \tag{2.5}$$

is the electronic wave function,

$$\Psi_{elec} = \Psi_{elec}(r_i, R_A) \quad , \tag{2.6}$$

which describes the motion of the electrons and explicitly depends on the electronic coordinates (r_i) but parametrically on the nuclear coordinates (R_A). Furthermore, to completely specify an electron, it is necessary to assign the corresponding spin (ω), so together with the spatial coordinates, we denote these four coordinates collectively by $\mathbf{x}$,

$$\mathbf{x} = \{r, \omega\} \quad , \tag{2.7}$$

and the wave function for an N-electron system is written as $\Psi(\mathbf{x}_1, \mathbf{x}_2, \cdots, \mathbf{x}_N)$.

The total energy of fixed nuclei will also include the constant nuclear repulsion term leading to,

$$E_{tot} = E_{elec} + \sum_{A=1}^{M}\sum_{B>A}^{M}\frac{Z_A Z_B}{R_{AB}} \quad . \tag{2.8}$$

Solving versions of Eq. (2.5) and (2.8) is the main focus of the research reported in this thesis and, indeed electronic structure calculations in general. In the following, the subscript "*elec*" will be dropped.

However, one should bear in mind that although we will solve versions of Eq. (2.5) and Eq. (2.8) in which the Born-Oppenheimer approximation is made, the Born-Oppenheimer approximation is certainly not universality valid. It is well known that the Born-Oppenheimer approximation will break down when there are multiple potential energy surfaces close to each other in energy or crossing each other. Dissociative adsorption of molecules on metal surfaces is a famous contemporary example. Similarly, reactions involving hydrogen and proton transfer may be susceptible to breakdowns in the Born-Oppenheimer approximation. More caution must be exerted when dealing with systems such as those [28, 29, 30, 31].

Despite the deceptively simple form of the Eq. (2.5), its exact solution for anything but the simplest of systems remains to the present day a major challenge. And, indeed, the all too often quoted words of Paul Dirac from 1929 [32] remain valid to the present day:

> *The underlying physical laws necessary for the mathematical theory of a large part of physics and the whole of chemistry are thus completely known, and the difficulty is only that the exact application of these laws leads to equations much too complicated to be soluble.*

The difficulties in solving Eq. (2.5) lies in the electron-electron interaction, $\frac{1}{r_{i,j}}$, which includes all the quantum effects of the electrons. Despite the intractable nature of these interactions, many approximate methods have been developed to solve Schrödinger-like equations. Some of these approximate solutions, the ones made use of in this thesis, will be introduced in the following. However, the Slater determinant will be introduced first due to its fundamental role in many aspects of electronic structure theory.

2.1.2 Slater Determinants

Electrons are fermions and obey the Pauli exclusion principle. This requires that the wave function of electrons should be antisymmetric with respect to the interchange of the coordinates $\mathbf{x}$ of any two electrons,

$$\Phi(\mathbf{x}_1, \cdots, \mathbf{x}_i, \cdots, \mathbf{x}_j, \cdots, \mathbf{x}_N) = -\Phi(\mathbf{x}_1, \cdots, \mathbf{x}_j, \cdots, \mathbf{x}_i, \cdots, \mathbf{x}_N) \quad . \tag{2.9}$$

Slater determinants nicely satisfy this antisymmetric condition through an appropriate linear combination of Hartree products, which are the non-interacting electron wave functions[1]. For example, a two electron case which we occupy the spin orbitals χ_i and χ_j. If we put electron one in χ_i and electron two in χ_j, we will have,

$$\Phi_{12}(\mathbf{x}_1, \mathbf{x}_2) = \chi_i(\mathbf{x}_1)\chi_j(\mathbf{x}_2) \quad . \tag{2.10}$$

[1]It is necessary to caution that a single Slater determinant will not be enough when a multireference system is under consideration which requires a linear combination of several Slater determinants.

On the other hand, if we put the electron one in χ_j and electron two in χ_i, we will have

$$\Phi_{21}(\mathbf{x}_1, \mathbf{x}_2) = \chi_i(\mathbf{x}_2)\chi_j(\mathbf{x}_1) \tag{2.11}$$

by taking a linear combination of these two products,

$$\Phi_(\mathbf{x}_1, \mathbf{x}_2) = 2^{-1/2}(\chi_i(\mathbf{x}_1)\chi_j(\mathbf{x}_2) - \chi_i(\mathbf{x}_2)\chi_j(\mathbf{x}_1)) \quad , \tag{2.12}$$

where the factor $2^{-1/2}$ is a normalization factor. It can seen the antisymmetry is guaranteed during interchange of the coordinates of electron one and electron two:

$$\Phi_(\mathbf{x}_1, \mathbf{x}_2) = -\Phi_(\mathbf{x}_2, \mathbf{x}_1) \quad . \tag{2.13}$$

The antisymmetric wave function of Eq. (2.12) can rewritten as a determinant,

$$\Phi_(\mathbf{x}_1, \mathbf{x}_2) = 2^{-1/2} \begin{vmatrix} \chi_i(\mathbf{x}_1) & \chi_j(\mathbf{x}_1) \\ \chi_i(\mathbf{x}_2) & \chi_j(\mathbf{x}_2) \end{vmatrix} \tag{2.14}$$

and this is called a Slater determinant. For an N-electron system, the Slater determinant becomes,

$$\Phi(\mathbf{x}_1, \mathbf{x}_2, \cdots, \mathbf{x}_N) = (N!)^{-1/2} \begin{vmatrix} \chi_i(\mathbf{x}_1) & \chi_j(\mathbf{x}_1) & \cdots & \chi_k(\mathbf{x}_1) \\ \chi_i(\mathbf{x}_2) & \chi_j(\mathbf{x}_2) & \cdots & \chi_k(\mathbf{x}_2) \\ \vdots & \vdots & & \vdots \\ \chi_i(\mathbf{x}_N) & \chi_j(\mathbf{x}_N) & \cdots & \chi_k(\mathbf{x}_N) \end{vmatrix} \tag{2.15}$$

Note that the rows of the N-electron Slater determinant are labeled by electrons: first row ($\mathbf{x}_1$), second row ($\mathbf{x}_2$),$\cdots$, final row ($\mathbf{x}_N$). The columns are labeled by spin orbitals: first column (χ_i), second (χ_j),$\cdots$, final column (χ_k). Interchanging the coordinates of two electrons equals to the interchange of two rows of the Slater determinant which will change its sign. Thus the Slater determinant meets the requirement of antisymmetry. Furthermore having two electrons occupying the same spin orbital corresponds to having two columns of the determinant identical which leads to the determinant being zero. It is convenient to use a short-hand notation for a Slater determinant which only shows the diagonal elements:

$$\Phi(\mathbf{x}_1, \mathbf{x}_2, \cdots, \mathbf{x}_N) = |\chi_i(\mathbf{x}_1)\chi_j(\mathbf{x}_2)\cdots\chi_k(\mathbf{x}_N)\rangle \quad . \tag{2.16}$$

Furthermore, if the order of electrons is always to be $\mathbf{x}_1, \mathbf{x}_2, \cdots, \mathbf{x}_N$, then

$$\Phi(\mathbf{x}_1, \mathbf{x}_2, \cdots, \mathbf{x}_N) = |\chi_i\chi_j\cdots\chi_k\rangle \quad . \tag{2.17}$$

2.2 The Hartree-Fock Approximation

Among the approximate ways to solve Eq. (2.5), the Hartree-Fock (HF) method has a prominent status as it often paves the way toward more accurate calculations in modern quantum chemistry. At the same time, the HF method is also used extensively by itself to study various materials science problems, such as adsorption

[33], defects in solids [34], and electronic structure of insulators [35]. In this section, we give a brief account of the HF method.

The Hartree-Fock method starts from using the single Slater determinant as an approximation the to wave function of the ground state of the N-electron system:

$$|\Phi\rangle = |\chi_1, \chi_2, \cdots, \chi_a, \chi_b, \cdots, \chi_N\rangle \quad . \tag{2.18}$$

Thus this choice of the approximation of wave function guarantees a proper description of the electron which obey the Pauli exclusion principle as shown in the previous section. Then we need to determine the "best" approximate wave function. According to the variational principle, the "best" spin orbitals are those that make energy stationary,

$$E = \frac{\int \langle \Phi(\mathbf{x})|\hat{H}|\Phi(\mathbf{x})\rangle \, d\mathbf{x}}{\int \langle \Phi(\mathbf{x})|\Phi(\mathbf{x})\rangle \, d\mathbf{x}} \tag{2.19}$$

then we can systematically vary the spin orbitals $\{\chi_a\}$, while constraining that they are orthonormal, $\langle \chi_a|\chi_b\rangle = \delta_{ab}$, until the electronic minimum E_0 is reached. This leads to the HF energy expression,

$$\begin{aligned} E_{\mathrm{HF}} = \langle \Psi_0|\hat{H}|\Psi_0\rangle = & \sum_a \int \chi_a^*(1)(-\frac{1}{2}\nabla^2 - \frac{Z_A}{r_{iA}})\chi_a(1)\, dx_1 \\ & + \frac{1}{2}\sum_{ab} \int \chi_a^*(1)\chi_a(1) r_{12}^{-1} \chi_b^*(2)\chi_b(2)\, dx_1 dx_2 \\ & - \frac{1}{2}\sum_{ab} \int \chi_a^*(1)\chi_b(1) r_{12}^{-1} \chi_b^*(2)\chi_a(2)\, dx_1 dx_2 \quad . \end{aligned} \tag{2.20}$$

Each term at the right hand side in Eq. (2.20) will be explained in the following. The first term,

$$\begin{aligned} \int \chi_a^*(1)(-\frac{1}{2}\nabla^2 - \frac{Z_A}{r_{iA}})\chi_a(1)\, dx_1 = & \langle \chi_a(1)|h|\chi_a(1)\rangle \\ h = & -\frac{1}{2}\nabla^2 - \frac{Z_A}{r_{iA}} \quad , \end{aligned} \tag{2.21}$$

is the kinetic energy and potential energy for the attraction to the nuclei of a single electron. The last two terms in Eq. (2.20) are involving two electrons, and the first one is the Coulomb term and the other one is the exchange term which arises from the antisymmetric nature of the Slater determinant. For the Coulomb term, it has the classical interpretation that it represents the Coulomb interactions between two electrons, It is convenient to define a Coulomb operator,

$$J_b(1) = \int |\chi_b(2)|^2 r_{12}^{-1}\, dx_2 \quad . \tag{2.22}$$

Then the Coulomb term can be written as,

$$\int \chi_a^*(1)\chi_a(1) r_{12}^{-1} \chi_b^*(2)\chi_b(2)\, dx_1 dx_2 = \langle \chi_a(1)|J_b(1)|\chi_a(1)\rangle \quad . \tag{2.23}$$

The exchange term, has no simple classical interpretation like the Coulomb term, but we can define an exchange operator by its effects when operating on $\chi_a(1)$:

$$K_b(1)\chi_a(1) = \left[\int \chi_b^*(2) r_{12}^{-1} \chi_a(2)\, dx_2\right] \chi_b(1) \quad . \tag{2.24}$$

As evident from the above equation, $K_b(1)$ leads to an exchange of the variable in the two spin orbitals. Furthermore, the exchange operator, $K_b(1)$ is said to be a nonlocal operator, as the results of $K_b(1)$ operating on the spin orbital χ_a will depend on the value of χ_a throughout all space. Then the exchange term can be written as,

$$\int \chi_a^*(1)\chi_b(1) r_{12}^{-1} \chi_b^*(2)\chi_a(2)\, dx_1 dx_2 = \langle \chi_a(1)|K_b(1)|\chi_a(1)\rangle \quad . \tag{2.25}$$

Up to this, we can write the Hartree-Fock equation as an eigenvalue equation:

$$\left[h(1) + \sum_{b\neq a} J_b(1) - \sum_{b\neq a} K_b(1)\right]\chi_a(1) = E_a\chi_a(1) \quad . \tag{2.26}$$

Furthermore, to eliminate the restriction on the summation ($b \neq a$), we define a new operator, the Fock operator, by

$$f(1) = h(1) + \sum_b J_b(1) - K_b(1) \quad . \tag{2.27}$$

The Fock operator is the sum of the operator $h(1)$ and an effective one-electron potential operator called the Hartree-Fock potential $v_{(1)}^{\mathrm{HF}} = \sum_b J_b(1) - K_b(1)$. From Eq. (2.27), Hartree-Fock theory is a single particle method. So that the Hartree-Fock equation becomes:

$$f|\chi_a\rangle = E_a|\chi_a\rangle \quad . \tag{2.28}$$

This is the usual form of the Hartree-Fock equation. Although, Eq. (2.28) is written as a linear eigenvalue problem, it will need to be solved by iterative procedures as the Fock operator has a functional dependence on $|\chi_a\rangle$ through the Coulomb and exchange operator.

2.3 Post-Hartree-Fock Methods

The major problem in the Hartree-Fock method is that it completely neglects correlations between electrons with same spin (beyond exchange). Following Löwdin [36], in quantum chemistry it is common to define the energy associated with the missing electron correlation energy as:

$$E_{\mathrm{corr}} = E_{\mathrm{exact}} - E_{\mathrm{HF}} \quad , \tag{2.29}$$

where E_{exact} is the exact energy of the system and E_{corr} is thus the missing energy associated with correlations in the exact many body ground state wave function.

E_{corr} is negative because E_{HF} is always the upper bound of the E_{exact}. The missing correlation energy is typically a very small fraction of the total energy. However it can be a very important contribution to many systems of physical and chemical interest. For example, the restricted Hartree-Fock method cannot describe the dissociation of H_2 into two open-shell H atoms. Or, at least one quarter of the strength of hydrogen bonds between water molecules comes from correlations beyond HF [37].

Post-Hartree-Fock methods in quantum chemistry aim to improve on Hartree-Fock by taking account of electron correlation. These methods include configuration interaction (CI), Møller-Plesset perturbation theory, and coupled cluster. For CI methods, a linear combination of Slater determinants rather than one single Slater determinant in Hartree-Fock is used to approximate the wave function. However, CI was not been used in this thesis [2], so it will not be further discussed. Møller-Plesset perturbation theory, as the name suggests, treats electron correlation in perturbative way. And in the coupled cluster method, the electron correlation is handled through use of a so-called cluster operator. Both Møller-Plesset perturbation theory and coupled cluster will be now briefly introduced.

2.3.1 Møller-Plesset Perturbation Theory

The principle of perturbation theory in general is to start from a simple model which has been solved exactly or approximately and gradually add the small "perturbation" to this simple model. If the disturbance is not so large, the various physical quantities of interest can be obtained from the starting model.

Suppose we wish to solve the eigenvalue problem,

$$\hat{H}|\Psi_i\rangle = (\hat{H}_0 + \hat{H}')|\Psi_i\rangle = \xi_i|\Psi_i\rangle \quad , \tag{2.30}$$

where $\hat{H}_0$ is the reference Hamiltonian which we know the eigenfunctions and eigenvalues of $\hat{H}_0$,

$$\hat{H}_0|\Phi_i\rangle = E_i^0|\Phi_i\rangle \quad . \tag{2.31}$$

We want to systematically improve the eigenfunctions and eigenvalues of $\hat{H}_0$ so that they become closer and closer to the eigenfunctions and eigenvalues of the total Hamiltonian $\hat{H}$. To do that, we introduce a perturbation parameter λ, and write

$$\hat{H} = \hat{H}_0 + \lambda\hat{H}' \tag{2.32}$$

and expand the exact eigenfunctions and eigenvalues in a Taylor series in λ,

$$|\Psi_i\rangle = |\Phi_i\rangle + \lambda|\Phi_i^{(1)}\rangle + \lambda^2|\Phi_i^{(1)}\rangle + \cdots \tag{2.33a}$$

$$\xi_i = E_i^{(0)} + \lambda E_i^{(1)} + \lambda^2 E_i^{(2)} + \cdots \tag{2.33b}$$

[2] It is well-known that truncated CI like CISD (truncated at double excitation level) is not size-extensive and the full CI calculations which is prohibitively expensive, are limited to the smallest system like H_2. In contrast CCSD or CCSD(T) do have this important property. Although there is also proposed the correction to the truncated CI for this missing size-extensive (J. Chem. Phys. **101**, 8908 (1994)), in this thesis we will use coupled cluster method for the high accuracy calculations.

then we take the eigenfunction of $\hat{H}_0$ to be normalized ($\langle\Phi_i|\Phi_i\rangle = 1$). Further, we choose the normalization of Ψ_i to be $\langle\Phi_i|\Psi_i\rangle = 1$. This choice is called intermediate normalization and can always be made unless $|\Phi_i\rangle$ and $|\Psi_i\rangle$ are orthogonal. Therefore, by multiplying Eq. (2.33a) by $\langle\Phi_i|$, we have

$$\langle\Phi_i|\Psi_i\rangle = \langle\Phi_i|\Phi_i\rangle + \lambda\langle\Phi_i|\Phi_i^{(1)}\rangle + \lambda^2\langle\Phi_i|\Phi_i^{(1)}\rangle + \cdots = 1 \tag{2.34}$$

The above equation holds for all values of λ and the coefficients of λ on both sides must be equal, and hence

$$\langle\Phi_i|\Phi_i^{(n)}\rangle = 0 \quad n = 1, 2, 3, \cdots \tag{2.35}$$

Substituting Eq. (2.33a) and Eq. (2.33b) into Eq. (2.30), and equating coefficients of λ^n, we find

$$\hat{H}_0|\Phi_i\rangle = E_i^{(0)}|\Phi_i\rangle \quad n = 0 \tag{2.36a}$$

$$\hat{H}_0|\Phi_i^{(1)}\rangle + \hat{H}'|\Phi_i\rangle = E_i^{(0)}|\Phi_i^{(1)}\rangle + E_i^{(1)}|\Phi_i\rangle \quad n = 1 \tag{2.36b}$$

$$\hat{H}_0|\Phi_i^{(2)}\rangle + \hat{H}'|\Phi_i^{(1)}\rangle = E_i^{(0)}|\Phi_i^{(2)}\rangle + E_i^{(1)}|\Phi_i^{(1)} + E_i^{(2)}|\Phi_i\rangle \quad n = 2 \tag{2.36c}$$

$$\hat{H}_0|\Phi_i^{(3)}\rangle + \hat{H}'|\Phi_i^{(2)}\rangle = E_i^{(0)}|\Phi_i^{(3)}\rangle + E_i^{(1)}|\Phi_i^{(2)} + E_i^{(2)}|\Phi_i^{(1)}\rangle + E_i^{(3)}|\Phi_i\rangle \quad n = 3 \tag{2.36d}$$

and so on. Multiplying each of these equations by $\langle\Phi_i|$ and using the orthogonality relation of Eq. (2.35), we obtain the following expressions for the nth-order energies

$$E_i^{(0)} = \langle\Phi_i|\hat{H}^0|\Phi_i\rangle \tag{2.37a}$$

$$E_i^{(1)} = \langle\Phi_i|\hat{H}'|\Phi_i\rangle \tag{2.37b}$$

$$E_i^{(2)} = \langle\Phi_i|\hat{H}'|\Phi_i^{(1)}\rangle \tag{2.37c}$$

$$E_i^{(3)} = \langle\Phi_i|\hat{H}'|\Phi_i^{(2)}\rangle \tag{2.37d}$$

The set of equations in Eq. (2.36) and Eq. (2.37) outline the basic task of the many body perturbation theory that solve Eq. (2.36) to get the wave function and Eq. (2.37) to determine the different order energy.

First consider Eq. (2.36b), which determines the first-order wave function $|\Phi_i^{(1)}\rangle$. This can be rewritten as

$$(E_i^{(0)} - \hat{H}_0)|\Phi_i^{(1)}\rangle = (\hat{H}' - E_i^{(1)})|\Phi_i\rangle = (\hat{H}' - \langle\Phi_i|\hat{H}'|\Phi_i\rangle)|\Phi_i\rangle \tag{2.38}$$

with $E_i^{(1)}$ substituted by using Eq. (2.37b). Furthermore, the first order perturbation wave function can be expanded as,

$$|\Phi_i^{(1)}\rangle = \sum_{n\neq i}|\Phi_n\rangle\langle\Phi_n|\Phi_i^{(1)}\rangle \tag{2.39}$$

where it does not include the term $n = i$. Multiplying Eq. (2.38) by $\langle\Phi_n|$, we will have

$$(E_i^{(0)} - E_n^{(0)})\langle\Phi_n|\Phi_i^{(1)}\rangle = \langle\Phi_n|\hat{H}'|\Phi_i\rangle \quad . \tag{2.40}$$

Using the expansion Eq. (2.39) and inserting into Eq. (2.37c) for the second-order energy, we obtain,

$$E_i^{(2)} = \langle \Phi_i | \hat{H}' | \Phi_i^{(1)} \rangle = \sum_{n \neq i} \langle \Phi_i | \hat{H}' | \Phi_n \rangle \langle \Phi_n | \Phi_i^{(1)} \rangle \quad , \tag{2.41}$$

and hence, using Eq. (2.40), we finally have

$$E_i^{(2)} = \sum_{n \neq i} \frac{\langle \Phi_i | \hat{H}' | \Phi_n \rangle \langle \Phi_n | \hat{H}' | \Phi_i \rangle}{E_i^{(0)} - E_n^{(0)}} \quad , \tag{2.42}$$

which is the desired expression for the second-order energy. Higher order energy terms can be obtained in a similar, although increasingly more complex manner.

So far the theory has been completely general. To apply perturbation theory to electron correlation calculations, the unperturbed Hamiltonian ($\hat{H}_0$) must be selected. The most common choice is to take this as a sum over Fock operators which is defined in Eq. (2.27), leading to the Møller-Plesset (MP) perturbative theory [38]:

$$\hat{H}_0 = \sum_{i=1}^{N} F_i = \sum_{i=1}^{N} \left(h_i + v_{(i)}^{\mathrm{HF}}) \right) \quad , \tag{2.43}$$

and the perturbative Hamiltonian is,

$$\hat{H}' = \hat{H} - \hat{H}_0 = \sum_{i<j} r_{ij}^{-1} - \sum_i v_{(i)}^{\mathrm{HF}} \quad . \tag{2.44}$$

Now we start to derive the electron correlation energy by using MP theory, especially, we focus on the second-order energy which is the MP2 method. First, the Hartree-Fock wave function $|\Phi_0\rangle$ is an eigenfunction of $\hat{H}_0$,

$$\hat{H}_0 |\Phi_0\rangle = E_0^{(0)} |\Phi_0\rangle \tag{2.45}$$

with the eigenvalue $E_0^{(0)}$. The general result for the second-order energy has been shown in Eq. (2.42). That involves the matrix elements of the perturbation operator between the Hartree-Fock reference wave function and all possible excited states. However, the perturbation operator is a two-electron operator which means all matrix elements involving triple, quadruple, etc., excitations are zero. This leaves only single and double excitations. Furthermore single excitation states bring no contributions as they are also zero as shown below,

$$\begin{aligned} \langle \Phi_0 | \hat{H}' | \Phi_i^a \rangle &= \langle \Phi_0 | \hat{H} - \sum_{j=1}^{N} F_j | \Phi_i^a \rangle \\ &= \langle \Phi_0 | \hat{H} | \Phi_i^a \rangle - \langle \Phi_0 | \sum_{j=1}^{N} F_j | \Phi_i^a \rangle \\ &= \langle \Phi_0 | \hat{H} | \Phi_i^a \rangle - E_a \langle \Phi_0 | \Phi_i^a \rangle \quad . \end{aligned} \tag{2.46}$$

The first bracket on the final line of above equation is zero due to the Brillouin theorem [39], and the second one is also zero because of the orthogonality of wave functions. Therefore, the only excitations left are double excitations. Here the occupied states are labeled as $(i, j, k, \cdots)$ and the unoccupied states are labeled as $(a, b, c, \cdots)$,

$$E_i^{(2)} = \sum_{i<j}^{occ} \sum_{a<b}^{vir} \frac{\langle \Phi_0 | \hat{H}' | \Phi_{ij}^{ab} \rangle \langle \Phi_0 | \hat{H}' | \Phi_{ij}^{ab} \rangle}{E_0^{(0)} - E_{ij}^{ab}} \quad . \tag{2.47}$$

The matrix elements between the Hartree-Fock and the doubly excited state are given by two-electron integrals over molecular orbitals. The difference in total energy between two Slater determinants becomes a difference in molecular orbital energies. Thus the explicit expression for MP2 becomes,

$$E_i^{(2)} = \sum_{i<j}^{occ} \sum_{a<b}^{vir} \frac{[\langle \phi_i \phi_j | \phi_a \phi_b \rangle - \langle \phi_i \phi_j | \phi_b \phi_a \rangle]^2}{\varepsilon_i + \varepsilon_j - \varepsilon_a - \varepsilon_b} \quad . \tag{2.48}$$

In the above equation, the ϕ_i, ϕ_j are the occupied orbitals and ϕ_a, ϕ_b are the virtual (unoccupied) orbitals. The $\varepsilon_i, \varepsilon_j, \varepsilon_a$, and ε_b are the corresponding orbital energies.

MP2 shows improvements over Hartree-Fock in many respects in electronic structure calculations [40, 41]. For example, MP2 can capture the weak non-covalent interactions like dispersion for which Hartree-Fock completely fails. Also the geometry (G3 test set) predicted from MP2 show much improvement over Hartree-Fock compared with experimental measurements [42]. It is worth cautioning, however, that Møller-Plesset perturbation theory is far from a panacea. For example, it is not appropriate for truly metallic systems and for some molecular properties like spectroscopic constants which are not necessarily converged when going to high orders, or the convergence is slow or oscillatory [43]. Thus MP5 or MP25 will not definitely bring better results than MP2! Despite this, MP2 is a very powerful and useful post-Hartree-Fock method considering its accuracy and scaling (N^5) and widely used in molecular system electronic structure calculations.

2.3.2 Coupled Cluster Methods

The coupled cluster method was introduced into quantum chemistry by Čížek and Paldus [44, 45] in the 1960's and emerged as perhaps the most reliable, yet computationally affordable method for the approximate solution of the electronic Schrödinger and the prediction of molecular properties [46, 47, 48]. A short account of this method is given now.

The coupled cluster wave function is written as,

$$\Psi_{\text{cc}} = e^T \Phi_0 \quad . \tag{2.49}$$

Here Φ_0 is a Slater determinant, and the exponential operator e^T can be expanded as a Taylor series,

$$e^T = 1 + T + \frac{1}{2}T^2 + \frac{1}{6}T^3 + \cdots = \sum_{k=0}^{\infty} \frac{1}{k!} T^k \quad , \tag{2.50}$$

where the cluster operator T is given by

$$T = T_1 + T_2 + T_3 + \cdots + T_N \quad . \tag{2.51}$$

The T_ith operator acting on a HF reference wave function will generate all ith excited Slater determinants,

$$\begin{aligned} T_1\Phi_0 &= \sum_{i}^{occ}\sum_{a}^{vir} t_i^a \Phi_i^a \quad , \\ T_2\Phi_0 &= \sum_{i}^{occ}\sum_{a}^{vir} t_{ij}^{ab} \Phi_{ij}^{ab} \quad . \end{aligned} \tag{2.52}$$

From Eq. (2.50) and Eq. (2.51), the exponential operator may be written as

$$\begin{aligned} e^T =& 1 + T_1 + \left(T_2 + \frac{1}{2}T_1^2\right) + \left(T_3 + T_1T_2 + \frac{1}{6}T_1^3\right) \\ &+ \left(T_4 + T_3T_1 + \frac{1}{2}T_2^2 + \frac{1}{2}T_2T_1^2 + \frac{1}{24}T_1^4\right) + \cdots \end{aligned} \tag{2.53}$$

The first term generates the reference Hartree-Fock states and the second are all singly excited states. The terms in first parenthesis generate all doubly excited states, and so on.

With the coupled cluster wave function in Eq. (2.49), the Schrödinger equation becomes

$$\hat{H}e^T\Phi_0 = Ee^T\Phi_0 \quad . \tag{2.54}$$

Multiplying from the left by Φ_0^* and integrating gives

$$E = \langle\Phi_0|\hat{H}e^T|\Phi_0\rangle \quad . \tag{2.55}$$

Expanding out the exponential in Eq. (2.50), we get

$$E = \langle\Phi_0|\hat{H}(1 + T + \frac{1}{2}T^2 + \frac{1}{6}T^3 + \cdots)|\Phi_0\rangle \quad . \tag{2.56}$$

Note that $\hat{H}$ is at most a two-particle operator and then T is at least a one-particle excitation operator. We can simplify the above equation,

$$E = \langle\Phi_0|\hat{H}(1 + T + \frac{1}{2}T^2)|\Phi_0\rangle \quad . \tag{2.57}$$

This is the natural truncation of the coupled cluster energy equation and it only depends on the form of $\hat{H}$ not on that of T or on the number of electrons.

Till now, everything is exact. Expansion of the cluster operator T up to T_N would mean all possible excited determinants are included, then coupled cluster results are equal to those obtained from full CI calculations. However, in practice a truncation of T must be performed. Only including T_1 does not improve anything upon Hartree-Fock because of the Brillouin theorem. So the lowest approximation

starts from T_2. If T is expanded as $T_1 + T_2$, this will be referred to as CCSD, which is the coupled cluster method with single and double excitations. Now we focus on CCSD to get E in Eq. (2.57). If $T = T_1 + T_2$, then Eq. (2.57) becomes,

$$\begin{aligned} E &= \langle\Phi_0|\hat{H}|\Phi_0\rangle + \langle\Phi_0|\hat{H}T_1|\Phi_0\rangle + \langle\Phi_0|\hat{H}T_2|\phi_0\rangle + \frac{1}{2}\langle\Phi_0|\hat{H}T_1^2|\Phi_0\rangle \\ E &= E_0 + \sum_i^{occ}\sum_a^{vir} t_i^a\langle\Phi_0|\hat{H}|\Phi_i^a\rangle + \sum_{i<j}^{occ}\sum_{a<b}^{vir}(t_{ii}{}^{ab} + t_i^a t_j^b - t_i^b t_j^a)\langle\Phi_0|\hat{H}|\Phi_{ij}^{ab}\rangle \end{aligned} \tag{2.58}$$

and the first matrix elements are zero and the second matrix elements are two-electron integrals over molecular orbitals. The energy can be written down as,

$$E = E_0 + \sum_{i<j}^{occ}\sum_{a<b}^{vir}(t_{ii}^{ab} + t_i^a t_j^b - t_k^b t_j^a)(\langle\phi_i\phi_j|\phi_a\phi_b\rangle - \langle\phi_i\phi_j|\phi_b\phi_a\rangle) \quad . \tag{2.59}$$

The above equation is the expression of the energy obtained from CCSD, with the coefficients of single and double excitation generally obtained iteratively. Once these coefficients are known, the energy and wave functions can be calculated.

CCSD calculations are already very expensive, scaling as N^6 where N is the number of basis functions in the calculation, and to go beyond CCSD makes the calculations extremely demanding. For example, CCSDT which iteratively treats the third-order excitations, scales as N^8 which makes it practically unfeasible for anything but the smallest of systems. To avoid this demanding scaling, the triple excitations can be obtained in a perturbative manner, with an approach widely known as CCSD(T) [49]. Starting from the energy at the CCSD level and following the procedure outlined in Eq. (2.36) and Eq. (2.37), the triple excitation energy can be expressed as [50],

$$E_{\mathrm{CCSD}}^{(T)} = \sum_{a<b<c}^{vir}\sum_{i<j<k}^{occ} \frac{\langle\Phi_0|(1+\Lambda_1+\Lambda_2)\bar{H}_{\mathrm{CCSD}}|\Phi_{ijk}^{abc}\rangle\langle\Phi_{ijk}^{abc}|\bar{H}_{\mathrm{CCSD}}|\Phi_0\rangle}{\varepsilon_i + \varepsilon_j + \varepsilon_k - \varepsilon_a - \varepsilon_b - \varepsilon_c} \tag{2.60}$$

where $\bar{H}_{\mathrm{CCSD}} = e^{(-T_1-T_2)}\hat{H}e^{(T_1+T_2)}$ and Λ is the deexcitation operator and expressed in second quantization as,

$$\begin{aligned} \Lambda_1 &= \sum_{i,a}\lambda_a^i i^+ a \\ \Lambda_2 &= \frac{1}{4}\sum_{\substack{i,j\\a,b}}\lambda_{ab}^{ij} i^+ a j^+ b \quad . \end{aligned} \tag{2.61}$$

CCSD(T) is often considered as the "gold standard" method of quantum chemistry due to its very high accuracy. For example, CCSD(T) predicts the binding energy of the water dimer to be 217.6 meV [51] which is in a good agreement with the experimental value of 216.8 meV [52]. In general, the results from CCSD(T) calculations are often used to benchmark other theoretical methods like MP2 and DFT [53, 54].

2.4 Gaussian Functions

In the preceding sections, the basic ingredients of the quantum chemistry methods (HF, MP2, and CCSD(T)) have been introduced. In this section, the concept of the basis set will be introduced which is almost always necessary to practically solve the electronic Schrödinger equation.

Essentially, almost all electronic structure methods today rely on an expansion on the unknown wave function in terms of a set of basis functions. Any type of basis functions may in principle to be used like exponential, Gaussian, polynomial, plane-wave, spline, Slater type orbitals, and numeric atomic orbitals, etc. However, some issues are useful to consider when selecting basis functions:

- The basis functions should allow for the wave function/density to be accurately described with as low a computational cost as possible.

- The behavior of the basis functions will ideally capture some of the physics of the problem. For example, for bound atomic or molecular systems this means functions should go to zero when the distance between the nucleus and the electron becomes large. Or in a condensed matter system basis functions with a periodicity matching the crystal lattice can be useful.

In part for these reasons the use of Gaussian functions has become very popular in the calculations of chemical problems. We will now discuss in more detail the specific Gaussian orbital basis sets employed in this thesis. When we discuss electronic structure calculations on condensed matter systems, plane-wave basis sets, which are very popular for such simulations, will be introduced.

2.4.1 Gaussian Functions as Basis Sets

Eearly in quantum chemistry, Slater type orbitals (STO) were used as basis functions because of their similarity with the solutions of the hydrogen atom. The Slater type orbitals have the form in spherical coordinates,

$$\phi_i(\zeta, n, l, m, r, \theta, \psi) = N r^{n-1} e^{-\zeta r} Y_{lm}(\theta\phi) \quad , \tag{2.62}$$

where N is the normalization constant, and Y are the spherical harmonic functions. n, l, and m are the quantum numbers: principal, angular momentum, magnetic, respectively. ζ is called the "exponent". The exponential dependence on distance reflects the exact form of the hydrogenie orbitals. However, the calculation of the three- and four-center two-electron integrals with Slater orbitals is extremely slow and has no analytical form. Thus in modern quantum chemistry calculations, the Slater orbitals are generally restricted to atomic and diatomic systems.

In contrast, it is much faster to work with Gaussian functions in the evaluation of the two-electron integrals than STO functions. Thus for this pragmatic reason, Gaussian functions have become the most popular basis functions in quantum chemistry. Numerous quantum chemistry codes employ Gaussian functions as basis

sets. The Gaussian function type orbital (GTO) has the following form in Cartesian coordinates:

$$g(\zeta, l_x, l_y, l_z, x, y, z) = Ne^{-\zeta r^2} x^{l_x} y^{l_y} z^{l_z} \quad . \tag{2.63}$$

Note that the l_x, l_y, l_z in Cartesian coordinate are not the quantum numbers but instead parameters. However, the sum of them, $L = l_x + l_y + l_z$ is analogous to the angular momentum for atoms, to mark function as s-type ($L = 0$), p-type ($L = 1$), d-type ($L = 2$), and f-type ($L = 3$), etc.

The Gaussian function described in Eq. (2.63) is generally known as a primitive Gaussian function. It is very common to group several primitive Gaussian functions into one Gaussian function and this new Gaussian function is known as a contracted Gaussian function,

$$g(c) = \sum_{i}^{k} a_i g(p) \quad , \tag{2.64}$$

where c and p designate contracted and primitive, respectively. By contracting, several primitive Gaussians into one, the computational effort can be reduced through the optimization of several coefficients in one go.

When using Gaussian function basis sets it is far from trivial to decide what set of (contracted) Gaussian functions are appropriate for the system under investigation. Generally some experience is required. However, the minimum basis set which must be used corresponds to the number of atomic orbitals in the system. For example, the minimum basis set for hydrogen is just a single s-function. For the first row elements in the periodic table, this means two s-functions and one set of p-functions ($2p_x$, $2p_y$, $2p_z$). For almost all practical problems the minimum basis set description is inadequate. The next improvement is to double all the basis functions which produce the double zeta (DZ) type basis. For hydrogen, a DZ basis set will use two s-functions ($1s$, $1s^{'}$). For the first row elements in the periodic table, this means four s-function ($1s$, $1s^{'}$, $2s$, $2s^{'}$) and two sets p-functions ($2p$, $2p'$). When the basis set has three sets of basis functions for each orbital, you will get the tripe zeta (TZ) basis and so on. As we will see below, it is common to make a distinction between core and valence electrons, with more sets of basis functions (larger zeta) allocated to the valence electrons compared to the core electrons.

Further improvements can be achieved by adding so-called polarization or diffuse functions. Although a free isolated atom will have spherical symmetry, the atoms in a molecule or some other chemical environment will exhibit some distortions in their electron density. To take account of this effect through the basis set, we need to augment basis sets with additional functions with the larger angular momentum. For example, hydrogen will be augmented by adding a p orbital into its minimum basis set. In Pople style basis sets, which will be introduced later, an asterisk represents the polarization function in the basis set like 6-31G*. In a similar spirit, so-called diffuse functions are sometimes also included in the basis set. The purpose of adding diffuse functions is to improve the description at large distances from the nuclei. This is especially important for anions as the additional electrons are loosely bound to nuclei. In general, diffuse functions have a very small exponent, ζ,

typically from 0.01 to 0.1, so it will extend far from the nucleus.

2.4.2 Pople and Dunning Basis Sets

Many and various Gaussian basis sets exist. Here we focus on the two different classes of Gaussian basis sets used in this thesis: Pople style basis sets and the correlation consistent basis sets of Dunning and co-workers [55, 56, 57]. For the Pople style basis sets, it is better to take an example to explain the meaning of the notation. For example, a 6-31G basis set is a double split valence basis set. This notation means that the core orbitals are described by one contracted Gaussian function comprised of six primitive Gaussians. The valence orbital has been split into two contracted Gaussians, one comprised of three primitive Gaussians and the other just one primitive Gaussian. As another example a 6-311G basis set is a triple split valence basis set. The core orbital is still a contraction of six primitive Gaussians. However the valence is now split into three parts which are contractions of three, one, and one primitive Gaussians, respectively.

The correlation consistent basis sets, from Dunning's group, are designed to systematically recover the correlation energy with the increasing size of the basis sets. Normally, the basis sets are obtained from the HF atomic calculations [58]. When coming to molecular calculations, the basis functions are augmented with polarization functions accounting for the distortion from the atomic state in the molecular environment. However, there is not a clear way to achieve the continuous improvements with increasing the basis functions. Thus the convergence is not easy to guarantee and the choice of the basis set is sometimes drawn from the researcher's own experience. In contrast, the correlation consistent basis set choose the basis functions depend on the similar contributions to the correlation energy from each function independent of the function type. For example, the contributions from $2d$ and $1f$ function are similar, so they belong to the same group and will be added together. By this way, Dunning proposed a series of correlation consistent basis sets which can approach the complete basis set (CBS) limit in a systematic manner (see Figure 2.1). In the current thesis, the following correlation consistent basis set are employed, cc-pVDZ ($3s2p1d$), cc-pVTZ ($4s3p2d1f$), cc-pVQZ ($5s4p3d2f1g$), and cc-pV5Z ($6s5p4d3f2g1h$) where the number of contracted Gaussian functions are indicated in brackets.

As with the Pople style basis sets, the correlation consistent basis sets can be augmented by the addition of diffuse functions. The augmentation consists of adding one extra function with a smaller exponent to every angular momentum channel. This is denoted by the new prefix of aug: aug-cc-pVXZ (X=D, T, Q, and 5). Furthermore, if the correlation between core-core and core-valence electrons needs to be recovered, the correlation consistent basis sets can be augmented with basis functions with large exponents. Based on the cc-pVXZ (X=D, T, Q) basis sets, ($1s1p$) functions are added to cc-pVDZ, ($2s2p1d$) to cc-pVTZ, ($3s3p2d1f$) to cc-pVQZ, etc. This produce a new series of basis sets: cc-pCVXZ (X=D,T, and Q).

As the key feature of the correlation consistent basis set is to systematically improve with basis set size, there are several different ways to extrapolate the results

to the CBS limit, which will be discussed below.

2.4.3 Basis Set Superposition Error

Localised basis functions, such as Gaussian functions, are prone to a problem known as basis set superposition error (BSSE) [59]. When two fragments A and B approach each other to form the new species, fragment A feels the basis functions of fragment B and fragment B also feels the basis functions of fragment A. Effectively each fragment feels a larger basis set than what it has as an isolated fragment and in so doing artificially stabilising the cluster.

One widely used method to assess the BSSE is the Counterpoise correction scheme of Boys and Bernardi [60]. To illustrate how this method works, consider the binding energy of the dimer (AB). The binding energy (E_{bind}) can be expressed as,

$$E_{\text{bind}} = E(AB)_{ab} - E(A)_a - E(B)_b \tag{2.65}$$

where $E(AB)_{ab}$, $E(A)_a$, and $E(B)_b$ are the energy of AB, monomer A, and monomer B, respectively. The subscript indicates the corresponding basis set for AB, A, and B. Because of the incompleteness of the basis set for A and B, there exists a BSSE in E_{bind}. When using the Counterpoise method, the BSSE can be evaluated with,

$$\Delta E_{\text{BSSE}} = E(A, AB)_{ab} + E(B, AB)_{ab} - E(A, AB)_a - E(B, AB)_b \tag{2.66}$$

where $E(A, AB)_{ab}$ represents the energy of monomer A in the structure it adopts in the dimer and with the full basis set of the dimer available. Likewise $E(B, AB)_{ab}$ represents the energy of the monomer B in the structure it adopts in the dimer and with the full basis set of the dimer available. $E(A, AB)_a$ and $E(B, AB)_b$ are then the energies of A and B, respectively, with only their own basis functions but again in the structure they adopt in the dimer. Thus Eq. (2.66) gives the difference between the energies of each fragment with the corresponding monomer and the full dimer basis sets. By this way, the artificial enhancements each monomer gains in the dimer can be established and eliminated if desired by obtaining a corrected binding energy: $E_{\text{bind}} - \Delta E_{\text{BSSE}}$.

If high accuracy is desired, BSSE should be removed. However, removal of BSSE is not sufficient to guarantee high accuracy in, e.g., binding energies because of the incompleteness of the basis sets. Fortunately, there are well established extrapolation schemes that can alleviate basis set incompleteness errors, which will be introduced in the following section.

2.4.4 Extrapolation to the Complete Basis Set Limit

As we have emphasized, one particular feature of Dunning's correlation consistent basis sets is that they systematically allow the correlation energy to be improved with increasing basis set size. This systematic convergence provides opportunities to extrapolate to the CBS, which could remove the errors from the incompleteness of the basis set. In general, the first step of the extrapolation is to separate the extrapolation of the Hartree-Fock energy and the electron correlation energy [61].

Many extrapolation schemes have been developed for obtaining CBS estimate with Dunning's basis sets [56, 61, 62, 63, 64]. For the extrapolation of the Hartree-Fock energy, the extrapolation is mostly done with expressions like,

$$E_X^{\mathrm{HF}} = E_{\mathrm{CBS}}^{\mathrm{HF}} + AX^{(-B)} \quad , \tag{2.67}$$

and

$$E_X^{\mathrm{HF}} = E_{\mathrm{CBS}}^{\mathrm{HF}} + Ae^{(-BX)} \quad , \tag{2.68}$$

where X is the cardinal number corresponding to the basis set (X=2, 3, and 4 for double zeta, triple zeta, and quadruple zeta). E_X^{HF} is the corresponding HF energy and $E_{\mathrm{CBS}}^{\mathrm{HF}}$ is the HF energy at the CBS. A and B are fitting parameters.

For electron correlation extrapolation, there are yet more options. For example, one of the popular three-parameter extrapolations schemes is,

$$E_X^{\mathrm{corr}} = E_{\mathrm{CBS}}^{\mathrm{corr}} + CX^{-3} + DX^{-5} \quad , \tag{2.69}$$

where E_X^{corr} is the corresponding electron correlation energy for a given cardinal number (X) and $E_{\mathrm{CBS}}^{\mathrm{corr}}$ is the electron correlation energy at the CBS. C and D are again the fitting parameters.

We will make use of extrapolation methods in chapter 6. To illustrate how the extrapolation schemes work the variation of the Hartree-Fock energy and electron correlation energy of a water molecule is shown in Figure 2.1. The energy of a single molecule has been calculated with cc-pVTZ, cc-pVQZ, and cc-pV5Z basis sets and the extrapolations were done for the Hartree-Fock energy and correlation energy by using Eq. 2.68 and Eq. 2.69, respectively. Two features of Figure 2.1 are apparent and worth very briefly commenting upon. First, E^{HF} and E^{corr} exhibit uniform convergence to the CBS limit upon increasing basis set size. Second, the variation in E^{HF} with basis set size in considerably (about 4 times) smaller than E^{corr} and E^{HF} is much faster in approaching the CBS limit than E^{corr}.

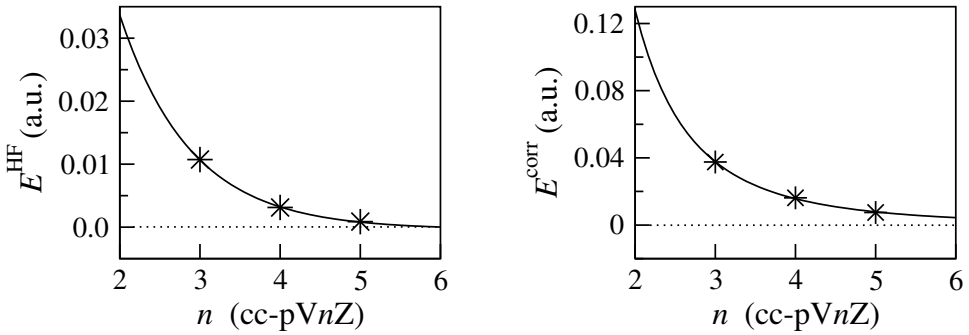

Figure 2.1: Extrapolation of the Hartree-Fock energy (E^{HF}) and electron correlation energy (E^{corr}) of a water molecule using Eq. (2.68) and Eq. (2.69), respectively. The electron correlation calculations are done at the MP2 level. The energy zero in both plots is the extrapolated CBS limit.

2.5 Density-Functional Theory

In the preceding section, we introduced several different ways to approximately solve the electronic Schrödinger equation such as the Hartree-Fock method, Møller-Plesset perturbation theory, and coupled cluster methods. These different methods share one common feature that they all rely on the many body wave function as a central quantity. Once the wave function is known, the energy of the system and all related properties will be determined. But the wave function itself is already a complicated quantity as it depends on $3N$ spatial variables together with the spin variable, where N is the number of electrons in the system. This severely limits the system sizes that can be treated with wave function based methods. Certainly systems with hundreds of atoms and large basis sets are beyond reach for most practical studies with wave function based methods.

DFT differs from the wave function based methods by using the electron density ($\rho(\mathbf{r})$) as the central quantity. The advantage of using the electron density over the wave function is the much reduced dimensionality. Regardless of how many electrons one has in the system, the density is always 3 dimensional. This enables DFT to be applied to much larger systems, hundreds or even thousands of atoms become possible. Partly for this reason, DFT has become the most widely used electronic structure approach today, particularly in the condensed matter physics community. In this section, a basic introduction to DFT will be given. Authoritative and comprehensive discussions of DFT can be found in a range of excellent review articles [65, 66, 67, 68] and textbooks [69, 70].

2.5.1 Thomas-Fermi Theory

The history of using the electron density rather than the wave function begins with the early work of Thomas and Fermi [71, 72]. First, let us define the electron density,

$$\rho(\mathbf{r}) = N \int \cdots \int |\Psi(\mathbf{x}_1, \mathbf{x}_2, \cdots, \mathbf{x}_N)|^2 \, d\mathbf{s}_1 \mathbf{x}_2 \cdots \mathbf{x}_N \quad . \tag{2.70}$$

$\rho(\mathbf{r})$ determines the probability of finding any of the N electrons within the volume $\mathbf{r}$ but with arbitrary spin while the other $N-1$ electrons have arbitrary positions and spin in the state represented by Ψ. This is a nonnegative simple function of three variables, x, y, and z, integrating to the total number of electrons,

$$\int \rho(\mathbf{r}) \, dr = N \quad . \tag{2.71}$$

In Thomas-Fermi theory, the kinetic energy of electrons are derived from the quantum statistical theory based on the uniform electron gas, but the interaction between electron-nucleus and electron-electron are treated classically. Within this model, the kinetic energy of the electrons is defined as,

$$T[\rho] = C_F \int \rho^{5/3}(\mathbf{r}) \, d\mathbf{r} \quad , \tag{2.72}$$

with

$$C_F = \frac{3}{10}(3\pi^2)^{2/3} = 2.871 \quad . \tag{2.73}$$

From the above equation, the approximation is made that the kinetic energy only of the electron depends exclusively on the electron density. By adding the interaction between electron-nucleus and electron-electron into Eq. (2.72), a total energy in terms of electron density is obtained,

$$E[\rho] = C_F \int \rho^{5/3}(\mathbf{r})\, d\mathbf{r} - Z \int \frac{\rho(\mathbf{r})}{r}\, d\mathbf{r} + \frac{1}{2} \iint \frac{\rho(\mathbf{r}_1)\rho(\mathbf{r}_2)}{|\mathbf{r}_1 - \mathbf{r}_2|}\, d\mathbf{r}_1 d\mathbf{r}_2. \tag{2.74}$$

The second and third terms are the electron-nucleus and electron-electron interactions, respectively.

The importance of this simple Thomas-Fermi model is not how well it performs in computing the ground state energy and density but more as an illustration that the energy can be determined purely using the electron density.

2.5.2 Hohenberg-Kohn Theorem

Modern density-functional theory was born in 1964 with the paper of Hohenberg and Kohn [73]. The two key results of this paper are: (i) a one to one mapping between external potential and electron density was established; (ii) it was shown that the ground state density can be found by using a variational principle.

The first part was proved in a simple and extremely elegant manner using the principle of *reductio ad absurdum*, and this is derived for a non-degenerate system[3]. Suppose there is a collection of electrons enclosed into a box influenced by an external potential $v(\mathbf{r})$. We assume we know the electron density of this system and it also determines $v(\mathbf{r})$ and thus all properties. If there is another external potential $v^{'}(\mathbf{r})$ which differs from $v(\mathbf{r})$ by more than a constant that can also give the same electron density $\rho(\mathbf{r})$ for the ground state, then we will have two different Hamiltonians $\hat{H}$ and $\hat{H}^{'}$ whose ground state electron density is the same but the normalized wave function Φ and $\Phi^{'}$ would be different. Then we will have

$$\begin{aligned} E_0 < \langle \Phi^{'} | \hat{H} | \Phi^{'} \rangle &= \langle \Phi^{'} | \hat{H}^{'} | \Phi^{'} \rangle + \langle \Phi^{'} | \hat{H} - \hat{H}^{'} | \Phi^{'} \rangle \\ &= E_0^{'} + \int \rho(\mathbf{r}) [v(\mathbf{r}) - v(\mathbf{r})^{'}]\, d\mathbf{r} \quad , \end{aligned} \tag{2.75}$$

where E_0 and $E_0^{'}$ are the ground-state energies for $\hat{H}$ and $\hat{H}^{'}$, respectively. Similarly, we can get

$$\begin{aligned} E_0^{'} < \langle \Phi | \hat{H} | \Phi \rangle &= \langle \Phi | \hat{H} | \Phi \rangle + \langle \Phi | \hat{H}^{'} - \hat{H} | \Phi \rangle \\ &= E_0 - \int \rho(\mathbf{r}) [v(\mathbf{r}) - v(\mathbf{r})^{'}]\, d\mathbf{r} \quad . \end{aligned} \tag{2.76}$$

Adding Eq. (2.75) and Eq. (2.76), we will obtain

$$E_0 + E_0^{'} < E_0^{'} + E_0 \quad . \tag{2.77}$$

[3]For degenerate system, see the article from M. Levy, Phys. Rev. A **26**, 1200 (1982).

This is an obvious contradiction. So there are no two different external potentials that can give the same $\rho(\mathbf{r})$. Thus $\rho(\mathbf{r})$ uniquely determines $v(\mathbf{r})$ and all ground-state properties.

Now we can write the energy E explicitly as a function of the electron density $\rho(\mathbf{r})$:

$$\begin{aligned} E[\rho] &= T[\rho] + T_{ne}[\rho] + V_{ee}[\rho] \\ &= \int \rho(\mathbf{r}) v(\mathbf{r})\, d\mathbf{r} + F_{\mathrm{HK}}[\rho] \quad , \end{aligned} \tag{2.78}$$

where

$$F_{\mathrm{HK}}[\rho] = T[\rho] + V_{ee}[\rho] \quad . \tag{2.79}$$

Here note that $F_{\mathrm{HK}}[\rho]$ is only dependent on ρ and independent from any external potential $v(\mathbf{r})$. Thus $F_{\mathrm{HK}}[\rho]$ is a universal functional of ρ.

The second Hohenberg-Kohn theorem demonstrates that that the ground state energy can be obtained variationally, with the density that minimizes the total energy being the exact ground state density. This is expressed as:

$$E_0[\rho_0] \leq E_v[\rho] \tag{2.80}$$

where $E_v[\rho]$ is the energy functional of Eq. (2.78). Following from the first part of the theorem, suppose the ground state wave function is Φ and its related electron density is ρ. Thus the ρ uniquely defined the external potential $v(\mathbf{r})$. If there is another wave function $\Phi^{'}$ with a arbitrary variation from Φ and its electron density is $\rho^{'}$, then we can obtain,

$$\langle \Phi^{'} | \hat{H} | \Phi^{'} \rangle = \int \rho^{'}(\mathbf{r}) v(\mathbf{r}) + F_{\mathrm{HK}}[\rho^{'}] = E[\rho^{'}] \geq E[\rho] \quad . \tag{2.81}$$

So the energy will reach the minimum only when the electron density is the ground-state electron density.

2.5.3 The Kohn-Sham Equations

From the Hohenberg-Kohn theorem, we can get the ground-state energy by minimizing the energy functional,

$$E[\rho] = \int \rho(\mathbf{r}) v(\mathbf{r})\, d\mathbf{r} + F_{\mathrm{HK}}(\rho(\mathbf{r})) \quad . \tag{2.82}$$

Although the Hohenberg-Kohn theorem provided a proof in principle that the total energy could be obtained from the ground state density it was not yet known how to obtain the $\rho(\mathbf{r})$ or $F_{\mathrm{HK}}(\rho(\mathbf{r}))$. In 1965, Kohn and Sham [74] published a paper which transformed density-functional theory into a practical electronic structure theory. Kohn and Sham recognized that the failure of Thomas-Fermi theory mainly resulted from the bad description of the kinetic energy. To address this problem they decided to re-introduce the idea of one electron orbitals and approximate the kinetic

energy of the system by the kinetic energy of non-interacting electrons. This lead to the central equation in Kohn-Sham DFT which is the one-electron Schrödinger-like equation expressed as:

$$(-\frac{1}{2}\nabla^2 + v(\mathbf{r}) + \int \frac{\rho(\mathbf{r}')}{|\mathbf{r}-\mathbf{r}'|}\, d\mathbf{r}' + v_{xc}(\mathbf{r}))\phi_i = \varepsilon\phi_i \quad . \tag{2.83}$$

Here ϕ are the Kohn-Sham orbitals and the electron density is expressed by,

$$\rho(\mathbf{r}) = \sum_i^N |\phi_i|^2 \quad . \tag{2.84}$$

The terms on the left side of Eq. (2.83) are the kinetic energy of the non-interacting reference system, the external potential, the Hartree potential, and exchange-correlation potential, respectively. The ε is the energy of the Kohn-Sham orbital. In addition, the exchange-correlation potential is given by,

$$v_{xc}(\mathbf{r}) = \frac{\delta E_{xc}[\rho]}{\delta\rho(\mathbf{r})} \tag{2.85}$$

and $E_{xc}[\rho]$ is the exchange-correlation functional which will be discussed in section 2.5.4. Furthermore, we can define an effective potential (v_{eff}) which is,

$$v_{eff} = v(\mathbf{r}) + \int \frac{\rho(\mathbf{r}')}{|\mathbf{r}-\mathbf{r}'|}\, d\mathbf{r}' + v_{xc}(\mathbf{r}) \quad . \tag{2.86}$$

This allows Eq. (2.83) to be rewritten in a more compact form,

$$(-\frac{1}{2}\nabla^2 + v_{eff})\phi_i = \varepsilon\phi_i \quad . \tag{2.87}$$

Clearly this is a Hartree-Fock like single particle equation which needs to be solved iteratively. Finally, the total energy can be determined from the resulting density through

$$E = \sum_i^N \varepsilon_i - \frac{1}{2}\iint \frac{\rho(\mathbf{r})\rho(\mathbf{r}')}{|\mathbf{r}-\mathbf{r}'|}\, d\mathbf{r}d\mathbf{r}' + E_{xc}[\rho] - \int v_{xc}(\mathbf{r})\rho(\mathbf{r})\, d\mathbf{r} \quad . \tag{2.88}$$

Equations (2.87), (2.84), and (2.85) are the celebrated Kohn-Sham equations. Note that the v_{eff} depends on $\rho(\mathbf{r})$ through Eq. (2.86). So the Kohn-Sham equation must be solved self-consistently. The general procedure is to begin with an initial guess of the electron density, construct the v_{eff} from Eq. (2.86), and then get the Kohn-Sham orbitals. Based on these orbitals, a new density is obtained from Eq. (2.84) and the process repeated until convergence is achieved. Finally, the total energy will be calculated from Eq. (2.88) with the final electron density. If each term in the Kohn-Sham energy functional was known, we would be able to obtain the exact ground state density and total energy. Unfortunately, there is one unknown term, the exchange-correlation (xc) functional (E_{xc}). E_{xc} includes the non-classical aspects of the electron-electron interaction along with the component of the kinetic energy of the real system different from the fictitious non-interacting system. Since E_{xc} is not known exactly, it is necessary to approximate it, which is the focus of the next section.

2.5.4 Exchange-Correlation Functionals

"*Density functional theory is in principle exact! But, in practice approximations have to be made.*"

W. Kohn
Oct. 14, 1997
Laboratoire de Chimie Theorique
Universite Pierre et Marie Curie
Paris, France

To use the Kohn-Sham equations we must know what the form of the exchange-correlation energy functional is. However, the exact form of E_{xc} is not known and may never be known (in some simple closed form). Thus since the birth of DFT some sort of approximations for E_{xc} have been used. By now there is an almost endless list of approximations with varying levels of complexity. Rather recently a useful way for categorizing the many and varied E_{xc} functionals that exist has been proposed by Perdew and is known as "Jacob's ladder" [8]. In this scheme functionals are grouped according to their complexity on rungs of a ladder which lead from the Hartree approximation on "earth" to the exact exchange-correlation functional in "heaven". We now very briefly discuss the first few rungs of this ladder as a means to introduce some of the most common types of exchange-correlation functionals in widespread use:

(a) The local-density approximation (LDA): This is simplest approximation, and can be written as

$$E^{xc-\mathrm{LDA}}[\rho(\mathbf{r})] = \int \rho(\mathbf{r})\varepsilon^{xc-\mathrm{unif}}(\rho(\mathbf{r}))\, d(\mathbf{r}) \quad , \tag{2.89}$$

where $\varepsilon^{xc-\mathrm{unif}}$ is the exchange-correlation energy per particle of the homogeneous electron gas of density $(\rho(\mathbf{r}))$, i.e. the exchange-correlation energy density is taken to be that of a uniform electron gas of the same density. The exchange energy is known exactly and the correlation energy is obtained by fitting to the many-body studies of Gell-Mann and Brueckner and Ceperly and Alder [75, 76]. Modern LDA functional tend to be exceedingly similar, differing only in how their correlation contributions have been fitted to the many-body free electron gas data. The Perdew-Zunger (PZ) [77], Perdew-Wang (PW) [78], and Vosko-Wilk-Nusair (VWN) [79] functionals are all common LDA functionals. Strictly, the LDA is valid only for slowly varying densities. Experience with calculations of atoms, molecules, and solids shows that Eq. (2.89) can in general also be applied to these systems. Indeed LDA works surprisingly well and much current understanding of metal or semiconductor (Si or GaAs) surfaces comes from LDA simulations. A partial rationalization of the success of LDA is provided by the observation that it satisfies a number of so-called sum rules [80, 81, 82, 83].

(b) The generalised gradient approximation (GGA): These are the second generation functionals (sitting on the second rung of Jacob's ladder) in which the gradient of the density, $\nabla\rho(\mathbf{r})$, at each coordinate is taken into account as well as the density itself:

$$E^{xc-\mathrm{GGA}}[\rho(\mathbf{r})] = \int \rho(\mathbf{r})\varepsilon^{xc-\mathrm{unif}}(\rho(\mathbf{r}))\nabla\rho(\mathbf{r})\, d(\mathbf{r}) \quad . \tag{2.90}$$

Thus GGAs are "semi-local" functionals, comprising corrections to the LDA while (again) ensuring consistency with known sum rules. For many properties, for example geometries and ground state energies of molecules, GGAs can yield better results than the LDAs. Although for the properties of metals and their surfaces, GGA results are not necessarily superior to LDA results. The most widely used GGAs in surface physics are the PW91 [84] functional, and its close relative PBE [85]. PBE actually has several off-spring[4]; revPBE [86], RPBE [5], PBE-WC [87], and PBEsol [88]. RPBE is the most popular of the off-spring, although the latest addition to the PBE family, PBE-WC and PBEsol, offers promise for the simulation of solids and their surfaces. Also the special designed functional, AM05 [89], dedicated to include the surface effect which has been shown a much improved performance for bulk properties, such as lattice constant and bulk modulous, and jellium surface energy than PBE and PW91 [90].

(c) The meta-GGAs: These are the third generation functionals (third rung of Jacob's ladder) and use the second derivative of the density, $\nabla^2\rho(\mathbf{r})$, and or kinetic energy densities, $\tau_\sigma(\rho(\mathbf{r})) = 1/2\sum_i|\nabla\phi_i|^2$, as additional degree of freedom. In gas phase studies of molecular properties meta-GGAs such as the TPSS [91] functional have been shown to offer improved performance over LDAs and GGAs. However, aside from some benchmark studies of bulk materials and jellium surfaces, these functionals have not yet been exploited to any great extend in the solid state.

(d) The hybrid functionals: These fourth generation functionals add "exact exchange" from Hartree-Fock theory to some conventional treatment of DFT exchange and correlation[5]. The most widely used, particularly in the quantum chemistry community, is the B3LYP [92, 93] functional which employs three parameters, a_{1-3}

[4]PBE and its off-spring differ only in how they treat electron exchange. The exchange component of GGA-PBE is

$$E_x^{\mathrm{PBE}}[\rho(\mathbf{r})] = \int \rho(\mathbf{r})\varepsilon^{xc-\mathrm{unif}}(\rho(\mathbf{r}))F_x^{\mathrm{PBE}}(\rho(\mathbf{r}),\nabla\rho(\mathbf{r}))\, d(\mathbf{r}) \quad ,$$

where F_x^{PBE} is an exchange enhancement factor given by

$$F_x^{\mathrm{PBE}}[\rho(\mathbf{r}),\nabla\rho(\mathbf{r})] = 1 + \kappa - \frac{\kappa}{1+\mu s^2/\kappa}$$

with the dimensionless reduced gradient, $s = |\nabla\rho(\mathbf{r})|/2n(3\pi^2\rho(\mathbf{r}))^{1/3}$. In the original PBE $\kappa = 0.804$. In revPBE $\kappa = 1.245$. In RPBE $F_x[\rho(\mathbf{r}),\nabla\rho(\mathbf{r})] = 1 + \kappa - \kappa exp(-\mu s^2/\kappa)$, and in PBE-WC μs^2 takes a more complex form.

[5]The philosophy behind the hybrid functional is simple and rooted in the adiabatic connection formula, which is a rigorous *ab initio* formula for the exchange-correlation energy of DFT. One

(determined through fitting to experiment) to control the mixing of the HF exchange and density functional exchange and correlation. It takes the following form:

$$E^{xc} = E^{x-\mathrm{LDA}} + a_1(E^{x-\mathrm{HF}} - E^{x-\mathrm{LDA}}) + a_2\Delta E^{x-\mathrm{GGA}} + a_3\Delta E^{c-\mathrm{GGA}} \quad . \tag{2.91}$$

Reformulating this to eliminate two parameters leads to an equation of the form

$$E^{xc} = E^{xc-\mathrm{GGA}} + a(E^{x-\mathrm{HF}} - E^{x-\mathrm{GGA}}) \quad , \tag{2.92}$$

and setting $a = \frac{1}{4}$ (based on the grounds of perturbation theory [94]) leads to a class of functionals with only as many parameters as their underlying GGAs. If PBE is the GGA used in Eq. (2.92) we arrive at the hybrid PBE0 functional [95]. Another popular hybrid functional worth mentioning here is BH&HLYP [96], which has 50% Hartree-Fock exchange. Such functionals have been shown to offer noticeably improved performance over LDA and GGA functionals for the calculation of gas phase properties of molecules and band gaps in solids.

Beyond these few rungs of Jacob's ladder, there are other E_{xc} functionals of increasing complexity. However, adding complexity by climbing higher on Jacob's ladder or by obeying more and more constraints [97] does not necessarily bring improved performance in total energies.

2.6 Plane-Waves and Pseudopotentials

As with the wave function based methods, when it comes to the practical application of DFT issues such as basis sets need to be considered. In calculations of solids or condensed matter, which will be the main types of systems that DFT is applied to in this thesis, plane-wave basis set is a very common choice. In many cases, combined with plane-wave is the pseudopotential approach for treating the strong interactions between core electron and nuclei. We will now briefly discuss plane-waves and then pseudopotentials.

2.6.1 Plane-Wave Basis Sets

When dealing with a crystal which has atoms periodically arranged, the electrons are in a periodic potential $U(\mathbf{r})$ where $U(\mathbf{r}+\mathbf{R}) = U(\mathbf{r})$ and $\mathbf{R}$ is the Bravais lattice

conventional expression of this formula is:

$$E^{xc} = \int_0^1 U_{xc}^{\lambda}\, d(\lambda) \quad ,$$

where λ is an interelectronic coupling strength parameter that switches on the $(1/r_{ij})$ Coulomb repulsion between electrons and U_{xc}^{λ} is the potential energy of exchange and correlation at λ. This formula connects the non-interacting reference system with the fully interacting one all at density $\rho(\mathbf{r})$. Recognizing that the non-interacting $\lambda = 0$ limit is nothing more than HF exchange, it is expected that exact exchange must play a role in "better" exchange-correlation functionals and thus DFT exchange and correlation functionals are mixed with a fractional of HF exchange.

vectors. Starting from Bloch's theorem [11], the eigenstates ϕ of the one-electron Hamiltonian $H = -\frac{1}{2}\nabla^2 + U(\mathbf{r})$ can be written as

$$\phi_{nk}(\mathbf{r}) = exp(i\mathbf{k}\cdot\mathbf{r})\mu_{nk}(\mathbf{r}) \quad , \tag{2.93}$$

where μ_{nk} is a function with the same periodicity as the potential ($U(\mathbf{r})$) that $\mu_{nk}(\mathbf{r}+\mathbf{R}) = \mu_{nk}(\mathbf{r})$. Furthermore, μ can be expanded as,

$$\mu_{i\mathbf{k}} = \frac{1}{\Omega_{cell}}\sum_m c_{i,m} exp(iG_m\cdot\mathbf{r}) \quad , \tag{2.94}$$

where G is the reciprocal lattice vector and $\Omega = N_{cell}\Omega_{cell}$. Here Ω is the whole volume.

We aim to solve the following Schrödinger-like equation and each electron moves in an effective potential $V_{eff}(\mathbf{r})$,

$$\hat{H}_{eff}\phi_i(\mathbf{r}) = \left[-\frac{1}{2}\nabla^2 + V_{eff}(\mathbf{r})\right]\phi_i(\mathbf{r}) = \varepsilon_i\phi_i(\mathbf{r}) \quad . \tag{2.95}$$

By the Bloch theorem in Eq. (2.93), the eigenfunctions can be written as

$$\phi_i(\mathbf{r}) = \sum_q c_{i,q}\frac{1}{\Omega}exp(i\mathbf{q}\cdot r) = \sum_q c_{i,q}\times|q\rangle \quad . \tag{2.96}$$

Here $c_{i,q}$ are the expansion coefficients and $q = \mathbf{k}+G$, in the basis of the orthonormal plane-wave $|q\rangle$ satisfying

$$\langle q^{'}|q\rangle = \frac{1}{\Omega}\int exp(i\mathbf{q}^{'}\cdot r)exp(i\mathbf{q}\cdot r) = \delta_{\mathbf{q}^{'}\cdot q} \quad . \tag{2.97}$$

Inserting Eq. (2.96) into Eq. (2.95) with the orthogonality of Eq. (2.97) and multiplying from the left by $\langle q^{'}|$, leads to the Schrödinger-like equation in Fourier space,

$$\langle q^{'}|\left[-\frac{1}{2}\nabla^2 + V_{eff}(\mathbf{r})\right]|q\rangle = \varepsilon_i\langle q^{'}|q\rangle c_{i,\mathbf{q}} = \varepsilon_i c_{i,\mathbf{q}} \quad . \tag{2.98}$$

Considering each term in the Hamiltonian. The first term, kinetic energy operator can be written as,

$$\langle q^{'}|-\frac{1}{2}\nabla^2|q\rangle = |q|^2\delta_{\mathbf{q}\cdot q'} \quad . \tag{2.99}$$

Second, for a crystal, the periodic potential $V_{eff}(\mathbf{r})$ can be expressed as a sum of Fourier components,

$$V_{eff}(\mathbf{r}) = \sum_m V_{eff}(G_m)exp(iG_m\cdot\mathbf{r}) \quad . \tag{2.100}$$

Together with Eq. (2.99) and Eq. (2.100), Eq. (2.95) can be rewritten as

$$H_{m,m'}(\mathbf{k})c_{i,m'}(\mathbf{k}) = \varepsilon_i(\mathbf{k})c_{i,m'}(\mathbf{k}), \tag{2.101}$$

where

$$H_{m,m'} = \langle\mathbf{k}+G_m|\hat{H}_{eff}|\mathbf{k}+G_m^{'}\rangle = |\mathbf{k}+G_m|^2 + V_{eff}(G_m - G_m^{'}). \tag{2.102}$$

Here q has been expanded as $\mathbf{k}+G$. Eq. (2.101) and Eq. (2.102) are the basic Schrödinger-like equations of a periodic crystal with a plane-wave basis set.

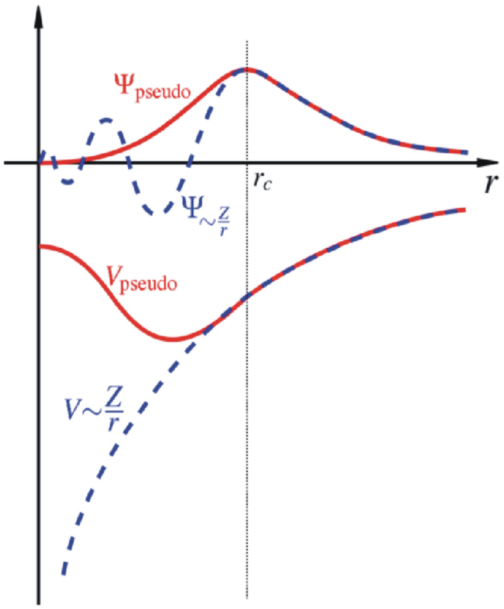

Figure 2.2: Schematic illustration of all-electron (dashed lines) and pseudopotential (solid lines) and their corresponding wave functions. The radius at which the all-electron and pseudo-electron values match is designated as r_c.

2.6.2 Pseudopotentials

It is well established that most physically interesting properties of solids are determined by the valence electrons rather than the core electrons. Meanwhile, the deeply bound core electrons within plane-wave basis sets, require a huge amount of basis functions for their description. Thus this leads to a contradiction that the less important core electrons will consume a lot of computational cost. To alleviate this problem, the pseudopotential approximation replaces the strong ionic potential with a weaker pseudopotential.

In general, there are two main purposes of the pseudopotential formalism. First, to use a much weaker pseudopotential to replace core electrons which due to their deep potential need to be described by many plane-wave basis functions. Second, to eliminate the rapid oscillations of the valence electron wave function in the core region. These issues are shown in Figure 2.2. From Figure 2.2, we can see the pseudopoential is much weaker than the all-electron one and pseudo wave function has no radial node inside the core region. It is essential within the pseudopotential scheme that outside the core region, the pseudo potential and wave function becomes the same with the corresponding all electron ones (Figure 2.2).

The most common general form of a pseudopotential is,

$$V_{ps} = \sum_{lm} |Y_{lm}\rangle V_l(r) \langle Y_{lm}| \tag{2.103}$$

where Y_{lm} are the spherical harmonics. One important class of pseudopotentials are so called norm-conserving pseudopotential. Norm conserving pseudopotentials

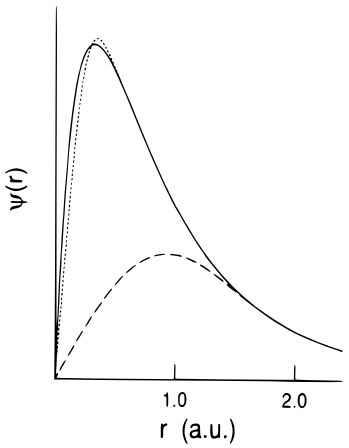

Figure 2.3: Oxygen $2p$ radial wave function (solid line) and corresponding pseudo wave function by using the norm-conserving HSC [98] (dotted line) and Vanderbilt ultrasoft methods [99] (dashed line). The figure was taken from [99].

require that the all-electron and pseudo wave function agree beyond a chosen radius (r_c) and the integrated density inside r_c for the all electron wave function and pseudo wave function are the same ("norm conservation"). There are many types of norm-conserving pseudopotentials from different authors such as Troullier and Martins [100], Kerker [101], Hamann, Schlüter, and Chiang [98], and Vanderbilt [102].

One issue with the norm-conserving pseudopotentials is that they can not generate smoother pseudo wave function than the all electron one when coming to the first row elements like O and the localized transition metals like Ni due to the "norm conservation" rule.

This situation can be seen in Figure 2.3 for the oxygen $2p$ orbital. There is hardly any improvement for the norm-conserving pseudopotential over the all-electron counterpart. To circumvent this difficulty, Vanderbilt [99] made a radical modification to break the norm conservation rule and relax the condition that the psudo wave function inside the core region must have the same density as the all-electron wave function. By this way, the pseudo wave function can be made much softer than the all-electron wave function (Figure 2.3). The full density will be added back before the normalization of the wave function. This kind of pseudopotential is called an ultrasoft pseudopotential, which enables much lower plane-wave cut-offs to be used in the calculations.

The combination of DFT, plane-wave basis set, and pseudopotentials has became a well-established methodology in electronic structure calculations of condensed matter [103, 104]. Usually such simulations are performed in periodic supercells to represent the physical system under consideration. Applying this methodology to the calculation of nonperiodic systems such as a defect in a crystal or a crystal surface is also possible but requires particular attention. To compute such systems a suitable periodic representation must be artificially constructed. An example of

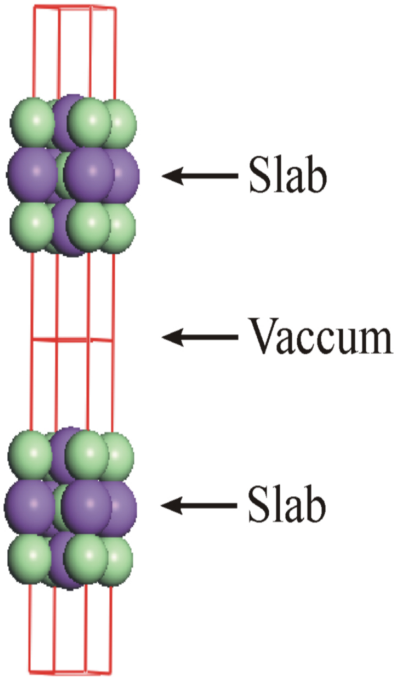

Figure 2.4: Schematic illustration of a supercell model of NaCl(001): the surface is represented by a 3 layers slab separated by vacuum. The supercell is repeated in all 3 dimensions, only 2 individual supercells are shown here.

a unit cell appropriate for the calculation of solid surface is shown in Figure 2.4 in which the surface is modelled as a slab of material separated by a region of vacuum.

Chapter 3

Bulk NaCl and NaCl(001)

3.1 Introduction

Common salt, NaCl, plays a key role in environmental chemistry, biology, and several other scientific disciplines, as well as being a material of obvious importance to many aspects of daily life. Since all bodies interact with their surroundings through their surfaces, it is necessary to explore the structure and properties of NaCl surfaces if an understanding of the role salt and salt particles play in the above disciplines is to be arrived at. On the basis that one must first understand the properties of bulk and clean surfaces before one can understand their interaction with atoms and molecules, the current chapter focuses exclusively on bulk NaCl and NaCl surfaces.

It is known, for example, from the cubic equilibrium shape of NaCl crystals, that the low energy surface of NaCl is the electrically neutral and stoichiometric (001) surface. It is understood that the Na and Cl atoms at such surfaces will undergo only small relaxations from their bulk truncated positions which has been observed in the experiments [105, 106]. However, quantitative insight into the properties of NaCl surfaces is to a large extent lacking. This is mainly because many of the popular surface science probes, which have been so successfully exploited to probe the surfaces of metals, such as scanning tunneling microscopy (STM), LEED, and photoelectron spectroscopies, can not easily be applied in a non-destructive manner to the surfaces of wide band-gap ionic materials, such as NaCl. The conventional application of these electron-based probes to insulators can lead to surface charging, electron-stimulated dissociation of the alkali halides, and alkali enrichment of the selvedge, all of which hampers characterization of the surface [107].

From experiment there are two main approaches to remedy or at least mitigate the destructive nature of the electron-based probes at insulating surfaces. One is to use a probe with a low electron current. With LEED, for example, this means the deployment of systems operating with very low primary currents in the pA or low nA range. The second approach is to investigate the properties of thin (nanometer) films of insulators supported on metallic substrates, rather than attempting to investigate pure single crystals of the ionic materials themselves. For NaCl(001) both techniques have been applied, leading to two independent LEED I-V structure determinations [105, 106] that provides valuable data with which to benchmark the

accuracy of our computational approach. Nonetheless our general understanding of salt surfaces falls far behind that of metal and semiconductor surfaces, with important issues such as the surface energy of NaCl(001) remaining unclear. Indeed this absence of insight into clean NaCl(001) persists despite several recent theoretical studies of atomic and molecular adsorption on NaCl(001) [22, 23, 108].

In this chapter, the computational details are elaborated in section 3.2. In section 3.3, bulk NaCl is discussed and in section 3.4 our calculations of flat NaCl(001) are presented. In section 3.5, the information from the electronic structure will be analyzed. Finally, we sum up all results and reach a conclusion.

3.2 Computational Details

All calculations in this chapter have been performed with DFT within the plane-wave pseudopotential approach [103, 104] as implemented in the CASTEP code [109]. Most properties reported here have been computed with the LDA [77] and the GGA PBE [85] exchange-correlation functionals. In addition, the modified PBE functional of Wu and Cohen (WC) [87] has been used for a number of bulk and surface calculations. This functional differs from PBE only in the functional form of the so-called exchange enhancement factor, in the same spirit as the revPBE [86] and RPBE [5] functionals. PBE-WC, as we refer to it here, has been designed to give the exchange hole a more diffuse radial cut-off than the original PBE has, which is believed to be more appropriate for the calculation of solids and their surfaces [87, 97]. Indeed PBE-WC lives up to this design feature by showing better performance for various properties of solids such as lattice constants, bulk moduli, and the surface energy of jellium [87].

In the current work the electron-ion interactions are described with Vanderbilt ultra-soft pseudopotentials [99] expanded up to a plane-wave cut-off energy of 400 eV. LDA pseudopotentials have been used for all LDA calculations and likewise GGA (PBE) pseudopotentials have been used for all GGA (PBE and PBE-WC) calculations. Further, we note that the well-known problem of nonlinear core-valence electron exchange and correlation for Na [110] has been eliminated in the present study by treating the Na $2s$ and $2p$ electrons as valence electrons.

The thicknesses of the NaCl slabs examined ranged from 2—12 layers and a variety of periodic supercells were used to model the different surface systems considered. For the flat NaCl(001) surface a 1×1 unit cell was employed as is observed in experiment [106]. In each case a Monkhorst-Pack [111] $\boldsymbol{k}$ point mesh with the equivalent of at least a 4×4 sampling within the 1×1 surface unit cell was used, and the vacuum region between slabs in adjacent cells was in excess of 11 Å. We note that in addition to the tests of the computational set-up discussed in the next section for bulk NaCl, careful tests on the dependence of our computed surface energies with regard to plane-wave cut-off and $\boldsymbol{k}$ sampling were performed. These tests, which are reported in **Appendix A**, reveal that our chosen cut-off energy (400 eV) and $\boldsymbol{k}$ point mesh (4×4 sampling within the 1×1 surface unit cell) yield surface energies and ledge energies converged to within 0.2 meV/Å^2 and 0.5 meV/Å, respectively,

of those obtained with a much higher cut-off (1200 eV) and much denser $\boldsymbol{k}$ point mesh (16×16 sampling within the 1×1 surface unit cell).

3.3 Bulk NaCl

The properties of bulk NaCl were examined, in particular the equilibrium lattice constant, bulk modulus, and various expressions for the energy of bulk NaCl were computed and compared to experiment and previous theory[112, 113, 114, 115, 116, 117]. This data, which we now discuss, is given in Table 3.1.

Our computed lattice constants with the LDA, PBE, and PBE-WC functionals are 5.46, 5.70, and 5.62 Å, respectively, and the computed bulk moduli are 32, 23, and 25 GPa. Compared to experiment, PBE overestimates the lattice constant and bulk modulus, whereas LDA underestimates the lattice constant and bulk modulus. This is consistent with what is generally known about the performance of these functionals for solids and, for the specific case of NaCl, consistent with previous LDA and PBE calculations. In particular, our values agree well with recent full-potential linearized-augmented plane-wave (FP-LAPW) [113] and projector augmented wave plus plane-wave (PAW-PW) [114] studies, as can be seen from Table 3.1. As expected, the PBE-WC functional shows improvements over both LDA and PBE, yielding a lattice constant (5.62 Å) and a bulk modulus (25 GPa) which are closer to experimental results than the two other functionals, also in agreement with the original PBE-WC paper [87].

The energetic stability of ionic crystals is typically reported in a variety of different manners, such as the formation energy, the cohesive energy, and the lattice energy. We have computed each of these quantities with the LDA, PBE and PBE-WC functionals and now discuss each in turn. The formation energy (E_f) of bulk NaCl at zero Kelvin (neglecting contributions from zero point vibrations) is defined as

$$E_f = E_{\mathrm{NaCl(s)}} - E_{\mathrm{Na(s)}} - \frac{1}{2}E_{\mathrm{Cl_2(g)}} \tag{3.1}$$

where $E_{\mathrm{NaCl(s)}}, E_{\mathrm{Na(s)}}$, and $E_{\mathrm{Cl_2(g)}}$ refer to the total energies of bulk NaCl, bulk Na, and gas phase Cl_2 molecules, respectively. Our computed formation energies with the LDA, PBE, and PBE-WC functionals are -3.89, -3.63, and -3.65 eV, respectively. The corresponding experimental value is -4.26 eV. Thus all functionals employed here predict too small a value of the formation energy. This underestimation is consistent with the only other GGA-PBE report of the formation energy of NaCl which gave -3.67 eV [114]. We have tried to identify the source of the error in the DFT formation energies. It does not appear to come from the Na bulk reference state since the cohesive energy of bulk Na is rather accurately computed with all three functionals: 1.25, 1.08, and 1.10 eV within the current computational set-up for the LDA, PBE, and PBE-WC functionals compared to the experimental value of 1.11 eV. A more likely source for the too low E_f is an error in the Cl_2 molecule, the bond strength of which is overestimated by all three functionals: 3.69, 2.91, and 3.13 eV for the LDA, PBE, and PBE-WC functionals compared to an experimental value of 2.52 eV. However, we caution that this is only part of the story and that

errors most certainly exist in the NaCl bulk total energies too, since the Cl_2 bond strengths alone do not provide a quantitative account of the computed E_f for all three functionals.

Table 3.1: Calculated and measured values for the equilibrium lattice constant (a_0), the bulk modulus (B_0), the formation energy (E_f), the cohesive energy (E^{coh}), and the lattice energy (LE) of NaCl. The computed values reported here that come closest to the experimental values for each of the above quantities are indicated in bold.

Note	Functional	a_0 (Å)	B_0 (GPa)	E_f (eV)	E^{coh} (eV)	LE (eV)
This work	LDA	5.48	32.0	**-3.89**	**6.96**	**8.39**
	PBE	5.70	23.2	-3.63	6.16	7.59
	PBE-WC	**5.62**	**24.7**	-3.65	**6.28**	7.91
			Previous DFT calculations			
AE-GTO[a]	LDA	5.48	35.2			8.52
AE-GTO[a]	PW91	5.75	22.9			7.65
FP-LAPW[b]	LDA	5.46	32.2			
FP-LAPW[b]	PBE	5.69	25.1			
PAW-PW[c]	PBE	5.70	23.4	-3.68	6.17	
PP-PW[d]	PBE-WC	5.62	25.4			
			Experiment			
		5.63[e]	26.6[f]	-4.26[g]	6.62[g]	8.20[e]

[a] All electron, full potential, Gaussian-type orbital (Ref. [112]).
[b] All electron, full potential, LAPW (Ref. [113]).
[c] All electron, frozen core PAW, plane wave (Ref. [114]).
[d] Pseudopotential, plane wave (Ref. [87]).
[e] Ref. [116].
[f] Ref. [115].
[g] Ref. [117].

The cohesive energy (E^{coh}) and lattice energy (LE) of NaCl at zero Kelvin (without corrections for zero point motion) are defined as follows:

$$E^{\text{coh}} = E_{\text{Na(atom)}} + E_{\text{Cl(atom)}} - E_{\text{NaCl(s)}} \tag{3.2a}$$

$$LE = E_{\text{NaCl(s)}} - E_{\text{Na}^+\text{(ion)}} - E_{\text{Cl}^-\text{(ion)}} \tag{3.2b}$$

where $E_{\text{Na(atom)}}$, $E_{\text{Cl(atom)}}$, $E_{\text{Na}^+\text{(ion)}}$, and $E_{\text{Cl}^-\text{(ion)}}$ refer to the total energy of isolated Na and Cl atoms and ions, respectively. The two quantities differ in how the isolated Na and Cl species are defined: for E^{coh} it is one comprised of Na and Cl atoms, whereas for LE it is one comprised of charged ions. From Table 3.1 it can be seen that all functionals do a reasonable job at predicting E^{coh}, coming within 0.5 eV (7%) of the experimental value (6.62 eV). Specifically the computed values are 6.96, 6.16, and 6.28 eV for LDA, PBE, and PBE-WC, respectively. Again, where comparison with previous DFT calculations is possible, our computed (PBE) value is very close (0.01 eV away) to the previous PAW-PW report [114].

For the calculation of the lattice energy similar quality results are obtained with the computed values of LE being 8.39, 7.59, and 7.91 eV with the LDA, PBE, and

PBE-WC functionals, respectively, compared to the experimental value of 8.20 eV. We note, however, that for the calculation of the charged (Na^+ and Cl^-) ions in our periodic supercell it was necessary to apply the correction of Makov and Payne [118] to obtain reliable ionization energies and electron affinities for Na and Cl. Our computed values for LE with the LDA (8.39 eV) and PBE (7.59 eV) functionals are close to the values of 8.52 and 7.65 eV reported before for the LDA and PW91 [119] functionals in a periodic DFT study of alkali halides with basis sets comprised of Gaussian-type orbitals [112].

In conclusion, we have established the accuracy of the current computational set-up, and made comparisons to experiment and previous theory when possible. As reported before, PBE-WC improves over PBE (and LDA) for the calculation of the lattice constant and bulk modulus of NaCl. However, when it comes to the calculation of the energetics of bulk NaCl it is difficult to see too much improvement with PBE-WC.

3.4 NaCl(001)

3.4.1 Structure of NaCl(001)

The NaCl(001) surface was examined with the LDA, PBE, and PBE-WC functionals. In Table 3.2, our computed DFT values for some key structural parameters of NaCl(001), obtained from calculations with 12 layer thick slabs, are reported. In particular the interlayer spacing and interlayer buckling of the Na and Cl atoms of the top three layers are given along with the experimental values determined from the two LEED I-V studies [105, 106]. It is encouraging that all three DFT functionals agree well with each other. Specifically a contraction of the interlayer distance between the first and second layer (Δ_{12}) of about 0.5% is predicted by all three functionals and a small buckling in the height of the Na and Cl atoms in the top layer of 0.07 to 0.11 Å is obtained.

Table 3.2: The relaxation of the interlayer distance (Δ) as a percentage of the lattice constant and interlayer buckling ($\Delta_{i(\mathrm{Cl-Na})}$) in Angstrom as obtained from DFT calculations with 12 layer NaCl slabs and from LEED I-V analyses. The subscripts designate the various NaCl layers with 1, 2, and 3 being the top layer, the first subsurface, and second subsurface layers, respectively.

	Δ_{12}(%)	Δ_{23}(%)	$\Delta_{1(\mathrm{Cl-Na})}$ (Å)	$\Delta_{2(\mathrm{Cl-Na})}$ (Å)	$\Delta_{3(\mathrm{Cl-Na})}$ (Å)
LDA	-0.55	0.07	0.072	-0.009	0.000
PBE	-0.60	0.02	0.110	-0.030	0.000
PBE-WC	-0.46	0.01	0.107	-0.035	0.000
NaCl(001)[a]	-1.43	0.10	0.14±0.003	-0.02±0.004	0.00±0.003
NaCl/Pd(100)[b]	-3.19	0.35	0.12±0.03	0.003±0.03	
NaCl/Pt(111)[b]	-2.84	0.35	0.12±0.04	0.01±0.04	

[a] Ref. [106].
[b] Ref. [105].

We note that a positive value for the buckling implies that the Cl atoms have relaxed outwards (towards the vacuum) relative to the Na atoms. The trends in the buckling and relaxations predicted here agree with the LEED analysis, although our predicted first to second layer relaxation at 0.5% is smaller than that obtained from LEED (1.4% from the single crystal study [106] and ∼3% from the experiments on the thin metal-supported NaCl films [105]). Aside from the relaxation and buckling of the top layer atoms, the atoms in other layers remain almost exactly at their bulk truncated positions.

Specifically, the interlayer spacing between the 2nd and 3rd layers (Δ_{23}) differs from the bulk value by ≤0.06% in our calculations and 0.11% in experiment [106], and the buckling of the Na and Cl atoms in the second layer ($\Delta_{2(\text{Cl-Na})}$) is reduced to -0.01 to -0.04 Å in our calculations and -0.02 Å in experiment [106]. By the time the third layer is reached both DFT and LEED agree that the bulk, non-buckled, limit has been reached.

3.4.2 Surface Energy of NaCl(001)

The surface energy is a basic thermodynamic quantity of a surface, of crucial importance to the equilibrium shape of crystals. However, it is an incredibly difficult quantity to determine experimentally [128, 129], and, indeed, most experimental surface energy measurements of NaCl (and other materials) go back to the 1960's and 1970's [120, 121, 122, 123, 124, 125, 126, 127]. For NaCl this has led to a large range of 11 to 24 meV/Å^2 for the surface energy of NaCl(001). We illustrate this with the plot in Figure 3.1 and aim here to make a contribution from first principles theory towards narrowing this range somewhat. The surface energy is defined as,

$$\gamma = (E_{\text{slab}} - NE_{\text{bulk}})/A \tag{3.3}$$

where E_{slab} is the total energy of the NaCl slab and E_{bulk} is the total energy of a NaCl formula unit in bulk NaCl. The number of NaCl formula units in the slab is N and A is the surface area of the slab. For all three exchange-correlation functionals, slabs of 2 to 12 layers thickness were examined, leading to the computed values of γ displayed in Figure 3.1. Two features of Figure 3.1 are apparent. First, γ is extremely insensitive to the number of layers used in the calculation. The computed values of γ with the 2 layer slabs differ from those computed with the 12 layer slabs, by <0.5 meV/Å^2 for all three functionals. Second, the choice of exchange-correlation functional has a noticeable and significant impact upon γ; with γ being ∼14.6, ∼9.0, and ∼9.4 meV/Å^2 with the LDA, PBE, and PBE-WC functionals, respectively.

In the absence of reliable experimental measurements of the surface energy of NaCl(001) it is difficult to say which functional yields the most reliable value of γ. However, we can make a qualitative judgement by drawing upon experience from other materials. When comparison to experiment is possible, as it most often is for metals, it is typically found that the PBE values are smaller than the experimental ones, with LDA being the closer of the two [1] [130, 131]. In addition the recent DFT and diffusion quantum Monte Carlo (DMC) [132] study for the surface energy

[1] This apparently superior performance of LDA compared to that of PBE for the surface energy

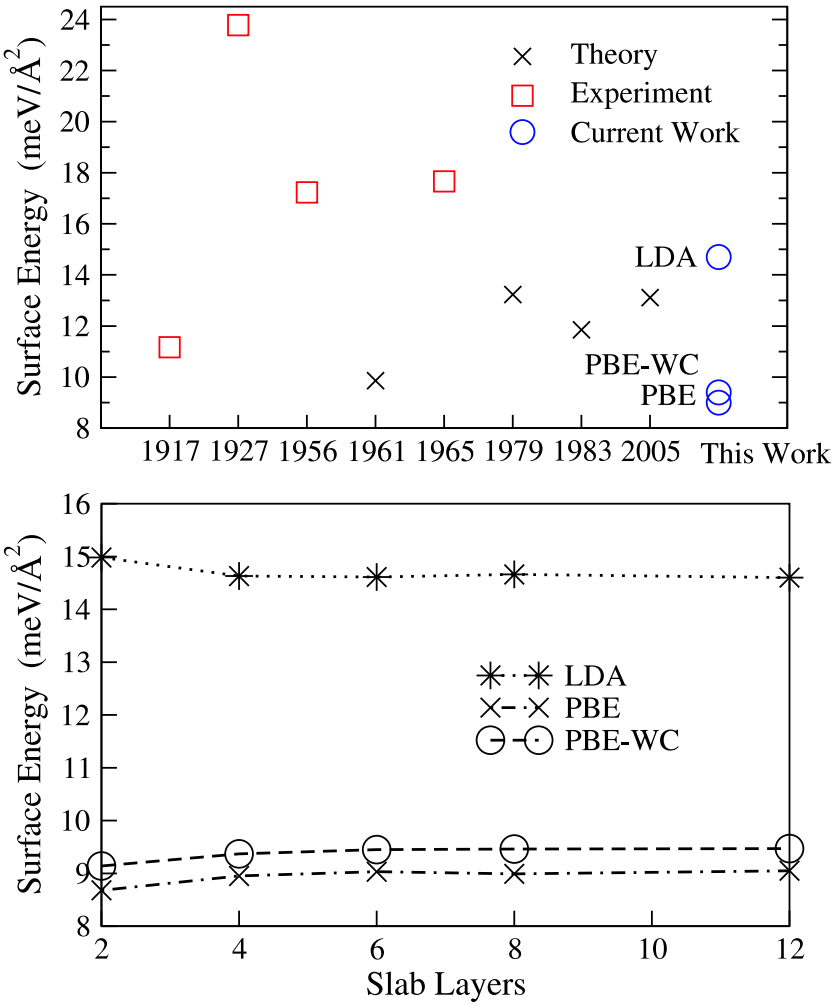

Figure 3.1: (a) Measured and computed values of the surface energy of NaCl(001) since 1917, along with the LDA, PBE, and PBE-WC values determined here. The references corresponding to the previously reported values are given in Ref.s [120, 121, 122, 123, 124, 125, 126, 127]. (b) The dependence of the computed surface energy of NaCl(001) on the number of NaCl layers and exchange-correlation functional used.

of MgO(001) finds that the LDA value is again about 30% larger than the PBE value and, moreover, that the LDA value is considerably closer to the, in principle, more reliable DMC result. Finally, we note that the surface energy of NaCl(001) predicted from the PBE-WC functional is about 4 meV/Å^2 larger than the one obtained with PBE. Thus for the surface energy of NaCl(001), PBE-WC does not appear to offer any significantly improved performance over PBE. Overall in the absence of a well-defined experimental value or calculation results superior to those provided by DFT here it seems reasonable to suggest that the best estimate of the surface energy of NaCl(001) is the one proposed here of 9.0–15.0 meV/Å^2.

3.5 Electronic Structure Analysis

Before ending we briefly address some aspects of the electronic structure of the NaCl surfaces examined here. In particular, we discuss how the electronic structures of the atoms at the clean and stepped surfaces differ from the atoms in bulk NaCl.

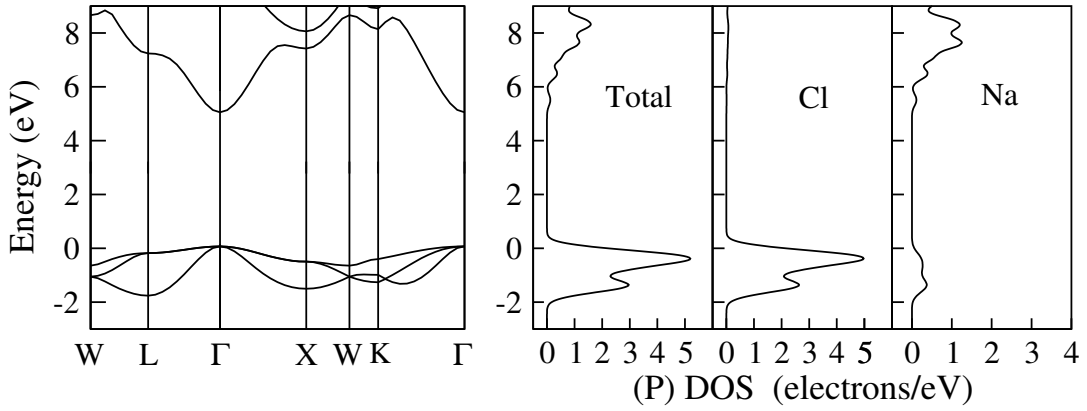

Figure 3.2: (a) Band structure of bulk NaCl, as obtained from a DFT-PBE calculation. (b) Total density of states (DOS) and partial densities of states (PDOS), partial onto Cl and Na atoms in bulk NaCl. Only the energy interval around the top of the valence band and bottom of the conduction band is shown. A smearing of 0.2 eV has been applied to all DOS and PDOS. The energy zero is the top of the valence band.

The band structure, density of states (DOS), and partial density of states (PDOS) for bulk NaCl, as obtained with the PBE functional, are plotted in Figure 3.2. NaCl is an insulator with a wide band gap. The computed PBE (direct) Kohn-Sham band gap within the current computational set-up is 5.0 eV. As expected with such a semi-local GGA functional this is significantly smaller than the experimental optical value of 8.5 eV [133]. The computed width of the valence band is, however, at 1.6 eV in better agreement with the experimental value of 1.8 eV [134]. The NaCl valence

of metals has been rationalized by recalling that due to a favorable cancellation of errors LDA outperforms PBE for the calculation of the surface energy of jellium too [97]. Of course, jellium is not a good model for NaCl, but nonetheless the relative magnitude of the LDA and PBE surface energies computed here is similar to what is seen for jellium.

band is essentially comprised of Cl $3p$ states, as can be seen from the PDOS plot in Figure 3.2(b). From the PDOS plot it can further be seen that the bottom of the conduction band is predicted to be of Na ($3s$) character. This is the conventional interpretation of the NaCl conduction band. However, there has been some discussion, which is indeed born out by closer inspection of the individual Kohn-Sham orbitals of the bulk NaCl electronic structure, that the Cl $4s$ contribution to the bottom of the valence band is not insignificant [135, 136, 137].

Moving to the surface, we plot the surface band structure and layer resolved PDOS in Figure 3.3, both of which were obtained from a 12 layer NaCl slab calculation. The computed valence band width (1.6 eV) and band gap (5.0 eV) are essentially identical to the values computed for bulk NaCl. Further, as predicted long ago by Levine and Mark [138], we find that the NaCl surface does not exhibit any surface states. Indeed, as could be partly anticipated from the small relaxation and buckling at the surface, we do not see any major changes in the electronic structure upon moving from the bulk of NaCl to the (001) surface.

By looking closely at the layer resolved PDOS (Figure 3.3(b)), a pronounced

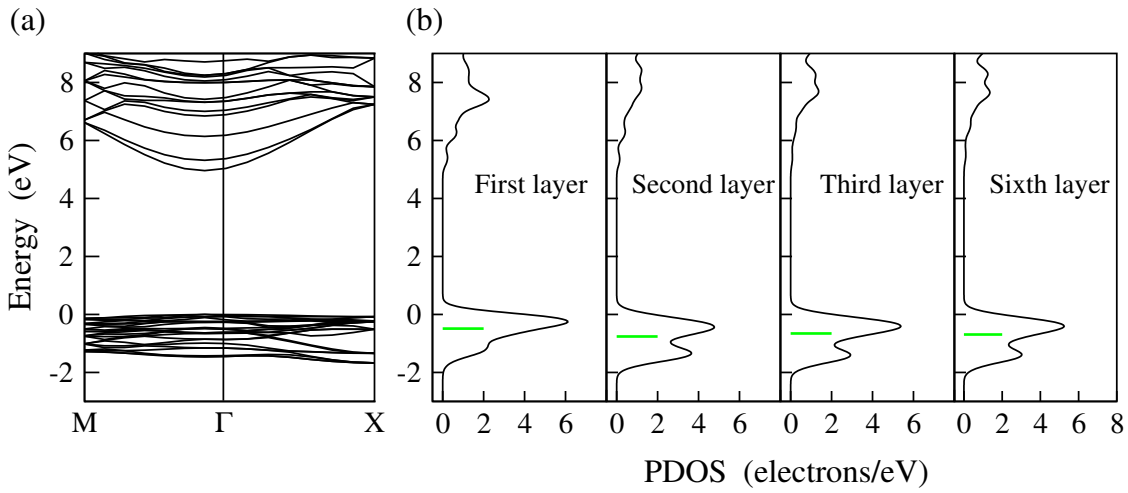

Figure 3.3: (a) Band structure of a 12 layer NaCl(001) slab, as obtained from a DFT-PBE calculation. (b) The layer resolved density of states of the first three layers and the sixth layer of a 12 layer NaCl(001) slab. The horizontal (green) line indicates the center of the valence band in each case. The energy zero is the top of the valence band.

but still small effect is visible. Specifically we see that as we move from the interior of the slab to the surface, the valence band narrows and its centre of gravity moves closer to the valence band maximum: compare the PDOS for layers six, three, two, and one in Figure 3.3(b). It is clear from Figure 3.3(b) however that, as with the structural relaxations at the NaCl(001) surface, the bulk properties are recovered almost immediately with the second layer DOS already very close to that of the bulk. A similar effect is also seen through the Cl PDOS plots displayed in Figure 3.4. Here the PDOS associated with a Cl atom in bulk NaCl, at the surface of NaCl(001), and at a step on NaCl(001) are displayed. Again one can see that the Cl

$3p$ valence band center moves closer to the valence band maximum as one goes from a Cl atom in bulk to one at a step. Correlated with these changes in the PDOS is an increase in the computed Mulliken charge of the Na and Cl atoms upon moving from the bulk to the surface, to the steps, as can be seen from Table 3.3

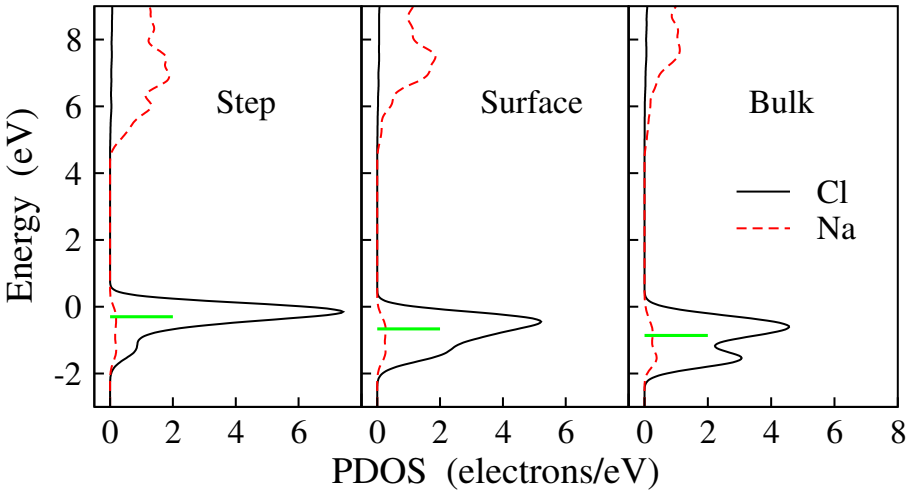

Figure 3.4: Partial density of states (PDOS) of a single Cl atom (solid line) and a single Na atom (dashed line) positioned at the step, the surface, and the interior (bulk) of a stepped NaCl(001) slab, as obtained from a DFT-PBE calculation. Only the top of the valence band (Cl $3p$) and the bottom of the conduction band are displayed. The horizontal (green) line indicates the position of the center of the valence band in each case. The energy zero is the top of the valence band.

3.6 Summary

To recap, bulk NaCl and flat NaCl(001) have been examined with density-functional theory. The properties of bulk NaCl have been computed with the LDA, PBE, and PBE-WC exchange-correlation functionals. Our results agree with previous theoretical studies and the new PBE-WC functional offers improved performance over both LDA and PBE in the description of key bulk properties such as the equilibrium lattice constant and bulk modulus. However, when it comes to the calculation of energetic properties of bulk NaCl such as the formation energy, cohesive energy, and lattice energy, it is difficult to see too much improvement with PBE-WC compared to PBE.

For the structure of NaCl(001) we find only a small inward relaxation of ∼0.6% for the top layer and a considerably smaller relaxation for the second to third interlayer distances (∼0.06%). A small buckling between Cl and Na atoms in the top layer, ∼0.1 Å, is also predicted. All three exchange-correlation functionals agree on this behavior, which is largely in agreement with the LEED I-V analyses, although the absolute magnitude of the top layer relaxation is somewhat smaller than the values of 1.4% and ∼3% that come from LEED.

Table 3.3: The computed DFT-PBE Mulliken charges on Cl and Na atoms in bulk NaCl, at the (001) surface of NaCl, and at the stoichiometric (100)-like step

Charge (e)	Na	Cl
Bulk	0.54	-0.54
Surface	0.61	-0.59
Step	0.67	-0.62

The surface energy of NaCl(001) is estimated to be in the range 9 to 15 meV/Å^2, as obtained from the three exchange-correlation functionals. In light of the absence of reliable experimental surface energy measurements of NaCl(001) it is difficult to identify one functional as being clearly superior to the others. However, we have discussed how the surface energies obtained from the LDA and PBE functionals often straddle the true value with LDA likely to be the closer of the two. An improved estimate of the surface energy of NaCl(001) must await either new experiments or more potent calculations than those provided in the current work, both of which are now clearly needed.

Finally, the electronic structure of bulk NaCl and flat NaCl(001) has been briefly discussed. As with the atomic structure, the electron density in the surface region is not perturbed to any great extent by the presence of the surface. The main effect is a small narrowing and up-shift of the valence band DOS as one moves from the bulk, to the sub-surface region, to the flat surface.

Chapter 4

Monoatomic Steps on NaCl(001)

4.1 Introduction

The role played steps and kinks is fundamental for understanding the morphology of crystal surfaces as well as equilibrium surface structure (ECS) [139]. There is a long history of employing Wulff construction to study the ECS and the thermal evolution of ECS. [140]. Although there are plenty of work have been done for metal surfaces (Pb, Cu) [141, 142, 143, 144, 145, 146] or semiconductor surfaces (Si) [147, 148], quantitative information from either experiment or first principles theory for steps on NaCl is absent, and in particular the energetic cost to create steps on NaCl is not known. Also the interaction between neighboring steps, whether this is repulsive or attractive, remains unclear. Here we aim to make a start at remedying this situation by determining the formation energies of steps and relative stabilities between stoichiometric (100)-like and non-stoichiometric (111)-like steps.

The remainder of this chapter is structured as follows. The computation details are listed in section 4.2. The non-polar (100)-like and polar (111)-like steps are discussed in section 4.3 and section 4.4, respectively. Finally, we draw conclusions in section 4.5.

4.2 Computational Details

For the calculations in this chapter of monoatomic steps on NaCl(001) a single layer stripe of NaCl(001) was placed on top of a 4 layer NaCl(001) slab. The stoichiometric "(100)-like" steps were constructed from 3 atom wide overlayer stripes of NaCl(001) separated by 1–5 atom wide lower terraces of NaCl(001) (Figure 4.1). Likewise the polar "(111)-like" steps were constructed from NaCl(001) overlayer stripes whose "edges" were cut in such a manner to yield either purely Cl terminated or purely Na terminated steps (Figure 4.1). The other details of the computational setup are the same as those reported in chapter 3.

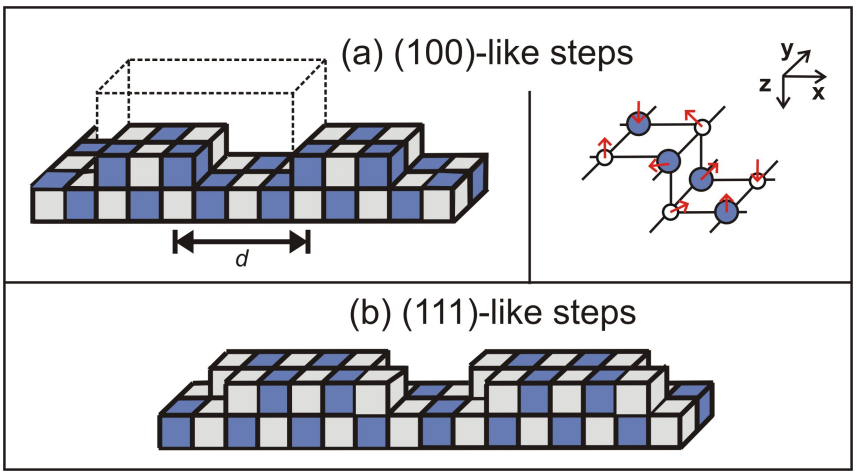

Figure 4.1: (a) Partial sketch of the model used in the calculation of neutral (100)-like steps on NaCl(001), comprising a "stripe" of NaCl atoms on top of the flat NaCl(001) surface. d is the lower terrace distance between adjacent steps, which is varied in separate calculations to extract the isolated step formation energies of (100)-like steps on NaCl(001). The dashed rectangular box represents the top half of one specific unit cell used in calculations of the value of d shown. On the right the direction of the computed displacements of the surface atoms in the vicinity of a step are indicated by the arrows. (b) A partial sketch of the model used in the calculation of the polar (111)-like steps on NaCl(001). The overlayer stripes are cut to yield either purely Cl terminated or purely Na terminated steps. Note that although only one layer of NaCl(001) is shown, four layer thick NaCl slabs were used in all step calculations. Dark (blue) cubes or circles represent Na atoms, whereas light (gray) cubes or circles represent Cl atoms.

4.3 Nonpolar (100)-like Steps

To begin we introduce a quantity, the ledge energy, which is defined as

$$E_{\text{ledge}} = (E_{\text{slab}} - NE_{\text{bulk}} - \gamma A)/2L \tag{4.1}$$

where E_{slab} is the total energy of the relaxed stepped surface, which contain N formula units of NaCl. As before, E_{bulk} is the bulk energy of a NaCl formula unit and γ is the computed NaCl(001) surface energy. The surface area of the slab is A, and L is the length of the step in the unit cell. One of the main goals of the current calculations on steps is to extract the formation energy of monoatomic height steps on NaCl(001). This quantity can be accessed once the step-step interaction is known and subtracted from the ledge energy. Steps can interact in several ways. The most studied interaction is the so-called elastic interaction which assume $1/d^2$ behavior where d is the distance between neighboring steps. The elastic interaction is due to the deformation fields around each steps. In addition , there are also entropic interaction, force dipole-dipole interaction, etc. between steps. Whether the combination of all these interactions leads to an attractive or repulsive interaction between steps depends very much on the system under consideration [149, 150]. Here we adopted this simplified $1/d^2$ relation to calculate the step formation energy, however our data fit well with this simple relation which will be discussed in the following. Thus by examining the dependence of the ledge energy on the width

of the terrace that separates neighboring steps, the isolated step formation energy (E_{step}) can be extracted with the aid of the following relation [139, 151, 152]:

$$E_{\text{ledge}} = E_{\text{step}} + B/d^2 \tag{4.2}$$

where B/d^2 represents the step-step interaction between neighboring steps and d is the lower terrace length, as shown in Figure 4.1.

To obtain the step energy of (100)-like steps, DFT PBE calculations with three different values of the lower terrace width d were performed. Specifically, calculations with d equal to 1, 2, and 3 Na-Cl-Na nearest neighbor distances were performed. With the DFT PBE Na-Cl-Na distance of 5.70 Å the width of the lower terrace thus ranges from 5.70 Å to 17.10 Å. The ledge energies obtained from these calculations are plotted in Figure 4.2 as a function of $1/d^2$, and from this a PBE step formation energy of ∼42 meV/Å for monoatomic (100)-like steps on NaCl(001) is determined.

An additional feature of the data displayed in Figure 4.2 is that the interaction between adjacent steps is quite weak since the slope of the fitted line is rather shallow. Indeed even for the system with the shortest intervening terrace between the steps, i.e., $d = 5.70$ Å, the ledge energy is within 5 meV/Å of the extrapolated value. For the systems with the two larger intervening terraces the step-step interaction across the lower terrace is essentially zero [1]. An implication of this is that for this system, although certainly not in general, E_{ledge} is an excellent approximation for E_{step}

The data fitted to Eq. (4.2) and used to extract E_{step} in Figure 4.2 were all obtained with a fixed upper terrace width of 1 Na-Cl-Na distance. A calculation of the ledge energy with a wider upper terrace, equal to 2 Na-Cl-Na distances, yields a value of E_{ledge} that differs from that obtained with the regular upper terrace by only 4 meV/Å. Such a small change demonstrates that E_{ledge} is also rather insensitive to the upper terrace width and indicates that our computed PBE step formation energy of 42 meV/Å is reasonably robust to changes in the surface model employed. For the exchange-correlation functional, however, it is a different story and as we saw with the surface energy the choice of exchange-correlation functional has a significant impact on the computed value. Specifically, the LDA ledge energy for a stepped surface with a lower terrace width of one Na-Cl-Na distance is 58 meV/Å, compared to the equivalent PBE result of 47 meV/Å. Thus, as with the surface energy, the LDA value exceeds the PBE one by 25% [2]. Again, in the absence of experimental measurements for the step formation energy on NaCl(001), we speculate that the real value of E_{step} is within the range provided by the PBE and LDA functionals (40–60 meV/Å).

Before moving to the (111)-like steps we briefly discuss the optimized structure

[1] The weak interaction between adjacent steps is further born out by analysis of the atomic and electronic structures of the relaxed (i.e., optimized) steps obtained from our calculations with the different sized terraces. Specifically, the relaxation of the atoms at the steps separated by the smallest intervening terrace (5.70 Å) differs from those with the largest terrace (17.10 Å) by 0.01 Å at most. Likewise the Mulliken charges and partial density of states of the atoms at the steps are essentially identical in the systems with the longer and shorter intervening terraces.

[2] The step formation energy calculated from LDA is ∼54 meV/Å.

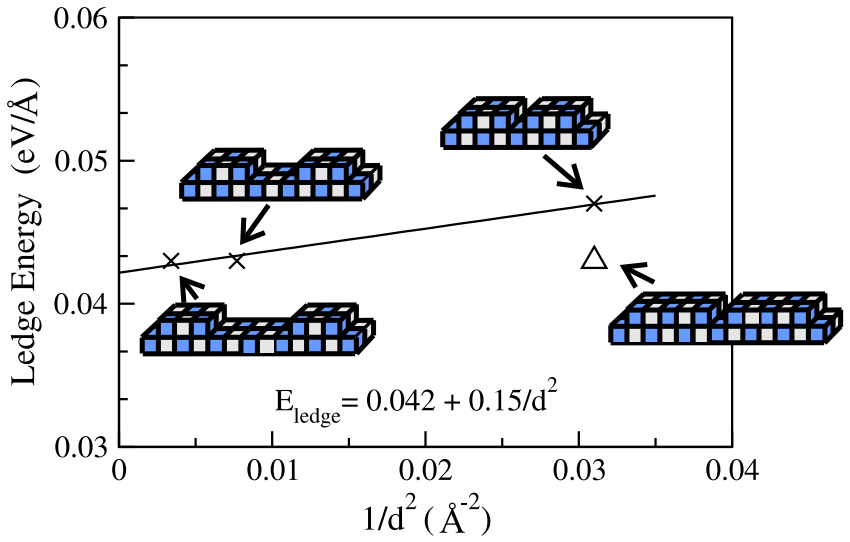

Figure 4.2: DFT-PBE ledge energy, as defined in Eq. (4.1), associated with a (100)-like step on NaCl(001) as a function of the inverse distance between neighboring steps. d is varied from 1 to 3 Na-Cl-Na distances, as indicated by the schematic structures. A linear fit (Eq. (4.2), solid line) to the three points yields a PBE based estimate of the isolated step formation energy 42 meV/Å. A single point (triangle) obtained with a wider upper terrace (2 Na-Cl-Na distances wide) indicates that the computed ledge energy is not very sensitive to the width of the upper terrace.

of the (100)-like steps computed here. How the atoms displace in the vicinity of the (100)-like step from their bulk truncated positions is indicated by the arrows on the right of Figure 4.1.

Overall we find that, as with the flat NaCl(001) surface, the atoms near the steps only undergo moderate displacements; displacements larger than 0.20 Å from their bulk truncated positions are not observed for any of the atoms in the step simulations. In particular, we find that the atoms not directly located at the step behave essentially as they do on the flat NaCl(001) surface, i.e., the surface layer Cl atoms are displaced towards the vacuum, whereas the surface layer Na atoms move towards the bulk. The Na and Cl atoms directly located at the top of the step undergo similar upward and downward movements, but now also undergo displacements inwards toward the step. The net result is a 0.13 Å displacement of the upper step Cl atoms along a plane tilted by 45° from the surface plane and a 0.18 Å displacement for the upper step Na atoms along a plane tilted by 27° from the surface plane. The atoms directly beneath the upper step atoms are naturally affected by the movement of their upper neighbors and both types of atom undergo an upward relaxation of 0.15 Å.

4.4 Polar (111)-like Steps

Coming to the polar-termination (111) steps, we focus on the relative stabilities between different termination steps which include (100), (111)-Cl, and (111)-Na

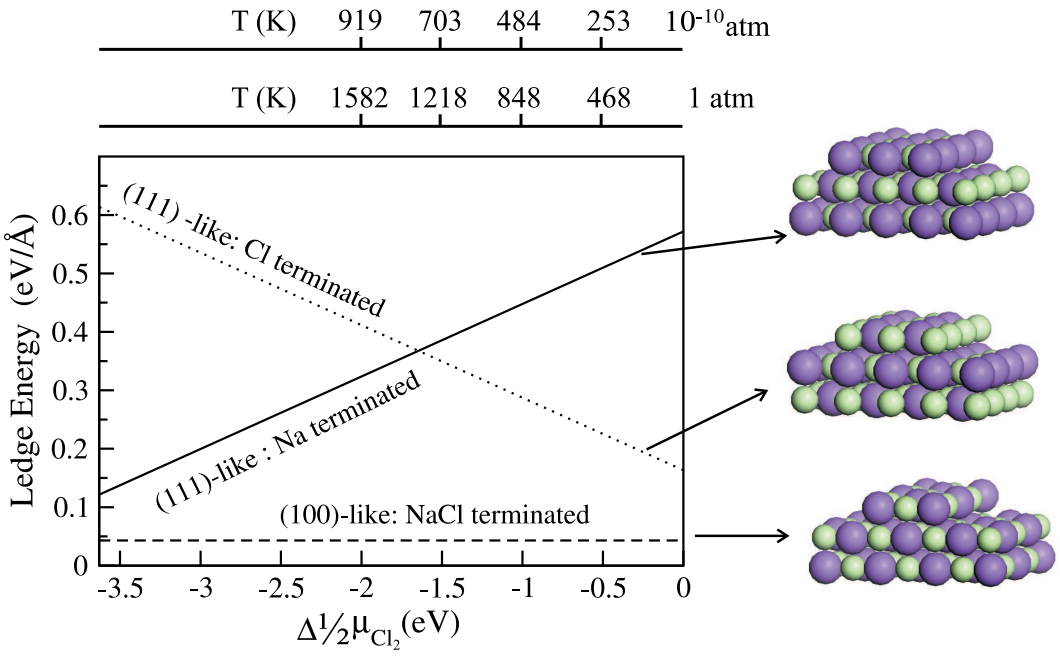

Figure 4.3: DFT-PBE ledge energy of (100)-like and (111)-like steps as a function of Cl_2 chemical potential. The zero of the Cl_2 chemical potential axis corresponds to the total energy of gas phase Cl_2 molecules, as defined in Eq. (B.2). Two temperature scales at 1 atm and 10^{-10} atm are also given as well as partial illustrations of the models used for each type of step calculation. Note that although only two layers of NaCl(001) are shown, four layer thick NaCl slabs were used in all step calculations.

terminations. The relative stabilities of (100) and (111) terminations of step are not known nor is it known under what conditions, if any, other types of step will become favorable. To explore this issue we have compared the stabilities of (100)-like steps with two alternative polar steps; specifically a purely Cl terminated (111)-like step and a purely Na terminated (111)-like step; illustrations of which are given in Figure 4.3.

Since the (111)-like terminations are non-stoichiometric, i.e., they contain a different number of Na and Cl atoms in the simulation cell, we are unable to directly determine the ledge energy from Eq. (4.1), as we did for the (100)-like step. However, it is reasonably straightforward to reformulate the ledge energy as defined in Eq. (4.2) into a thermodynamic expression based on chemical potentials. This has been done in **Appendix B** and leads to the following expression for the ledge energy [142, 153]:

$$\begin{aligned} E_{\text{ledge}} = \Big\{ & E_{\text{slab}} - N_{\text{Na}} \left[E_{\text{Na(s)}} + \left(E_f - \frac{1}{2}\mu_{\text{Cl}_2} \right) \right] \\ & - \frac{1}{2} N_{\text{Cl}} (E_{\text{Cl}_2\text{(g)}} + \mu_{\text{Cl}_2}) - \gamma A \Big\} / 2L \end{aligned} \tag{4.3}$$

where N_{Na} and N_{Cl} are the numbers of Na and Cl atoms in the simulation cell. The only other new quantity introduced in Eq. (4.3) is μ_{Cl_2}, the chemical potential of Cl_2 molecules in the gas phase. Thus we have an expression for the ledge energy, dependent solely on the chemical potential of Cl_2 molecules, which allows us to compare the relative stability of stoichiometric and non-stoichiometric steps. Further, as shown in **Appendix B**, an estimate of the temperature and pressure dependence of the relative stabilities of differently terminated steps can be obtained by expressing μ_{Cl_2} in terms of temperature and pressure of the Cl_2 gas phase.

The change of ledge energy of the purely Cl or purely Na terminated (111)-like steps as well as the stoichiometric (100)-like steps are plotted as a function of μ_{Cl_2} in Figure 4.3. In addition, the temperature dependence of the ledge energy at two specific pressures (1 atm and UHV pressure (10^{-10} atm)) are also given. The two key conclusions we draw from Figure 4.3 are: (i) the (100)-like step is significantly more stable than either termination of (111)-like step at all allowed values of the Cl_2 chemical potential. Typically, the ledge energy for the (100)-like step is at least 0.1 eV/Å lower than either of the non-stoichiometric steps; and (ii) the (111)-like Cl terminated step is more stable than the Na terminated step at all values of the Cl_2 chemical potential down to -1.7 eV. From the temperature and pressure scales given one can thus see that the Cl terminated step is more stable than its Na counterpart at all experimentally accessible temperatures and pressures.

4.5 Summary

The energetics of steps on NaCl(001) have been examined. The formation energy of isolated (100)-like steps on NaCl(100) is ∼42 meV/Å as obtained from PBE, with the LDA value about 20% larger. Placing our computed step energy in a broader context, we note that it is a rather small step formation energy, close to the calculated noble metals silver and copper, for example [154]. Further, the interaction between neighboring steps is small, never more than 5 meV/Å for the systems examined here. The ledge energy of polar (111)-like steps has also been evaluated, allowing us to compare the relative stabilities of purely Cl or purely Na terminated steps with each other and with the neutral (100)-like steps. It is found that the (100)-like terminated steps are significantly more stable than either of the (111)-like terminated steps at all allowed values of the chlorine chemical potential. Further, it is found that the Cl terminated steps are more stable than the Na terminated steps down to values of μ_{Cl}= -1.7 eV, which effectively means that Cl terminated steps are more stable than Na terminated steps at all accessible temperatures and pressures.

Chapter 5

Halogen Adatoms on Alkali Halide Surfaces

5.1 Introduction

Alkali halides are classical wide band gap insulating materials. They have long been studied as model systems to better understand basic notions in solid state physics [11] and because of their important optical properties [155]. In recent years there has been increased interest in the surface properties of alkali halides due to their potential role in emerging nanoscale technologies [13, 156] and because of their importance to environmental chemistry such as ozone depletion and precipitation [157, 158].

Nonetheless, our basic understanding of such surfaces remained shallow; certainly when compared to that for metal or even metal-oxide substrates. Thus, one of the simplest questions one could ask concerning adsorption at such surfaces remains unanswered: How do (additional) halogen adatoms adsorb? This question is important to answer for the materials science technologies mentioned above and for understanding alkali halide crystal growth and dissolution as well as understanding basic principles of adsorption and bonding. Conventional wisdom would lead one to conclude that the halogen adatoms should bond to alkali substrate atoms since this is the correct location for continued crystal growth. However, we show here for a series of sodium halide surfaces—NaF(001), NaCl(001), and NaBr(001)—that first principles calculations predict halogen adatom adsorption and bonding to halide substrate atoms instead. The explanation for this "non-textbook" adsorption is that covalent bonds are formed. Specifically, a two-center three-electron bond [18] is created in each system. Effectively the bonding in these systems resembles that of an "embedded molecular ion"; an analogy that proves to be helpful also in explaining the subtle differences observed between each adsorption system as well as the dynamical properties of the NaCl adsorption system. The above conclusions are reached based on a series of DFT and MP2 calculations for halogen adsorption on sodium halide slabs and sodium halide clusters.

In this chapter, the computational details are shown in section 5.2. The novel adsorption site preference for halogen adatom is discussed in section 5.3. The two-

center three-electron classical chemical bond behind this adsorption site preference is analyzed in section 5.4. Finally, the short summary of the results are in section 5.5.

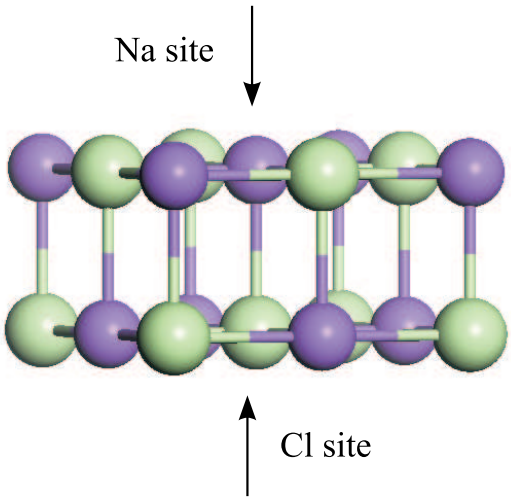

Figure 5.1: The Na_9Cl_9 cluster model used. Cl atom adsorption was considered above the central Cl (bottom) or central Na (top). The Na atoms are the purple (darker) spheres.

5.2 Computational Details

All periodic slab calculation in this chapter have been performed with the CASTEP code [109] with a plane-wave basis set and Vanderbilt ultrasoft pseudopotentials [99]. Six layer thick slab are used to examine F on NaF(001), Cl on NaCl(001), and Br on NaBr(001) within a square unit cell comprised of 8 sodium and 8 halide atoms per layer. During structure optimizations the two central layers of each sodium halide slab were kept fixed, whilst the remaining four layers plus two halogen adatoms (one on either side of the slab) were allowed to relax. The experimental lattice constants for NaF, NaCl, and NaBr were used throughout. A 2×2×1 Monkhorst-Pack $\boldsymbol{k}$ point mesh [111] has been used and spin-polarised calculations were performed when necessary. The all-electron B3LYP, BH&HLYP, and MP2 calculations on the frozen Na_9Cl_9 cluster have been carried out with the Gaussian 03 code [159].

5.3 Adsorption Sites

Table 5.1 lists the adsorption energies and adsorbate-substrate distances for each system at the high-symmetry atop sites. It is clear from Table 5.1 that the halogen adatoms bind most strongly at the halide sites, rather than at the Na sites. In every case there is a preference of 0.2–0.4 eV for adsorption at the halide site. Two interesting trends are also apparent from Table 5.1, which we discuss again

below: the halide atom adsorption energies decrease and the adsorbate-substrate bond lengths increase as one moves down the halogen group from F to Cl to Br.

Table 5.1: Adsorption energies, E_{ads} (eV/atom) and optimized adatom—substrate distances, d (Å), for F/NaF(001), Cl/NaCl(001), Br/NaBr(001) and Cl on the Na_9Cl_9 cluster all with the PBE functional and the plane-wave pseudopotential method. The bond strengths and bond lengths of the corresponding gas phase molecular ions, i.e., F_2^-, Cl_2^-, and Br_2^-, calculated within the same computational framework, are given in parentheses.

Binding site		NaF(001)	NaCl(001)	NaBr(001)	Na_9Cl_9
Halide	E_{ads}	1.07(2.07)	0.72(1.73)	0.58(1.58)	0.77
	d	1.97(2.07)	2.61(2.66)	2.87(2.91)	2.61
Na	E_{ads}	0.70	0.41	0.31	0.47
	d	2.25	2.72	2.87	2.75

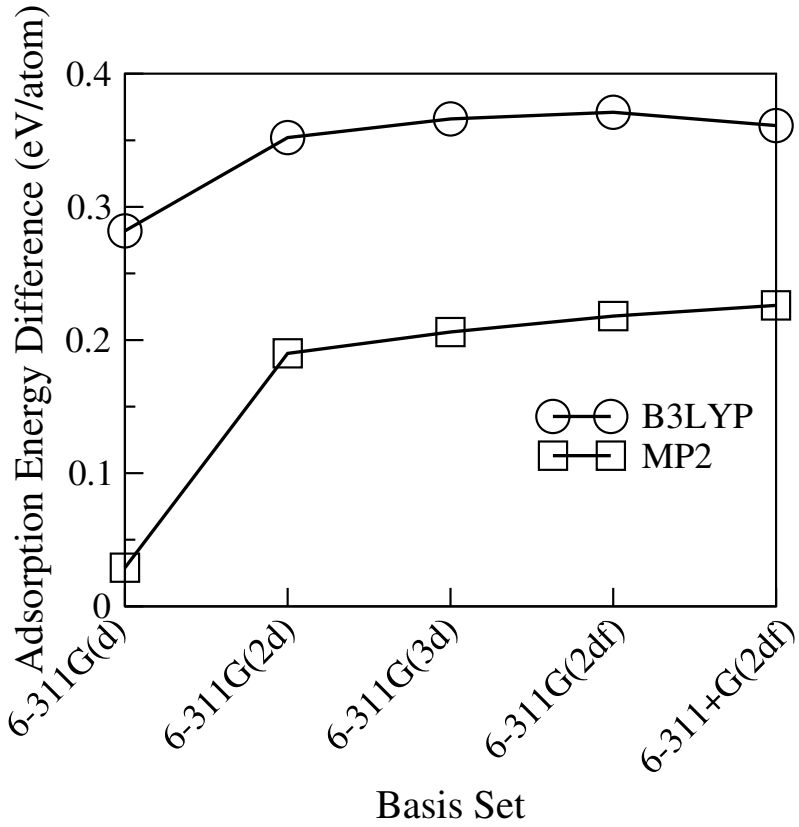

Figure 5.2: The adsorption energy difference ($E_{\mathrm{ads}}(\mathrm{Cl}) - E_{\mathrm{ads}}(\mathrm{Na})$) of Cl adatom between Cl site and Na site obtained by using B3LYP and MP2 methods with the Na_9Cl_9 cluster for a series different basis sets.

Noting that the energy difference between the two high symmetry adsorption sites on each surface is on the order of 0.2–0.4 eV it is not inconceivable that the theoretical approach employed here may simply be incorrectly predicting the halide site as the preferred one for adsorption. We make this seemingly over-cautious

statement because, as we will show below, the adsorption bonds above the halide sites (but not above the Na sites) are comprised of two-center three-electron bonds. Almost all density functionals on the market, including the PBE functional used here and the popular B3LYP hybrid functional, significantly overestimate the strength of such bonds [160]. MP2, on the other hand, and the hybrid BH&HLYP functional [96] generally yield accurate predictions for two-center three-electron bond strengths when compared to high-level quantum chemical methods such as coupled cluster [160, 161].

We now employ these alternative quantum chemical methods to test the trends identified here. Specifically a series of all-electron DFT B3LYP, BH&HLYP, and MP2 calculations for Cl adsorption on NaCl clusters were performed. The NaCl system was selected because it is the one most likely to be representative of the three systems under consideration and, of course, is the most generally interesting of the three.

Table 5.2: Adsorption energies, E_{ads} (eV/atom), and optimized adatom—substrate distances, d (Å), at the all-electron B3LYP, BH&HLYP, and MP2 levels for Cl above the central Na or central Cl site of the Na_9Cl_9 cluster shown in Figure 5.1.

Binding site		B3LYP	BH&HLYP	MP2
Cl site	E_{ads}	0.51	0.35	0.39
	d	2.59	2.69	2.50
Na site	E_{ads}	0.17	0.10	0.16
	d	2.80	2.98	2.97

First we used the plane-wave pseudopotential method to identify a suitable cluster model that would faithfully mimic Cl adsorption on NaCl(001), and then used the same cluster to compute Cl adsorption at the BH&HLYP and MP2 together with B3LYP. The plane-wave pseudopotential calculations reveal that the frozen two layer Na_9Cl_9 cluster shown in Figure 5.1 is a good model since the adsorption energies and adsorption structures obtained with it for Cl adsorption at both types of adsorption site are close to those obtained with the periodic slab model (see Table 5.1). All-electron calculations were then performed for Cl adsorption on the Na_9Cl_9 cluster with a 6-311+G(2df) Gaussian function basis set. As is clear from Table 5.2 the BH&HLYP and MP2 calculations fully support the binding site preference predicted by the GGA-PBE pseudopotential approach; with BH&HLYP the site preference is 0.25 eV and with MP2 it is 0.23 eV.

Exhaustive tests on the dependence of the results presented here to basis set size and cluster size were performed, some of which are shown in Figure 5.2. With regard to basis set it was found that a 6-311G(2d) basis set was already sufficient to capture the binding energy difference between the two sites since, even at the MP2 level, the binding energy difference with this smaller basis set was within 20 meV of the binding energy difference obtained with the 6-311+G(2df) basis set reported here. With regard to cluster size, DFT and MP2 calculations were performed for Cl adsorption on Na_5Cl_5, $Na_{13}Cl_{13}$, and $Na_{25}Cl_{25}$ clusters as well as the Na_9Cl_9 cluster.

In every case the Cl site remained the preferred one for adsorption.

5.4 Electronic Structure Analysis

More confident in the validity of the binding site assignment made here, we now ask: Why do halogen adatoms bond preferentially to halide substrate atoms? This result is unexpected for the reasons outlined above and, furthermore, from a simple comparison of the relative bond strengths of alkali halide dimers versus halogen dimers in the gas phase which reveals that for the systems examined here the strength of the alkali halide dimer (i.e., NaF, NaCl or NaBr) always exceeds that of the respective halogen dimer (i.e., F_2, Cl_2, or Br_2) [116]. An analysis of the electronic structures obtained from our DFT-PBE slab calculations reveals the answer for the predicted binding site preference.

In all three adsorption systems a covalent bond forms when the halogen atoms bond to the halide substrate atoms. The difference of the total densities of states (ΔDOS) and partial densities of states (ΔPDOS) between the adsorbate and clean surfaces plots displayed in Figure 5.3 reveal this. For each system the energy range in the vicinity of the alkali halide valence band is shown. Prior to adsorption the valence band is comprised of a single (large) peak of p orbital character. After adsorption new peaks are visible at the top and bottom edges of the valence band. Inspection of the individual Kohn-Sham eigenstates in each system reveals that a series of adsorbate-substrate bonding and antibonding states of p(adatom) and p(substrate) character are created within this energy interval.

Specifically, a set of σ-type bonding ($p_z + p_z$) and anti-bonding ($p_z - p_z$) states and a set of π-type bonding ($p_{x/y} + p_{x/y}$) and anti-bonding ($p_{x/y} - p_{x/y}$) states are formed. In each case the bonding and antibonding states of π character are fully occupied and reside within the valence band (or in the case of NaF also below the valence band).

Hence the fully occupied π-type states do not contribute to the overall net bonding. The σ-type states, on the other hand, straddle the valence band and are the key states responsible for bonding because one of the anti-bonding σ-type states remains unoccupied. Or, more precisely, within the spin-polarized ΔPDOS picture of Figure 5.3(b),(c) there is a single unoccupied one-electron state of σ-type antibonding character above the valence band maximum. Examples of the eigenstates of σ-type bonding and antibonding character from each system are shown in Figure 5.3(a) and a schematic diagram of the bonding picture that has emerged is shown in Figure 5.4 The σ-type covalent bond formed between the adatom and the substrate is also clear from the electron density difference plot for Cl on NaCl(001) (Figure 5.5(a)). Furthermore, the electron density difference plot for Cl adsorbed at the unfavorable Na site of NaCl(001) (Figure 5.5(b)) illustrates the clear difference between the adsorption bond at each site. The covalent bonding character is absent when Cl is at the Na site[1]. Instead there is an indication of an electrostatic

[1]This is also clear from inspection of the density of states and Kohn-Sham eigenstates when Cl is adsorbed at the Na site.

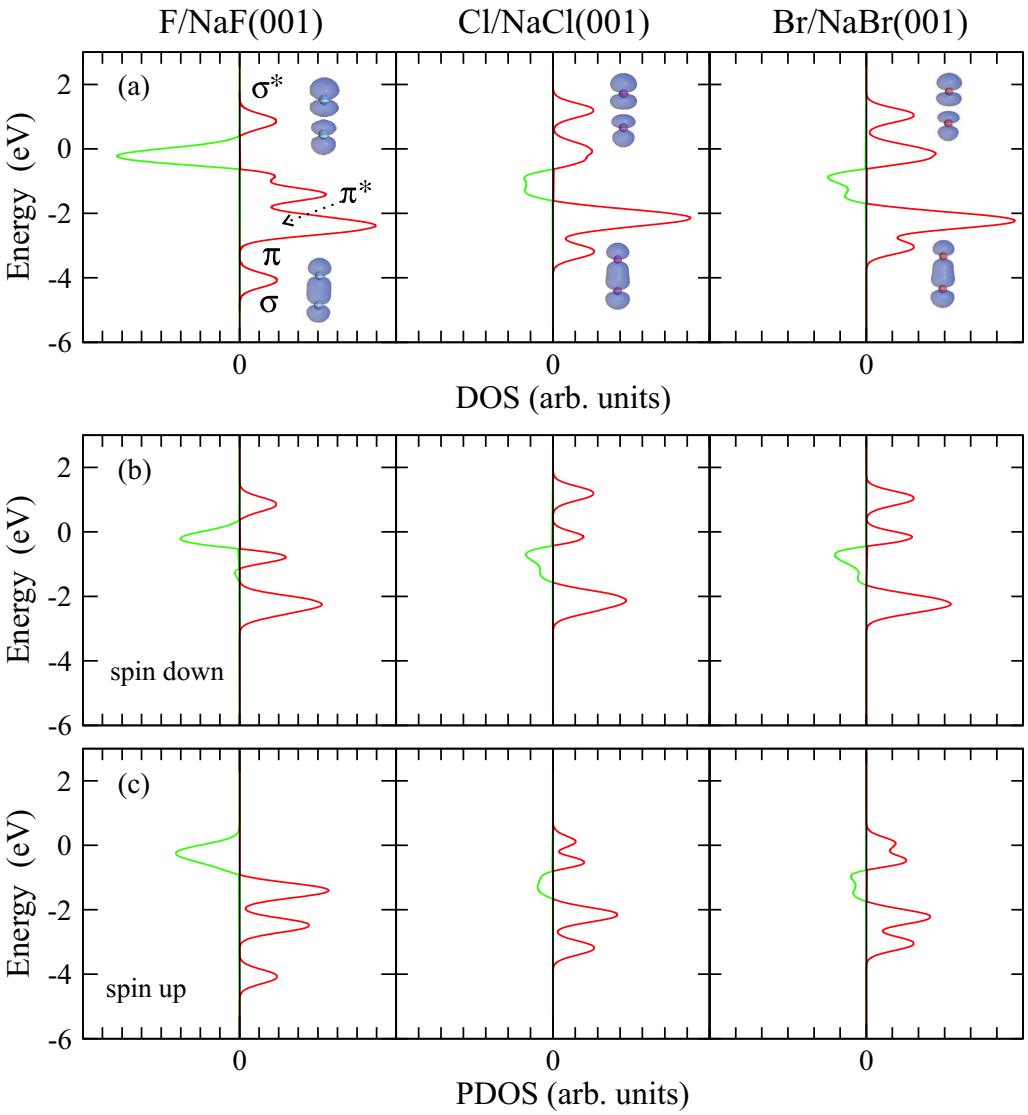

Figure 5.3: (a) the difference of density of states (ΔDOS) between the adsorbate and clean covered alkali halide (001) surfaces. $\Delta\mathrm{DOS} = \mathrm{DOS}_{(\mathrm{adsorbate})} - \mathrm{DOS}_{(\mathrm{clean})}$, where $\mathrm{DOS}_{\mathrm{adsorbate}}$ and $\mathrm{DOS}_{\mathrm{clean}}$ is the total density of states of adsorbate and clean alkali halide surfaces, respectively. The insets display isosurfaces of constant electron density for individual Kohn-Sham eigenstates and the labels indicate the character of certain key adsorbate-substrate states. The difference of the spin resolved partial density of states (ΔPDOS) with same definition of ΔDOS for the three adsorption systems. (b) spin down; (c) spin up. The red is positive and the green is negative. All results in (a), (b), and (c) have been obtained with the PBE functional and the plane-wave pseudopotential method. The energy zero has been set to the highest occupied Kohn-Sham eigenstate in each system.

interaction, illustrated by the (small) charge transfer from the substrate toward the adsorbate (Figure 5.5(b)). One might then expect that if the halogen adatom gains an electron to become a halide anion, X^-, the covalent bond at the halide site will be weakened and conversely the electrostatic attraction at the alkali (Na) site will be strengthened. It is plausible that this will result in a switch in adsorption site with the alkali site becoming the preferred one for anion adsorption. Indeed, a site switch is precisely what we see when we model the adsorption of a Cl^- by either adding an extra electron to our simulation cell or by replacing the Cl atom on the underside of the NaCl(001) slab with a neutral Na atom.

In the latter case, for example, the Na site is favored over the Cl site by 0.49

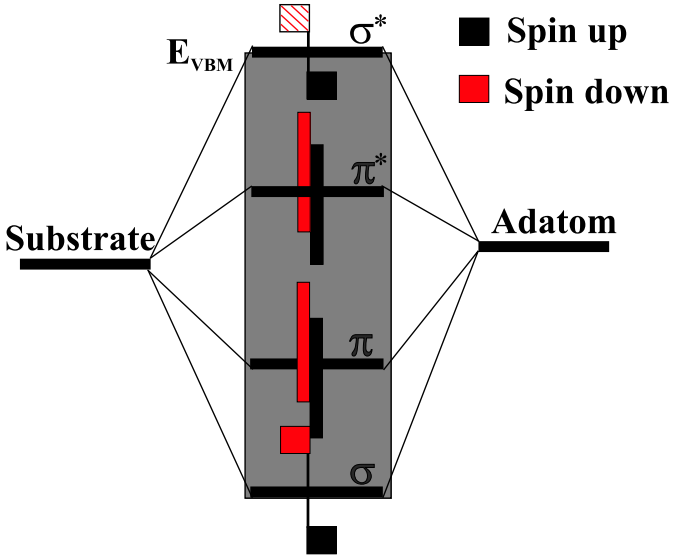

Figure 5.4: Schematic illustration of the bonding model proposed here for halogen adatom adsorption at the halide sites of alkali halide (001) surfaces. The gray rectangle designates the substrate valence band. A solitary σ-type orbital resides above the valence band maximum (E_{VBM}) and is not occupied.

eV/Cl adatom. Further, the bond length of the adsorbed Cl^- to the underlying Na is >0.10 Å shorter than it is for neutral Cl atom adsorption, and 0.80 Å shorter than the bond length for Cl^- adsorption at the (now unfavorable) Cl site. Thus we see that when the system has enough charge to have all the atoms assume their formal (integer) charges it behaves as anticipated. When this is not the case the system forms the most appropriate charged ion, by way of a textbook covalent bond.

The basic physical picture that has developed for the bonding at the preferred sites in these systems is thus that of a textbook two-center three-electron covalent bond. Essentially each adsorption system is equivalent to an X_2^- (X = F, Cl, or Br) species adsorbed upright at a halide vacancy on the surface. Indeed this analogy of an "embedded molecular ion" proves to be illuminating in two key respects. First, the trend of both the adsorption energies and adatom-substrate bond lengths correlate with the computed gas phase X_2^- bond strengths. Specifically, for the gas phase X_2^- and the respective adsorption systems the computed PBE bond strength

decreases and the bond length increases upon going from F to Cl to Br (Table 5.1). The correspondence is particularly striking between the bond lengths since each adsorption bond is within 0.2 Å of its respective molecular ion bond length (Table 5.1). Second, the short-time dynamics, as determined from a 12.5 ps *ab initio* molecular dynamics simulation (see **Appendix C**) for the Cl/NaCl(001) system, resembles that of an adsorbed chlorine molecule in a vacancy rather than an adsorbed atom on a flat surface. The motion of the two chlorine atoms is strongly correlated: they rotate and vibrate in concert in the "Cl vacancy". The dynamics also reveals that the potential energy surface for tilting the embedded Cl_2^- is rather flat. Indeed as confirmed by subsequent structure optimization 75 meV can be gained by tilting the Cl_2^- by ∼30 degrees from the surface normal.

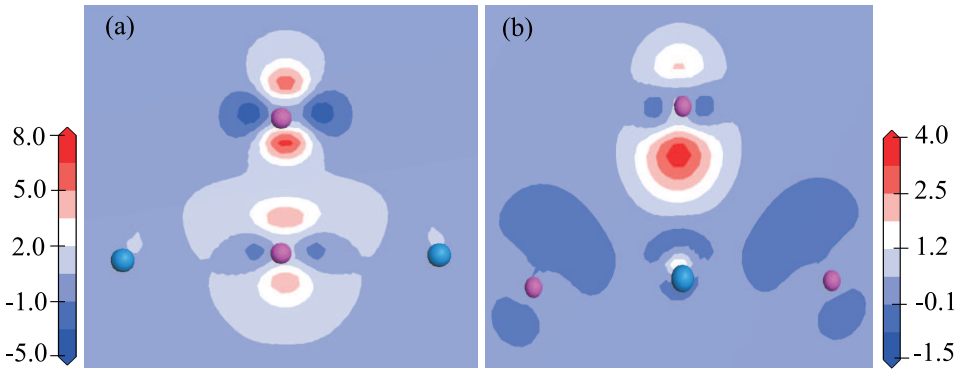

Figure 5.5: Electron density difference ($\Delta\rho$) for Cl adatom adsorption at the Cl substrate site (a) and the Na substrate site (b) of NaCl(001). $\Delta\rho$ is defined as $\Delta\rho = \rho_{\mathrm{Cl/NaCl}} - \rho_{\mathrm{NaCl}} - \rho_{\mathrm{Cl}}$, where $\rho_{\mathrm{Cl/NaCl}}$, ρ_{NaCl}, and ρ_{Cl} are the electron densities of the total system, the isolated NaCl(001) surface, and the Cl atom in the gas phase, respectively. The plane of the cut is along the (001) direction, perpendicular to the surface and the units of both legends are $10^{-4}\mathrm{eÅ}^{-3}$.

5.5 Summary

In summary, DFT slab calculations predict textbook covalent bond formation at the non-textbook halide adsorption sites on some prototype ionic materials. For the case of Cl on NaCl(001), this binding site preference is supported by BH&HLYP and MP2 cluster calculations. Aside from the clear esoteric interest, the present results are significant because they dictate the initial binding site for epitaxial alkali halide crystal growth and possible intermediate states in alkali halide dissolution.

Chapter 6

Towards a High Precision Estimate of the Adsorption Energy of Water on Salt

6.1 Introduction

The adsorption of atoms and molecules at solid surfaces is of great importance to many scientific disciplines such as catalysis, corrosion, and environmental science [162]. An accurate description of the energetics of the adsorption bond is often the first step toward deeper understanding in each of the above areas. Indeed, countless experimental and theoretical studies have been dedicated to the determination of high accuracy estimates of adsorption energies [163, 164, 165]. However, the reliable determination of the strength of the bond between an atom or molecule and a solid surface remains a major challenge for both experiment and theory, especially when the adsorption energy is small such as for physisorbed adsorbates.

Focusing specifically on theory, in recent years DFT [73, 74] has become the most popular electronic structure approach for treating adsorption and its success is substantial. If combined with the supercell approach, one can ensure that the treatment of the *xc* functional remains the only relevant approximation, enabling full geometry optimization of systems with hundreds of atoms with fully converged basis sets. However the adoption of an approximate *xc* functional leads practical DFT calculations to suffer from various well-known deficiencies, such as the missing dispersion interactions which may be relevant to some adsorption systems (like the one under consideration here) or the self interaction error which plagues others [166, 167, 168, 169]. Quite often in adsorption at solid surfaces DFT exhibits a strong sensitivity to the *xc* functional employed and in the absence of reliable experimental estimates, it is not known which functional is suitable for a particular problem [170, 171]. Indeed it is unclear what level of accuracy can be obtained from DFT with existing *xc* functionals. It is unlikely, for example, that current *xc* functionals popular in treating surfaces such as PBE [85] (PW91 [84]), RPBE [5], and LDA [77] can deliver so-called "chemical accuracy" an accuracy of 1 kcal/mol ($\sim$43 meV) in adsorption energies. Such a precision is desirable since it is the level

of accuracy necessary in order to reliably predict rates of process at surfaces such as desorption.

There are, of course, remedies to account for certain deficiencies within the density-functional theory framework. Van der Waals correction schemes [172, 173, 174] would be appropriate for the missing dispersion interactions and "hybrid" functionals for the self-interaction error [167]. Such techniques offer great promise. However, given their partly *ad hoc* nature and the frequent absence of definitive experimental values, accurate theoretical reference data against which their reliability can at first be benchmarked is highly desirable. Obvious alternatives to DFT are quantum Monte Carlo [9] or quantum chemistry approaches such as Møller-Plesset perturbation theory [38], coupled cluster theory [46] or configuration interaction. Again these approaches have had some success for adsorption at surfaces and offer further promise for the future [168, 175, 176, 177, 178, 179, 180, 181, 182, 183, 184]. However, at this stage none enables a full geometry optimization of a molecule above a periodic substrate at the complete basis set limit, which is now routine for DFT. So if one chooses to adopt one of these alternative methodologies to DFT new "headaches" are encountered such as the use of cluster models of the substrate or concerns about basis set incompleteness, which must be overcome.

In the current chapter, we apply MP2 and coupled cluster to obtain an estimate of the adsorption energy of an individual water monomer on salt. The focus here is exclusively on adsorption of an individual "isolated" water molecule and the many interesting questions relating to water clustering or the liquid water—salt interface are not considered here. Our interest in water on salt stems from its relevance mainly to environmental science and biology and also as an example of an important molecular physisorption system [19, 20, 21, 22, 23, 24, 25, 26]. Here, an attempt is made to push the quantum chemistry methods as far as we possibly can and ensure that the sensitivity of the results obtained to cluster size, basis set, and level of correlation treatment are understood and controlled. The specific procedure we follow to achieve a high accuracy estimate of the adsorption energy of water on salt involves a division of the total adsorption energy into contributions from Hartree-Fock and electron correlation, the use of embedded cluster models of the substrate, and extrapolations to CBS. For the treatment of electron correlation we employ MP2 and CCSD(T). These quantum chemistry calculations are also accompanied by a detailed discussion on the possible errors introduced at each stage of the "roadmap" followed as well as a careful series of DFT studies and comparison with experimental results.

In the following, section 6.2 provides details of the computational setup for both the periodic DFT and explicitly correlated quantum chemistry cluster calculations. Then in section 6.3, water adsorption on flat NaCl(001) with three different xc functionals and at various (low) coverages is discussed. The explicitly correlated quantum chemistry cluster calculations are then reported in section 6.4. This is followed with an analysis of the possible sources of error associated with our embedded cluster calculations in section 6.5. In section 6.6 some links between the current theoretical estimate and experimental results are made and we close with a brief discussion and conclusions in section 6.7.

6.2 Computational Details

Here the computational details for both the periodic DFT and quantum chemistry cluster calculations are briefly described. All periodic DFT calculations have been performed within the plane-wave pseudopotential approach as implemented in the CASTEP code [109]. The DFT calculations were carried out with three different exchange-correlation functionals: LDA [77], PBE [85], and RPBE [5]. The electron-ion interactions are described with Vanderbilt ultrasoft pseudopotentials [99] expanded up to a plane-wave cut-off energy of 400 eV. LDA pseudopotentials have been used for all LDA calculations, and likewise, GGA (PBE) pseudopotentials have been used for all GGA (PBE and RPBE) calculations. Further, we note that the well-known problem of nonlinear core-valence electron exchange and correlation for Na has been eliminated in the present study by treating the Na $2s$ and $2p$ electrons as valence electrons [110]. Four layer thick NaCl slabs separated by 15 Å of vacuum have been used. Most calculations were performed in a large p($2\sqrt{2} \times 2\sqrt{2}$) unit cell. Although for certain calculations on NaCl steps a p($3\sqrt{2} \times \sqrt{2}$) unit cell was used which, following chapter 4, comprised of a single layer "stripe" of NaCl atoms on top of the 4 layer NaCl slab. Brillouin zone sampling was performed at the Γ point only. Unless stated otherwise, during geometry optimizations all atoms in the unit cell were allowed to relax until a force convergence threshold of 0.01 eV/Å was met. As detailed in **Appendix A**, all of the above choices in computational setup were carefully checked for convergence, and capable of yielding adsorption energies which are reasonably expected to be within 10 meV of "absolute" convergence.

The all-electron calculations have been carried out with the NWChem4.7 [185], Gaussian03 [159], and Crystal06 [186] codes[1]. To model the substrate the following series of 2-layer stoichiometric NaCl clusters were used: Na_5Cl_5, Na_9Cl_9, $Na_{13}Cl_{13}$, and $Na_{25}Cl_{25}$. The clusters were embedded in large finite arrays of point charges as well as a combination of point charges and effective core potentials. The details of the embedding and the sensitivity of the results to the strategy employed will be discussed in detail in Section 6.4. A variety of localized Gaussian function basis sets were used, ranging from small Pople-style basis sets such as 6-311G*, 6-31G, 86-311G, and 8-511G to Dunning's larger correlation consistent basis sets [55, 187]. In particular, for the extrapolations to the complete basis set limit cc-pVXZ, aug-cc-pVXZ, and aug-cc-pCVXZ (X= 3, 4, 5) basis sets were used as described in Section 6.4. Electron correlation was treated at the MP2 [38] and CCSD(T) [46] levels. For most of the explicitly correlated calculations the optimized adsorption geometry obtained from the periodic PBE calculations was employed. Again the sensitivity of the results to this approximation will be discussed below.

Adsorption energies are defined as:

$$E_{\text{ads}} = E_{\text{water}} + E_{\text{NaCl}} - E_{\text{water/NaCl}} \quad , \tag{6.1}$$

[1]The quantum chemistry cluster calculations were mainly carried with the NWChem and Gaussian codes. The adsorption energies obtained from these codes never differed by more than 1 meV and so the two codes were used interchangeably; Gaussian for the smaller jobs and NWChem, in parallel, for the larger jobs. The usage of Crystal06 is purely for the periodic HF calculations.

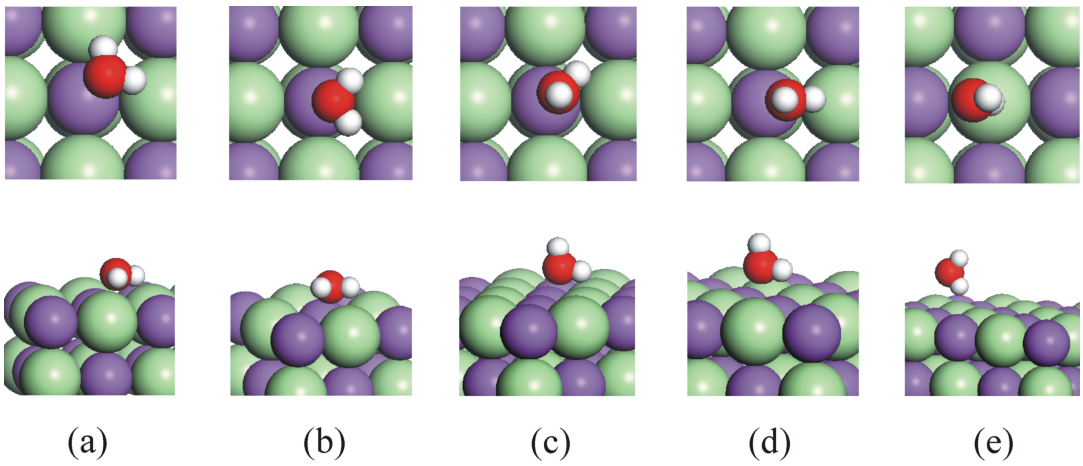

Figure 6.1: Top and side views of various initial structures tested at $\frac{1}{8}$ ML coverage for a water molecule adsorbed on NaCl(001). The purple, green, red, and white spheres are Na, Cl, O, and H, respectively.

where $E_{\text{water}}, E_{\text{NaCl}}$, and $E_{\text{water/NaCl}}$ are the total energies of the isolated water molecule, the clean NaCl(001) slab or cluster, and the water/NaCl adsorption system, respectively. With this definition, a positive adsorption energy corresponds to an exothermic adsorption process. When adsorption on the NaCl clusters is examined with the explicitly correlated methods, we find that is proves useful to split E_{ads} into contributions from Hartree-Fock ($E_{\text{ads}}^{\text{HF}}$) and electron correlation ($E_{\text{ads}}^{\text{corr}}$), i.e.,

$$E_{\text{ads}} = E_{\text{ads}}^{\text{HF}} + E_{\text{ads}}^{\text{corr}} \quad . \tag{6.2}$$

6.3 Periodic DFT Calculations for Water on Flat NaCl(001)

In this section a series of periodic DFT calculations for water monomer adsorption on NaCl(001) is reported. The focus is on the low coverage regime; from half a monolayer (ML) to $\frac{1}{8}$ ML, with the monolayer defined as one water molecule for each pair of surface NaCl atoms. So as to minimize the effects of numerical noise, the same large p($2\sqrt{2} \times 2\sqrt{2}$) unit cell was used for all water coverages and only the number of water molecules within the unit cell was altered. Three different *xc* functionals (LDA, PBE, and RPBE) were employed. PBE was selected because it is an extremely popular *xc* functional for water adsorption studies [188, 189, 190]. The RPBE functional [5] was selected because it is also popular in adsorption studies and was specifically designed to improve upon PBE for adsorption energies of CO on metals [191, 192]. And LDA is considered because there are indications that it outperforms PBE for certain surface properties such as the surface energy of metals and oxides [131, 132].

First, at $\frac{1}{8}$ ML we sought to determine the most stable structure for a water

monomer. To this end, several different initial configurations of a water molecule were considered. The initial structures tested are displayed in Figure 6.1. After optimization with all three *xc* functionals, only the configurations labeled (a) and (b) survived, as structures (c), (d), and (e) collapsed to (a). Of the two minimum energy structures, (a) was the most stable with an adsorption energy of 640, 383, and 286 meV/H_2O with the LDA, PBE, and RPBE *xc* functionals, respectively. The adsorption energy of structure (b) with these three functionals is 473, 297, and 251 meV/H_2O, respectively. Both structure (a) and (b) have the water molecule located approximately above a Na site with a small displacement ($\Delta_{\mathrm{O—Na}}$) toward the neighboring Cl site(s). In the most stable configuration (a), the H atoms of the water molecule are directed toward adjacent Cl atoms, indicating an additional attractive Cl—H interaction. Thus, DFT with three *xc* functionals offers a clear indication that the Na site is the most stable one for water adsorption, an assignment that matches the experimentally determined adsorption site for water on NaCl(001) at 1 ML coverage [19]. In addition, the conclusion that structure (a) is the most stable one agrees with several previous DFT studies [20, 21, 22, 23].

Considering the structures obtained from each functional in more detail, we

Table 6.1: Selected structural parameters of water at the most stable adsorption site (configuration (a) in Figure 6.1) at $\frac{1}{8}$ ML, $\frac{1}{4}$ ML, and $\frac{1}{2}$ ML with the LDA, PBE, and RPBE functionals. The units of length are in Å and angles are in degrees.

Functional	$d_{\mathrm{O—Na}}$[a]	$\perp$O[b]	$d_{\mathrm{Cl—H}}$[c]	$\Delta_{\mathrm{O—Na}}$[d]	$d_{\mathrm{O—H}}$[e]	$\angle\phi$[f]	$\angle$HOH[g]
			$\frac{1}{8}$ ML				
LDA	2.32	2.17	2.23	0.89	0.99	29.1	103.7
PBE	2.44	2.34	2.50	0.87	0.98	19.4	104.1
RPBE	2.44	2.37	2.70	0.82	0.98	14.7	104.4
			$\frac{1}{4}$ ML				
LDA	2.34	2.15	2.28	0.91	0.99	27.3	103.6
PBE	2.43	2.32	2.50	0.88	0.98	19.8	104.2
RPBE	2.45	2.39	2.59	0.90	0.98	15.2	104.7
			$\frac{1}{2}$ ML				
LDA	2.33	2.16	2.38	0.82	0.99	18.6	104.0
PBE	2.42	2.31	2.61	0.85	0.98	12.8	104.1
RPBE	2.45	2.38	2.72	0.85	0.98	10.3	104.3

[a] Distance between O and Na.
[b] Height of the oxygen atom above NaCl(001).
[c] Average distance between H and Cl .
[d] Displacement of O away from the Na site.
[e] Average distance between O and H.
[f] Angle between water dipole moment and NaCl(001). A positive value indicates that the H atoms are closer to the surface than O.
[g] H$\cdots$O$\cdots$H angle.

report in Table 6.1 a selection of key structural parameters characterizing adsorption structure (a). In particular, the water molecule, as indicated by the height of O ($\perp$o), resides about 2.2 to 2.4 Å above the surface. This range reflects a sensitivity of the height of the molecule above the surface to the *xc* functional employed,

with LDA predicting the shortest water-NaCl distance and RPBE the largest. Likewise, the related O—Na distance ($d_{O—Na}$) ranges from ∼2.32 Å (LDA) to ∼2.45 Å (RPBE). The tilt angle of the molecule (defined as the angle between the dipole moment of the molecule and the surface) with respect to the surface is 29°, 19°, and 15° with the LDA, PBE, and RPBE functionals, respectively. The lateral displacement of the water molecule from the precise atop site is ∼0.8–0.9 Å with all three *xc* functionals. The internal structure of the molecule is not perturbed much from its gas phase value with the ∠HOH angle within 1° of its equilibrium gas phase value for all three functionals and also the OH bond length within 0.01 Å of their gas phase values. On clean NaCl(001) there is a buckling between the Cl and Na atoms, with the Cl atoms residing 0.1 Å higher than the Na atoms. However upon water adsorption on top of Na, the Na is pulled out of the surface slightly and the buckling in the immediate vicinity of the adsorption site is alleviated.

To further address the issue of substrate relaxation, we have specifically examined the effect of surface relaxation on the water adsorption energy with a set of calculations on fixed NaCl slabs. For all three functionals it was found that the adsorption energy on the frozen NaCl slab was about 30 meV less. Specifically, the adsorption energy on the frozen (relaxed) surfaces was 611 (640), 355 (383), and 252 (286) meV/H_2O with the LDA, PBE, and RPBE functionals, respectively. Thus, whether the substrate is frozen or relaxed does not have a major impact on the adsorption of water on NaCl(001). Likewise, the structure and location of the adsorbed water molecule is quite insensitive to whether the atoms in the NaCl slab are fixed or relaxed. For example, the difference in the height of the molecule above the fixed and fully relaxed surfaces does not vary by more than 0.03 Å with all three *xc* functionals.

Next, the dependence of the adsorption energy and adsorption structure on water coverage was examined. The purpose of these calculations is not to perform an extensive examination of the coverage dependence of water adsorption, but rather to simply establish how sensitive the adsorption energy is to variations in coverage in this low regime and whether a $\frac{1}{8}$ ML coverage is low enough to be representative of an "isolated" monomer. To this end, we considered adsorption of the most stable adsorption structure (a) at $\frac{1}{4}$ and $\frac{1}{2}$ ML. Selected structural parameters and the adsorption energy at $\frac{1}{4}$ and $\frac{1}{2}$ ML are reported in Table 6.1 and Figure 6.2, respectively. Overall we find that for all three functionals the structural and energetic properties of the water molecule at $\frac{1}{4}$ and $\frac{1}{2}$ ML are rather similar to those obtained at $\frac{1}{8}$ ML. Throughout the entire coverage range ($\frac{1}{8}$ to $\frac{1}{2}$ ML) the adsorption energy changes less than 20 meV (Figure 6.2). Likewise, the structural parameters such as the height of the molecule and its displacement from the precise Na site are not particularly sensitive to coverage changes in this regime, varying by 0.03 Å at most. Overall it can be seen that in this coverage regime the water adsorption structure and energy is rather insensitive to water coverage and the $\frac{1}{8}$ ML adsorption structure can reasonably be considered as being representative of an isolated water on NaCl(001).

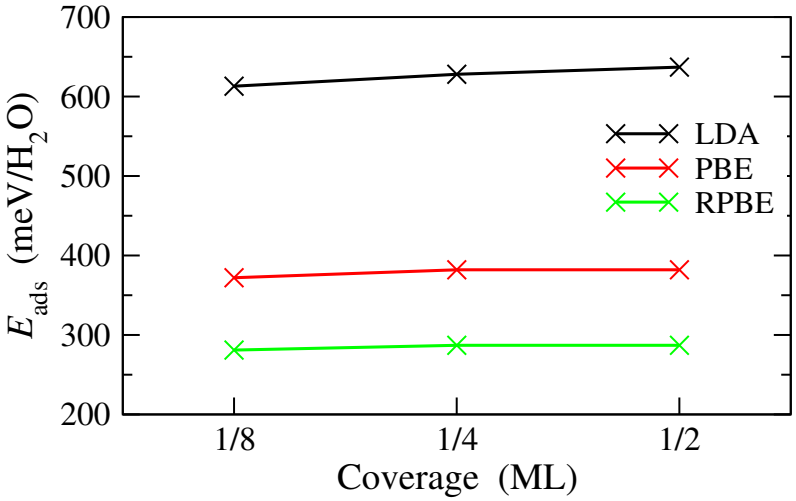

Figure 6.2: Coverage dependence of the water molecule adsorption energy with the LDA, PBE, and RPBE functionals, respectively.

6.4 Quantum Chemistry Cluster Calculations

The large dependence of the adsorption energy on the chosen *xc* functional observed here (Figure 6.2), is not very satisfactory, with the "range" of 350 meV being almost ten times larger than chemical accuracy. This prompted us to consider MP2 and CCSD(T) as alternatives to DFT which should, in principle, be able to deliver higher accuracy estimates of the adsorption energy. However, it is, of course, not (yet) possible to use MP2 or CCSD(T) to perform a full geometry optimization with a periodic slab model of the substrate at the complete basis set limit, as it is for DFT. Thus the process of obtaining a converged adsorption energy is considerably less straightforward than it is with DFT and involves the application of cluster models for the substrate, a careful consideration of basis set convergence, as well as several other issues which we now address.

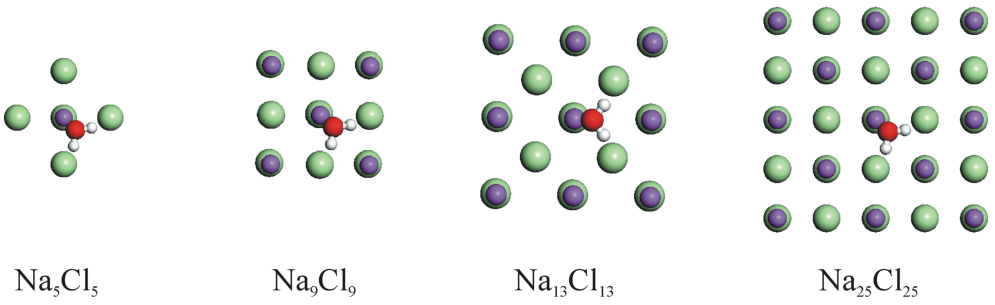

Figure 6.3: Top views of the stoichiometric 2 layer clusters used (Na_5Cl_5, Na_9Cl_9, $Na_{13}Cl_{13}$, and $Na_{25}Cl_{25}$) along with the adsorbed water molecule. The purple, green, red, and white spheres are Na, Cl, O, and H, respectively.

6.4.1 Cluster Size and Embedding

To enable methods like MP2 and CCSD(T) to wield their power to water/NaCl(001), it is necessary at present to move from the periodic supercell representation of the adsorption system to one based on finite cluster models. When examining adsorption on clusters, the first step is to establish the sensitivity of the results to cluster size and, if applicable, embedding strategy. To this end we examined adsorption on the series of stoichiometric two layer NaCl clusters shown in Figure 6.3, which range from an Na_5Cl_5 to an $Na_{25}Cl_{25}$ cluster. Adsorption on bare as well as embedded versions of these clusters was examined.

To begin, we focus on the Hartree-Fock contribution, $E_{\mathrm{ads}}^{\mathrm{HF}}$, to the adsorption energy and display in the top part of Figure 6.4 the variations in $E_{\mathrm{ads}}^{\mathrm{HF}}$ for non-embedded "naked" clusters (a), clusters embedded in point charges (PCs) (b), and clusters embedded in a shell of Na effective core potentials (ECPs) (at the Na^+ sites directly adjacent to the NaCl cluster) and PCs (c). Data for three rather small basis sets are displayed. Several interesting pieces of information can be gleaned from Figure 6.4, which we now discuss. First, without embedding, $E_{\mathrm{ads}}^{\mathrm{HF}}$ depends sensitively on the chosen cluster size. A large change in adsorption energy of over 100 meV for the different clusters is observed. Moreover, there is no apparent "convergence" with respect to cluster size and it is unclear if even the largest $Na_{25}Cl_{25}$ cluster is a suitable model for the true NaCl(001) surface. Second, after embedding the clusters in point charges, the variations in $E_{\mathrm{ads}}^{\mathrm{HF}}$ with cluster size are much smaller with the difference between the smallest Na_5Cl_5 and largest $Na_{25}Cl_{25}$ clusters being only 20 meV. Given the highly ionic nature of NaCl (and associated large band gap), along with the large body of literature on embedding of ionic solids [168, 175, 176, 177, 178, 180, 182, 183, 184, 193], this improvement is to be expected.

Table 6.2: Hartree-Fock contribution ($E_{\mathrm{ads}}^{\mathrm{HF}}$), correlation energy contribution ($E_{\mathrm{ads}}^{\mathrm{corr}}$) and total adsorption energy (E_{ads}) calculated with different point charge arrays of dimension X×Y×Z. Calculations were done at the MP2 level with a cc-pVTZ basis set. Units are in meV.

X×Y×Z	$E_{\mathrm{ads}}^{\mathrm{HF}}$	$E_{\mathrm{ads}}^{\mathrm{corr}}$	E_{ads}
11×11×6	230	273	503
21×21×6	230	273	503
31×31×6	230	274	504
41×41×6	229	274	503
21×21×2	228	273	501
21×21×4	230	274	504
21×21×8	230	274	504

The particular point charge set-up employed for the embedded cluster calculations displayed in Figure 6.4 (b) is a finite ±1.0 e array of dimension X×Y×Z = 21×21×6. A series of tests with alternative point charge arrays established that this particular array was large enough to achieve convergence with respect to the number of point charges of $E_{\mathrm{ads}}^{\mathrm{HF}}$ to within about 1 meV (Table 6.2). Third, after

embedding with a combination of point charges and ECPs the variation with cluster size is again small (Figure 6.4c). The specific recipe adopted for the ECP plus PC embedding was to replace all the cation point charges directly adjacent to anions of the cluster with Na LANL2DZ (Los Alamos National Laboratory 2-double-ζ) [194] ECPs which will replace the inner core electrons. The rationale for this this approach is the desire to minimize the artificial polarization of the anions caused by the point charges directly adjacent to them. However, whilst a combination of ECPs and point charges is known to be necessary for other ionic materials such as MgO [178], no clear improvement over the simple point charge embedding (Figure 6.4c) is observed here. Given the smaller polarizability of Cl^- compared to O^{2-} this observation is not entirely unexpected.

As a further assessment of the embedding strategy employed here, periodic

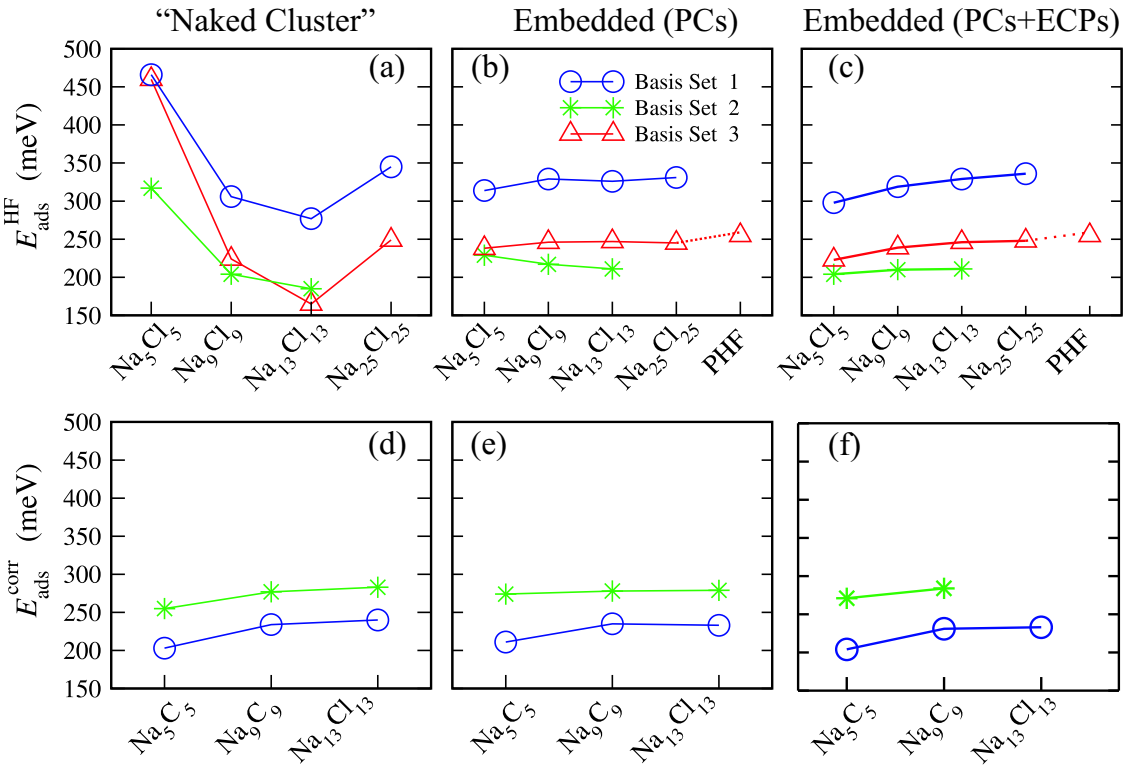

Figure 6.4: Variation of the HF (E_{ads}^{HF}, top) and electron correlation (E_{ads}^{corr}, bottom) contribution to the adsorption energy with respect to cluster size for three basis sets. Results for "naked", non-embedded clusters are shown (left column) together with clusters embedded with point charges (PCs) (middle), and clusters embedded with a combination of PCs and effective core potentials (ECPs) (right). PHF: periodic HF calculations. Basis set 1: O, H, Cl = 6-311G*, Na = 6-31G; Basis set 2: all = cc-pVTZ; Basis set 3: O, H = 6-311G*, Cl = 86-311G, Na = 8-511G.

Hartree-Fock calculations were performed with one particular basis set at a low coverage of $\frac{1}{8}$ ML. The difference between E_{ads}^{HF} with the largest embedded cluster and with periodic Hartree-Fock is 12 meV, further demonstrating that a clear understanding of the sensitivity of E_{ads}^{HF} to cluster size has been determined and that the embedding scheme employed here allows for the missing long range electrostatic

potential at the adsorption site to be recovered.

Now we move on to the electron correlation contribution, $E_{\rm ads}^{\rm corr}$, to the adsorption energy, computed at this stage with MP2. The first thing that is clear from Figure 6.4d-f is that $E_{\rm ads}^{\rm corr}$ is quite insensitive to the different clusters used. It can be seen that even before embedding the variation of $E_{\rm ads}^{\rm corr}$ for the different clusters is less than 36 meV. Nonetheless, embedding helps to reduce the dependence on cluster size slightly to 22 and 28 meV for embedding with PCs and PCs plus ECPs, respectively. The weak dependence of $E_{\rm ads}^{\rm corr}$ to cluster size likely reflects the local nature of electron correlation in adsorption on a wide band gap material like NaCl [195].

Overall, the results reported here reveal that through embedding it is possible to obtain a clear understanding of both the Hartree-Fock and correlation (MP2) contributions to the adsorption energy. Indeed, it is clear that the smallest Na_5Cl_5 cluster, when suitably embedded, already provides for water adsorption a rather good model of NaCl(001). We now use this cluster to do better quality calculations. Specifically we address three important and related issues, namely, basis set incompleteness, the question of which electrons need to be correlated, and an improvement upon the MP2 treatment of electron correlation.

6.4.2 Basis Set Extrapolations

So far we have mostly employed rather small basis sets which permitted the examination of rather large NaCl clusters. Now we focus on adsorption on the embedded Na_5Cl_5 cluster and employ considerably larger basis sets which enable extrapolation to CBS. To this end, we employ Dunning's correlation consistent basis sets (cc-pVXZ, aug-cc-pVXZ, and aug-cc-pCVXZ (X= 3, 4, 5)) along with standard heuristic extrapolation schemes [196, 197]. Specifically, for extrapolation of the Hartree-Fock part we use:

$$E_X = E_{\rm CBS}^{\rm HF} + Ae^{(-BX)} \quad , \tag{6.3}$$

and for the correlation part:

$$E_{\rm CBS}^{\rm corr} = \frac{X^3}{X^3-(X-1)^3}E_{(X)} - \frac{(X-1)^3}{X^3-(X-1)^3}E_{(X-1)} \quad , \tag{6.4}$$

where E_X is the energy computed with the corresponding basis set (X= 3, 4, 5), $E_{\rm CBS}$ is the energy at the CBS limit, and A and B are fitting parameters. As input to the extrapolation we use BSSE corrected triple-, quadruple-, and pentuple-ζ data for Hartree-Fock and BSSE corrected triple- and quadruple-ζ data for the (MP2) electron correlation. All BSSE corrections have been carried out with the Counterpoise method of Boys and Bernardi [60]. Using the above scheme we obtain CBS HF and MP2 correlation contributions to the adsorption energy of 191 and 244 meV, respectively. This leads to a preliminary estimate of the adsorption energy of 435 meV. Later, when attempting to place error bars on our computed adsorption energy, we will attempt to assess the quality of the CBS extrapolations provided by Eq. (6.3) and Eq. (6.4).

6.4.3 Sub-Valence Electron Correlation

Until now in the (MP2) correlation calculations only the valence electrons of each element have been correlated. This is the so-called "frozen core" approach which often provides a good compromise between accuracy and computational effort [198]. However, when high precision is required in, e.g., the calculation of binding energies, sub-valence correlations can make non-negligible contributions, especially for alkali group elements [199, 200, 201, 202]. To address the importance of sub-valence electron correlation, several full electron correlation calculations were performed along with a careful series of tests in which individual shells of electrons of the various elements were either correlated or frozen. These tests revealed a large difference between the valence only correlation and full electron correlated calculations of 62 meV (Table 6.3). Upon closer inspection, we find that the difference of 62 meV is mainly caused by the Na $2s$, $2p$ states. As can be seen from Table 6.3 activating Na $2s$, $2p$ electrons while keeping the Cl and O cores frozen almost all of the missing correlation contribution to the adsorption energy is recovered. Taking this 62 meV contribution from core-valence electron correlation, we arrive at an updated value of the adsorption energy of 497 meV.

Table 6.3: Variation of $E_{\text{ads}}^{\text{corr}}$ (at the MP2 level) on the electrons correlated and frozen in the system for water adsorption on an embedded Na_5Cl_5 cluster.

elements	frozen	correlated	$E_{\text{ads}}^{\text{corr}}$ (CBS)
O	$1s$	$2s$, $2p$	
Cl	$1s$, $2s$, $2p$	$3s$, $3p$	244
Na	$1s$, $2s$, $2p$	$3s$	
O	$1s$	$2s$, $2p$	
Cl	$1s$, $2s$, $2p$	$3s$, $3p$	303
Na	$1s$	$2s$, $2p$, $3s$	
O	none	$1s$, $2s$, $2p$	
Cl	"	$1s$, $2s$, $2p$, $3s$, $3p$	306
Na	"	$1s$, $2s$, $2p$, $3s$	

6.4.4 Beyond MP2 for Electron Correlation

To evaluate the effect of higher level correlations beyond the MP2 level, CCSD(T) has been applied to this system. CCSD(T) calculations are obviously computationally very expensive, scaling as $\sim N^7$, where N is the number of basis functions. Therefore, we limit the CCSD(T) calculations to the triple–ζ level and make use of the so-called ΔCCSD(T) scheme [203] to obtain an indication of the CCSD(T) adsorption energy at the CBS limit. This scheme simply relies on the fact that the MP2 and CCSD(T) binding energies exhibit similar convergence with respect to basis set size, and so by determining the difference of between MP2 and CCSD(T) at one particular basis set one can obtain an indication of the CCSD(T) at complete basis set limit. Upon doing this at the triple-ζ level a difference of 10 meV in $E_{\text{ads}}^{\text{corr}}$ between CCSD(T) and MP2 was obtained. Specifically, $E_{\text{ads}}^{\text{corr}}$ is 10 meV less with

CCSD(T), thus leading to a reduced adsorption energy at the ΔCCSD(T) CBS level of 487 meV.

6.4.5 Bringing it All Together

Table 6.4 lists the various contributions to the adsorption energy. Summing all the contributions leads to our best estimate of the adsorption energy on the embedded Na_5Cl_5 cluster of 487 meV. This value represents adsorption without any contributions from relaxation of the substrate. In section 6.3 we established that DFT provides a consistent picture for the relaxation contribution to the adsorption energy: ≈30 meV with the LDA, PBE, and RPBE *xc* functionals. Therefore, we estimate that the adsorption energy of a water monomer on the relaxed NaCl slab is ≈517 meV. Having arrived at these estimates through a series of necessary steps, we now attempt to establish appropriate error bars for the results obtained.

Table 6.4: A breakdown of the various contributions to the water molecule adsorption energy on an embedded Na_5Cl_5 cluster, as a model for NaCl(001).

Contribution	Value (meV)
HF/CBS	191
Correlation/CBS (MP2)	244
Core-valence electron correlation	62
ΔCCSD(T)	-10
Best estimate (fixed slab)	487
Best estimate (relaxed slab)	517

6.5 Establishing "Error Bars" for the Adsorption Energy

We now perform a detailed analysis of the various factors and assumptions made that might influence our estimated adsorption energy. Based on this, error bars are estimated for the adsorption energy and an indication of how close to chemical accuracy we have come is given.

6.5.1 The Structure of the Adsorbed Water Molecule

The first possible factor which could lead to errors in the estimated adsorption energy is likely to come from the structure of the water molecule adsorbed on NaCl(001). As we have said, in the cluster calculations we have adopted the DFT-PBE structure. This was a somewhat arbitrary choice, necessitated by the fact that full geometry optimizations for this adsorption system with something beyond DFT and with a suitably large basis set is exceptionally expensive computationally. To evaluate the sensitivity of the adsorption energy obtained to the structure employed, single

point calculations at MP2/cc-pVTZ level were performed on the optimized LDA and RPBE structures structures as well as a full geometry optimization with MP2 (with fixed Na and Cl atoms). The adsorption obtained from the MP2 optimization is very close to the one obtained from the PBE and RPBE optimized structures with the differences are 12 and 9 meV while the value from MP2 is larger. However, we do see a big difference between LDA optimized structure and the one from MP2, with the adsorption energy on the LDA structure is 63 meV less that MP2. Therefore, we see that for this system adopting the PBE structure proved not be an unreasonable choice for the subsequent explicitly correlation calculations. Before moving on it is, of course, appropriate to caution that the MP2 optimization was performed with the frozen core option and with only a medium sized triple zeta basis set.

6.5.2 Basis Set Extrapolations

For the basis set extrapolations in section 6.4, the particular procedure embodied in Eq. (6.3) and Eq. (6.4) was applied. However, there are a variety of popular extrapolation schemes, some of which which we test now in order to assess the sensitivity of the CBS extrapolation to the methods employed [204, 205, 206]. Specifically, as an alternative for the Hartree-Fock extrapolation procedure of Eq. (6.3), we use:

$$E_X = E_{\mathrm{CBS}}^{\mathrm{HF}} + AX^{-B} \quad . \tag{6.5}$$

And as alternatives for the extrapolation of the correlation contribution of (2) we use

$$E_X^{\mathrm{corr}} = E_{\mathrm{CBS}}^{\mathrm{corr}} + AX^{-2.4} \quad , \tag{6.6}$$

and

$$E_{\mathrm{CBS}}^{\mathrm{corr}} = E_X^{\mathrm{corr}} + A/(X+1/2)^3 \quad , \tag{6.7}$$

where each term in Eq. (6.5)-(6.7) has the same meaning as in Eq. (6.3) and Eq. (6.4). For the Hartree-Fock extrapolation, Eq. (6.3) and Eq. (6.5) are very popular non-linear three-parameter extrapolation schemes. For the electron correlation extrapolation, we are limited to two-point schemes as our data set for the extrapolation is limited to two points: Eq. (6.4) is a widely used X^{-3} extrapolation, and Eq. (6.6) and (6.7) are alternative two-point extrapolation schemes recently proposed [207, 208]. The results obtained from the various extrapolation schemes for $E_{\mathrm{CBS}}^{\mathrm{HF}}$ and $E_{\mathrm{CBS}}^{\mathrm{corr}}$ are listed in Table 6.5. For the Hartree-Fock extrapolation, the two schemes tested give binding energies which differ by only 5 meV. The difference among the three extrapolation schemes for $E_{\mathrm{CBS}}^{\mathrm{corr}}$ is likewise small at 3 meV. Although these tests do not represent an exhaustive analysis of all available extrapolation schemes, the similar results obtained with the various CBS extrapolations indicates that the total adsorption energy obtained here is unlikely to be subject to basis set errors in excess of 10 meV.

Table 6.5: $E_{\mathrm{CBS}}^{\mathrm{HF}}$ and $E_{\mathrm{CBS}}^{\mathrm{corr}}$ as obtained by various extrapolation schemes with cc-pVXZ (X = 3, 4, 5) and aug-cc-pVXZ (X = 3, 4) basis sets, respectively.

Method	$E_{\mathrm{CBS}}^{\mathrm{HF}}$ (meV)	$E_{\mathrm{CBS}}^{\mathrm{corr}}$ (meV)
Eq. (6.3)	191	
Eq. (6.5)	196	
Eq. (6.4)		244
Eq. (6.6)		247
Eq. (6.7)		245

6.5.3 Electron Correlation and the ΔCCSD(T) Approach

In section 6.4, we applied the so-called ΔCCSD(T) approach in order to move beyond the MP2 treatment of electron correlation. This approach relies on a similar convergence behavior of the MP2 and CCSD(T) binding energies with respect to basis set size. Because similar convergence behavior is often observed ΔCCSD(T) has proved useful for specific systems in which high accuracy binding energies are required but CCSD(T) calculations with basis sets larger than double- or triple-ζ are prohibitively expensive [203, 209]. However, the precise accuracy of the ΔCCSD(T) approach is not known for water adsorption on NaCl(001). To investigate this we performed a series of calculations on a model system comprising a Na cation and a water molecule, i.e., $(\mathrm{Na—H_2O})^+$. Furthermore, the exact adsorption structure identified from the water/NaCl calculations was adopted. This model system is small enough to allow CCSD(T) calculations with large basis sets to be performed while at the same time resembling, to some extent, the water/NaCl adsorption system. For this system, two parallel sets of calculations were carried out with MP2 and CCSD(T) with cc-pCV(T,Q)Z basis sets for Na^+, aug-cc-pCV(T,Q)Z basis sets for O, and aug-cc-pV(T,Q)Z basis sets for H. As for water monomer adsorption on NaCl(001), Eq. (6.4) has been used for extrapolation of the electron correlation energy contribution to the binding energy ($E_{\mathrm{bind}}^{\mathrm{corr}}$). Again all calculations have been corrected for BSSE errors with the Counterpoise method.

The results are shown in Table 6.6. For this system the correlation contribution to the binding energy is 39 and 41 meV with MP2 and CCSD(T), respectively at the triple zeta level, i.e., the difference between MP2 and CCSD(T) is only 2 meV. At the CBS limit this difference is similar, 3 meV. Thus for the model $(\mathrm{Na—H_2O})^+$ system the ΔCCSD(T) approach introduces a negligible error compared to a full CCSD(T)/CBS calculation. This suggests that the ΔCCSD(T) correction is, at least, not unsuitable for estimating the CCSD(T)/CBS value for water on NaCl as we have done here.

As a final point we note that we have also performed a full CCSDT calculation for the $(\mathrm{Na—H_2O})^+$ system and in so doing go beyond the perturbative treatment of the connected triple excitations. For this comparison, a triple zeta basis set was employed and the difference between CCSD(T) and CCSDT was only 1 meV. Thus for this particular system going beyond CCSD(T) does not appear to be necessary.

Table 6.6: Evaluation of the ΔCCSD(T) approach on $(Na—H_2O)^+$ with the $(Na—H_2O)^+$ structure taken from the H_2O/NaCl adsorption system. cc-pCV(T,Q) basis sets were used for Na, aug-cc-pCV(T,Q)Z basis sets for O, and aug-cc-pV(T,Q)Z basis sets for H. All electrons in the system are correlated and results are corrected for BSSE errors. Extrapolation was done with Eq. (6.4).

Method	Basis Set	$E_{\text{bind}}^{\text{corr}}$ (meV)
MP2	TZ	39
	QZ	45
	CBS	49
CCSD(T)	TZ	41
	QZ	47
	CBS	52
ΔCCSD(T)	TZ	2
CCSD(T)-MP2	CBS	3

6.5.4 The Final Error Estimate

Now we sum up the individual errors and try to put a final error bar on the adsorption energy estimate of 517 meV. First, we have the issue of the cluster szie. For the final adsorption energy estimate the embedded Na_5Cl_5 cluster was used. For this embedded cluster it was estimated that finite size errors are on the order of 20 and 22 meV at the Hartree-Fock and MP2 levels, respectively. Second, we concluded in section 6.5.1 that the error introduced by adopting the PBE adsorption structure was likely to be around 12 meV. From the basis set extrapolation and ΔCCSD(T) approach there is a further 10 meV. Thus we arrive at a final error bar of ±62 meV. This is likely to be conservative estimate. Moreover, the largest errors come from cluster size effects for which we know from Figure 6.4 how larger clusters perform. Specifically we find that larger clusters predict larger adsorption energies and so it is most likely that the true value for the adsorption energy will be on the larger binding side of the 517±62 meV range.

6.6 Discussion

Having arrived at a value for the adsorption energy of 517±62 meV, which we believe improves considerably on the alternative initial range from DFT of 286 to 640 meV, it is, of course, interesting to compare this value to experiment. Unfortunately, however the majority of the experimental measurements obtained for water on NaCl(001) relate to higher coverage, specifically the 2D (1×1) and c(4×2) structures. In this regime heats of adsorption of 50–60 kJ/mol (518–612 meV/H_2O) have been obtained [26, 210]. The only available experimental estimate of the adsorption energy for a low coverage of water monomers on NaCl(001) to have been reported comes from the HAS study of Bruch *et al.* [19], where a value of 63 kJ/mol (653 meV/H_2O) was reported for water monomers in the temperature range 140 to 150 K. This is noticeably larger than the 517±62 meV obtained in the current work. When

striving to bridge the gap between the computed adsorption energy and measured adsorption enthalpy, it is necessary to take into account the zero point contribution to the adsorption energy (∼80 meV)[2] and finite temperature effects (∼50 meV). Correcting for these effects, our estimated adsorption enthalpy at 145 K becomes 387 meV. This is about 263 meV less than the experimental value and well outside our estimated error bar on the adsorption energy. We suggest, therefore, that the value reported for water monomer adsorption does not correspond to water adsorption on perfect terrace but instead adsorption at defective sites. Indeed, Bruch *et al.* were also somewhat suspicious of their large adsorption energy in the low coverage regime stressing how "It is difficult to derive the adsorption energy of a very low coverage layer from the isotherms because heterogeneities and defect site effects may then be dominant in the data." Indeed, it is known from AFM studies that water molecules preferentially adsorb on defect sites such as steps or kinks on NaCl(001) [211, 212].

To specifically investigate the influence of water adsorption at defect sites in the low coverage regime a series of DFT-PBE studies have been performed for water adsorption at monoatomic (100) steps. Several different adsorption structures were considered with the water molecule at various locations and orientations. The most stable adsorption structure is the one shown in Figure 6.5. In this structure the oxygen of the water molecule is located between two Na atoms with its molecular dipole plane directed away from the surface. The PBE adsorption energy obtained for this structure is 540 meV, which is 157 meV larger than the PBE adsorption energy on the perfect terrace. Taking this 157 meV as a rather crude correction to our finite temperature adsorption enthalpy leads to an approximate adsorption enthalpy at steps site on NaCl of 544 meV, which is somewhat closer to the experimental estimate. However, it remains ∼100 meV smaller than the experimental value, a difference that we cannot at present reconcile. A set of experiments specifically aimed at determining the adsorption energy of water monomers on terraces of NaCl with, for example, microcalorimetry [163] would be highly beneficial in resolving this discrepancy.

Finally, we close by comparing the adsorption energies obtained with the various *xc* functionals to the benchmark value of 517 meV. Clearly at 286 and 383 meV the RPBE and PBE functionals predict too weak an adsorption energy, where at 640 meV the LDA functional overbinds by 123 meV. This is largely consistent with what is known about the performance of these *xc* functionals for weakly interacting systems [213]. However, the finding that of the three *xc* functionals tested LDA comes closet to the quantum chemistry result is quite unexpected. Certainly this is accidental agreement, reminiscent of the superior performance of LDA over PBE in certain van der Waals systems such as graphite or the inert gases [214, 215]. Given the very bad performance of LDA for H bonded systems [216], future simulations

[2]The phonon frequency calculations have been carried out by using the harmonic approximation at the Gamma point of the vibrational Brillouin zone with the finite displacement method for LDA, PBE, and RPBE functionals at $\frac{1}{8}$ ML coverage. The zero point vibration contribution to the adsorption energy is 89, 69, and 71 meV for LDA, PBE, and RPBE, respectively. The average value of these three is 80 meV.

with LDA for, e.g., water clusters or liquid water on NaCl are not recommended. It will be interesting to see how other functionals, in particular hybrid functionals such as PBE0 or B3LYP, perform for this adsorption system. Indeed, this will be discussed in the next chapter.

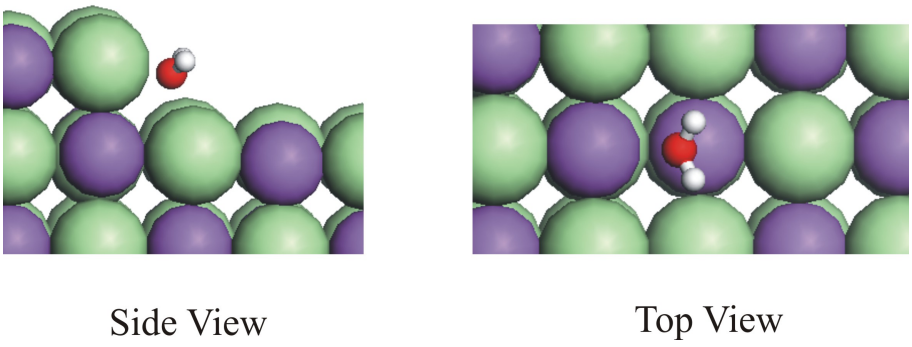

Figure 6.5: The most stable structure of the water molecule adsorbed at a monoatomic (100) step on NaCl(001), obtained from DFT-PBE calculations. The purple, green, red, and white spheres are Na, Cl, O, and H atoms respectively.

6.7 Summary

In summary, through an extensive set of DFT and explicitly correlated quantum chemistry calculations for water adsorption on NaCl, we have obtained an estimate of the adsorption energy of a water monomer on salt of 517 meV. A detailed analysis of the possible errors associated with this estimate gives an error bar of ± 62 meV, with the true value most likely to be on the larger binding side of this error bar. The value reported falls between those predicted by LDA and PBE.

In the future, it will be interesting to see how other functionals, in particular hybrid functionals perform for this adsorption system. It will also be interesting and important to reduce the error bars on the adsorption energy obtained here below the current value of 62 meV and reconcile the discrepancy between experiment and theory.

Chapter 7

Hybrid xc Functionals for Water Adsorption on NaCl(001) and Electronic Structure Analysis

7.1 Introduction

In chapter 6, quantum chemistry methods were used to obtain a high precision estimate of adsorption energy of a water molecule on NaCl(001) together with comparisons with DFT GGA (PBE, RPBE) and LDA results. To further explore the influence from different exchange-correlation functionals, hybrid functionals are employed. Hybrid functionals, such as B3LYP [92, 93] and PBE0 [95], are of interest because of the considerably improved performance these functionals offer over regular GGAs for the energetics of atoms and small molecules in the gas phase [217, 218, 219, 220]. For this reason hybrid functionals, especially B3LYP, have been widely used for the calculations of atomic and molecular systems by the quantum chemistry community for many years.

Recently, the application of hybrid functionals to extended periodic systems with plane-wave basis sets has been introduced [221, 222, 223]. The comparisons between hybrid functionals and regular GGAs show improved performance in some aspects such as lattice constants, bulk moduli, and atomization energies [221] of insulators and semiconductors. In addition, improved performance in adsorption has been observed [3, 168]. It is thus interesting to evaluate the performance of certain hybrid functionals for water adsorption on NaCl surfaces and see if they can yield adsorption energies in better agreement with the reference values obtained in chapter 6. Here we use B3LYP and PBE0 to calculate the adsorption energy of water on NaCl(001) at low coverage. The main conclusion from these calculations is that the hybrid functionals *do not* offer any clear improvement over the functionals tested in chapter 6. Indeed, the results obtained from B3LYP and PBE0 are within 30 meV of their regular GGA counterparts, BLYP and PBE.

A second aspect of this chapter is that we analyze the nature of electronic structure that lies behind this adsorption system. Although extensive DFT and quantum chemistry studies have been performed for water/NaCl(001), we still have not ad-

dressed what the nature of the interaction between water and NaCl(001) is. Electrostatics are believed to dominate this adsorption bond [20, 224], but whether there is any covalent interaction or H bonding interaction between H_2O and the Cls remains unclear. To answer these questions, information from electron density differences, density of states (DOS), partial density of states (PDOS), Mulliken charges, and electron localization functions (ELF) [225] are collected to give an understanding of the interaction between water and NaCl(001).

7.2 Computational Details

DFT calculations reported in this chapter are very similar to those reported in chapter 6 except that they have been performed with the CPMD code [226]. Periodic B3LYP, PBE0, BLYP, and PBE calculations have been performed. The electron-ion interactions are described with norm-conversing pseudopotentials and expanded up to a 180 Rydberg plane-wave cut-off energy. PBE pseudopotentials have been used for the PBE and PBE0 calculations, and likewise BLYP pseudopotentials have been used for BLYP and B3LYP calculations. A four layer thick NaCl slab separated by 15 Å of vacuum space in a 2×2 unit cell ($\frac{1}{4}$ ML) has been used. Brillouin zone sampling was performed at the Γ point only. During the structure optimization, the four layer NaCl slab was fixed and only the water molecule was allowed to relax. The experimental lattice constant was adopted.

7.3 Hybrid Functional Calculations

Table 7.1 lists the adsorption energies and selected structural parameters obtained with the B3LYP and PBE0 *xc* functionals. For the purpose of comparison the results obtained with BLYP and PBE are also reported. From Table 7.1, it is clear that the

Table 7.1: The adsorption energy, E_{ads}, computed from B3LYP and PBE0 together with BLYP and PBE with a fixed slab at $\frac{1}{4}$ ML. Three key structure parameters (in Å) of water on NaCl(001) which have been defined in Table 6.1 are also included.

Functional	E_{ads} (meV)	$d_{\text{O—Na}}$	$\perp_{\text{O}}$	$d_{\text{Cl—H}}$
PBE	326	2.45	2.33	2.55
PBE0	317	2.42	2.31	2.58
BLYP	230	2.48	2.39	2.66
B3LYP	259	2.44	2.34	2.66

adsorption energies obtained from PBE0 and B3LYP are similar to those obtained from PBE and BLYP with the difference between them being 9 and 29 meV, respectively. Therefore, the adsorption energies of B3LYP (259 meV) and PBE0 (317 meV) are still far away from the benchmark results obtained in the previous chapter (487 meV on a frozen NaCl slab). Considering the much larger computational cost for the hybrid functional calculations over LDA or GGA calculations, the results

are somewhat discouraging and the use of the hybrid functionals for this system is clearly not worth the effort.

Likewise, the predicted structural parameters from the hybrid functionals are also very close to the values obtained from the corresponding GGA functionals. In detail, the difference between B3LYP and BLYP distances are within 0.05 Å of each other and PBE0 and PBE values within 0.03 Å of each other. So there is no obvious improvement from the hybrid functionals over the GGAs for both energetics and structures for the adsorption of water on NaCl(001). Indeed, of all the functionals tested in this chapter and the preceding one LDA predicts the adsorption energy in best agreement with the quantum chemistry result.

7.4 Electronic Structure Analysis

The basic ingredients of water adsorption on NaCl(001), such as the structure and energetics have now been discussed in detail. The focus of this section is to start to elucidate the nature of the interaction between the water molecule and NaCl(001). To this end we analyze the electronic structures that lie behind the DFT calculations with a variety of analysis tools such as electron density differences, total and partial density of states, Mulliken population analysis, and electron localization functions. This analysis has been performed with both the LDA and PBE *xc* functionals.

To begin, electron density differences ($\Delta\rho$) plots are displayed in Figure 7.1 for both PBE and LDA *xc* functionals. $\Delta\rho$ is defined as:

$$\Delta\rho = \rho_{\text{water/slab}} - \rho_{\text{slab}} - \rho_{\text{water}} \quad , \tag{7.1}$$

where $\rho_{\text{water/slab}}$ is the density of the adsorption system, ρ_{slab} is the density of the clean surface, and ρ_{water} is the density of the water molecule. The electron density difference plots provide a general overview for how the total density of the water molecule and the NaCl surface rearrange upon formation of the adsorption bond. The first thing that is clear from Figure 7.1 is that the electron density differences are similar for LDA and PBE, with only marginally larger charge rearrangement in the case of LDA. Considering the nature of the electron density rearrangement two planes (P1 and P2 in Figure 7.1) in $\Delta\rho$ are displayed. Both planes are perpendicular to the surface with P1 bisecting an O–Na plane and P2 an O–H–Cl plane. The $\Delta\rho$ plots reveal a polarization of charge on the O and Na atoms with a build up in electron density just beneath the O and a depletion in electron density just above the Na (P1). Overall it appears that electron density is transferred from Na to water. This interpretation is consistent with the Mulliken charge analysis shown in Table 7.2 which indicates that the adsorbed water molecule has acquired 0.1 e from the Na atom of the substrate. The Mulliken charge transfer with the LDA and PBE *xc* functionals are essentially the same. A second feature of the adsorption bond that is clear from $\Delta\rho$ along P2 is the presence of an O–H$\cdots$Cl interaction. Specifically, there is a region of charge depletion on the H with a build up in density just above the Cl. Charge rearrangement such as this is reminiscent of hydrogen bond formation. For example, DFT electron density difference plots for the hydrogen

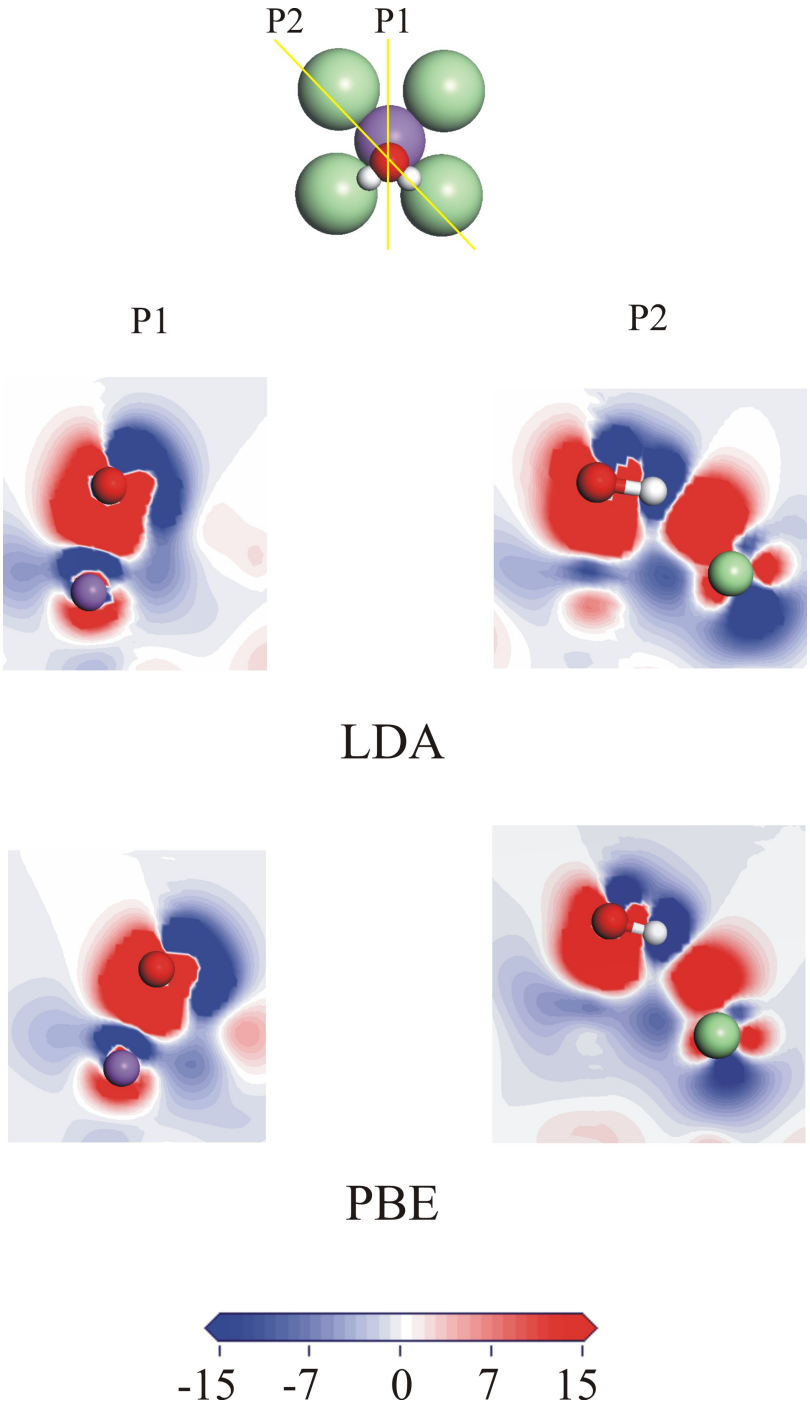

Figure 7.1: Electron density difference ($\Delta\rho$) contours for water/NaCl(001) computed with the LDA and PBE functionals at $\frac{1}{8}$ ML coverage. Here $\Delta\rho = \rho_{\text{water/slab}} - \rho_{\text{slab}} - \rho_{\text{water}}$, where $\rho_{\text{water/slab}}$ is the density of the adsorption system, ρ_{slab} is the density of the clean surface, and ρ_{water} is the density of the water molecule, each is in the precise positions they adopt in the adsorption system. Two 2D cuts are shown (P1 and P2) as indicated by the cartoon on the top. The units are in 10^{-4}eÅ^3. The purple, green, red, and white spheres are Na, Cl, O, and H atoms respectively.

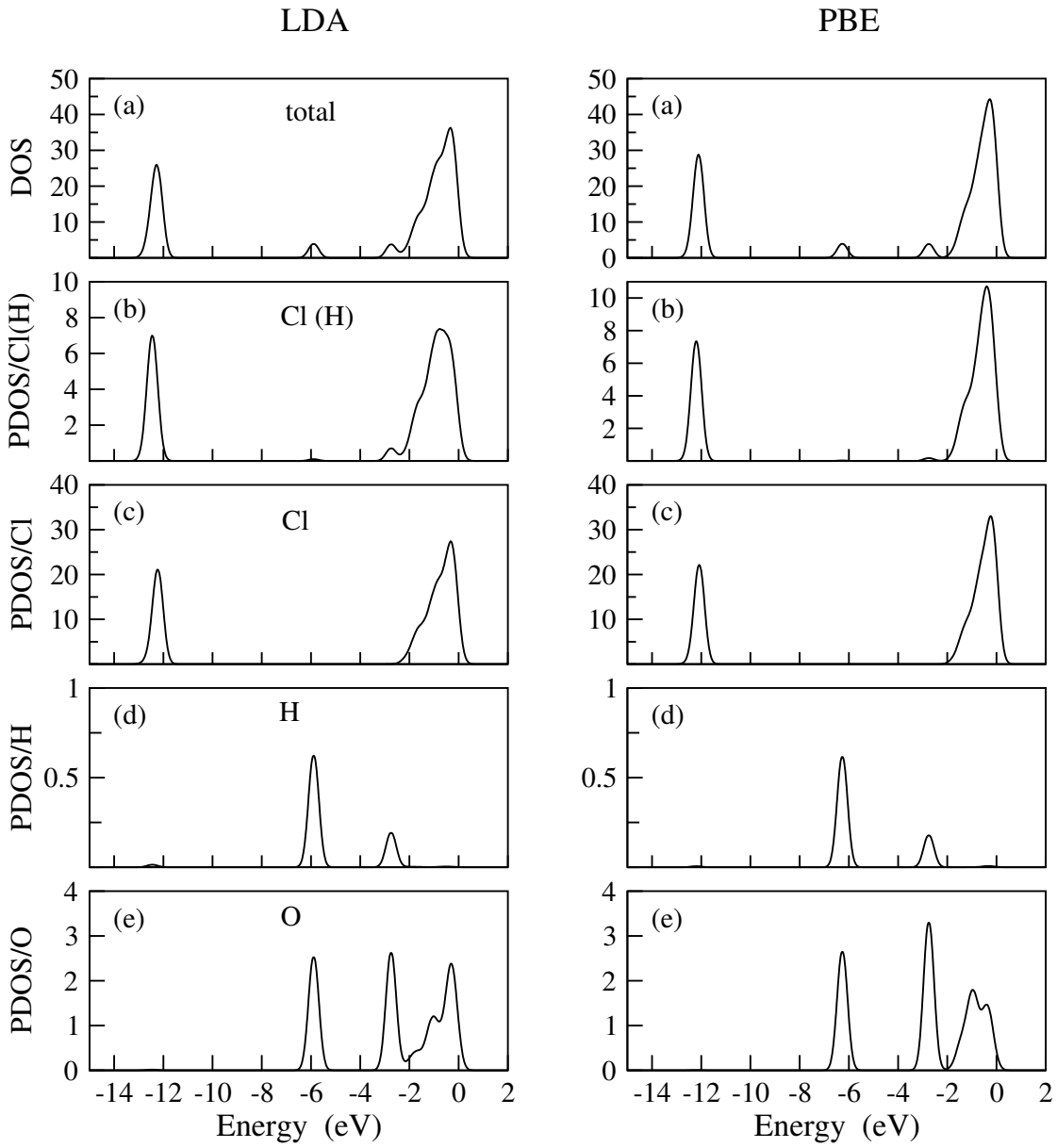

Figure 7.2: Density of states (DOS) and partial density of states (PDOS) for the valence electrons of water/NaCl(001) obtained from LDA and PBE. Units are electrons/eV. (a) Density of states of the top layer of NaCl(001) and adsorbed water molecule. (b) Partial density of states of the Cls which are interacting with Hs in water molecule. (c) Partial density of states of the surface Cls not directly interacting with water. (d) Partial density of states of H. (d) Partial density of states of O. The energy zero is the valence band maximum.

Table 7.2: Mulliken charges (e) for water/NaCl(001), bare NaCl(001) (top layer), and the water molecule in the gas phase.

Functional	O	H	Cl(H)	Cl	Na
water/NaCl(001)					
LDA	-0.90	0.39	-0.53	-0.53	0.67
PBE	-0.91	0.40	-0.58	-0.59	0.71
NaCl(001)					
				Cl	Na
LDA				-0.53	0.56
PBE				-0.58	0.60
water molecule in gas phase					
LDA	-1.08	0.54			
PBE	-1.05	0.53			

bond in the water dimer exhibit a similar decrease in density on the H atom involved in the hydrogen bond with an associated build up in density in the intermolecular region between the O and H atoms [227]. This leads to the suggestion that part of the water/NaCl interaction is mediated by a weak hydrogen bond between the hydrogen atoms and the chlorines. This interpretation is also consistent with the finding in chapter 6 that adsorption structure (a)—with the Hs directed at the Cls—is more stable than (b)—with the Hs directed at the neighboring Nas—as shown in Figure 6.1.

So far a picture based on electrostatics and charge transfer (including hydrogen bonding) appears to explain the adsorption bond. To determine whether there is any covalent nature to the adsorption bond a careful analysis of the total and partial densities of states has been performed as well as an analysis of the electron localization function in this system. First the DOS and PDOS analysis, which is reported in Figure 7.2, is discussed. Again the DOS and PDOS obtained with LDA and PBE are similar, each exhibiting a large conduction band peak 2–3 eV wide and a second large peak ∼13 eV below the valence band maximum, with two smaller peaks in between. Upon inspection of the PDOS for each type of atom in the adsorption system, it is found that the valence band is comprised of Cl $3p$ states and the large peak at ∼13 eV below the valence band maximum is comprised of Cl $3s$ states. The O and H PDOS plots (Figure 7.2(d)-(e)) reveal that there are essentially three water related states in the energy interval depicted. Examination of the individual Kohn-Sham eigenstates associated with each of the water resonances reveals that these are, in order of increasing energy, the $1b_2$, $3a_1$, and $1b_1$ states. These are the three highest occupied orbitals of water and essentially no mixing of these states with the substrate is observed. The only small mixing present is, in the case of LDA, at about -3 eV between the Cl involved in the hydrogen bond and the bottom of the $3a_1$ resonance. Thus, from the DOS and PDOS analysis no significant covalent interaction of the water with the substrate is observed.

The ELF [225, 228] provides a powerful approach to distinguish electrostatic and covalent interactions. The range of values for the ELF is between 0 and 1, with the

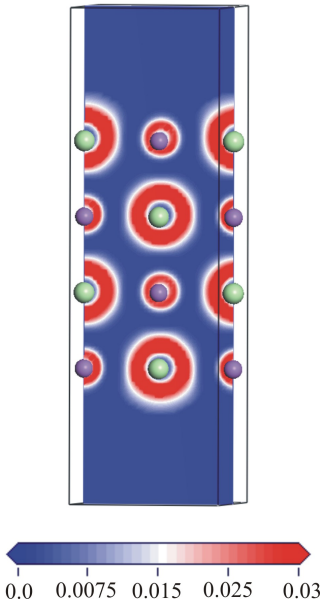

Figure 7.3: The ELF of a 4-layer clean NaCl(001) as obtained with DFT-PBE. The 2D cut is through (010) direction and perpendicular to the surface. The unit cell was turned around by a small angle to facilitate the view.

high values of ELF indicating well localized electrons which could be part of a chemical bond, atomic shell, or lone pair[1]. An example of an ELF plot computed with PBE for the clean 4-layer NaCl slab is shown in Figure 7.3. The shell structure for each Na and Cl, which is $2s$, $2p$ for Na and $3s$, $3p$ for Cl (given the pseudopotentials employed), is clearly observed. In the interatomic regions the ELF quickly goes to zero characteristic of an ionically bonded solid. Returning now to the water adsorption system, the ELFs from LDA and PBE are plotted in Figure 7.4. The same two planes used for the $\Delta\rho$ analysis are again shown and, as before, the features observed are similar for LDA and PBE. From the ELF plots of the adsorption system the Na and Cl atomic shell structure is again clear as is the lone pair character of the $3a_1$ orbital. Further, consistent with the PDOS analysis there is no indication of covalent bond formation with the ELF going to zero in the internuclear O–Na and H–Cl regions. Thus we conclude that in this adsorption system the interaction is mediated through electrostatics and not covalency.

7.5 Summary

In this chapter, the hybrid functionals, B3LYP and PBE0, have been employed to study water adsorption on NaCl(001) and further complement the performance comparisons of different *xc* functionals in the previous chapter. The main conclusion, however, is that we did not find any big difference between the hybrid functionals

[1]Specifically, high ELF values show that at the examined position the electron is more localized than in a uniform electron gas of the same density.

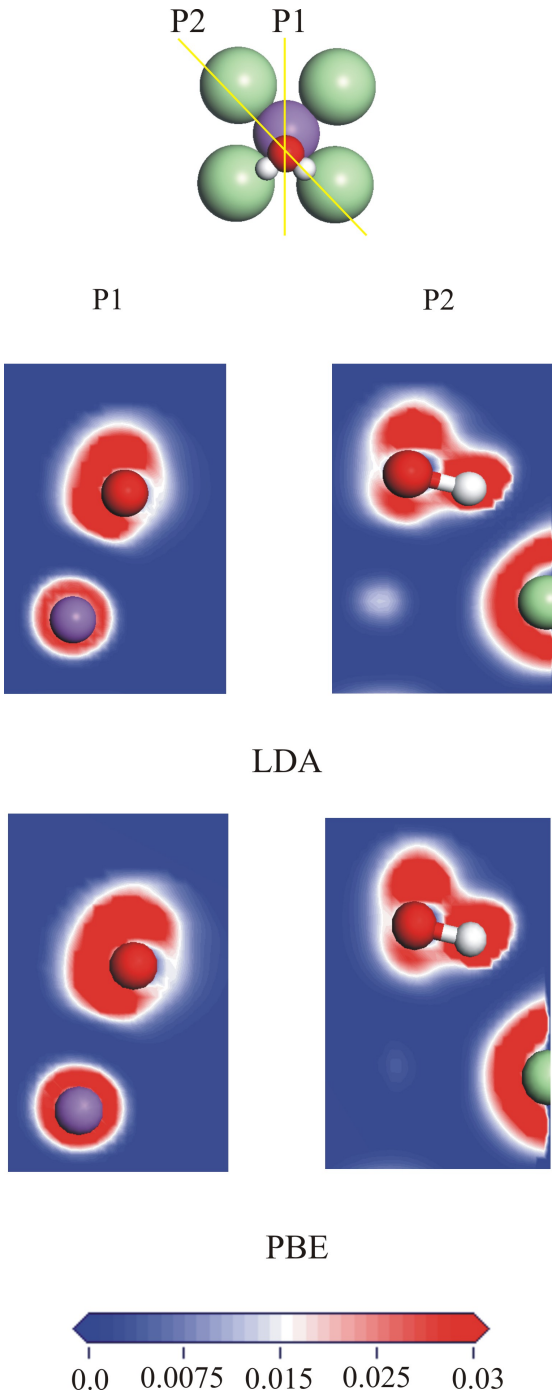

Figure 7.4: ELFs of water on NaCl(001) obtained with the LDA and PBE functionals. The 2D cuts are shown (P1 and P2) as indicated by the cartoon on the top.

and the corresponding GGA functionals (BLYP and PBE). The adsorption energies obtained from the hybrid functionals are still away from the quantum chemistry calculations by ∼228 and ∼170 meV for B3LYP and PBE0, respectively. Thus for this specific system, the hybrid functionals do not offer any clear improvements in performance of the energetics despite their increased computational cost. Similarly, the difference in the optimized structures obtained with the hybrid functionals and their GGA counterparts is small, within 0.05 Å.

To further understand the interaction between the adsorbed water molecule and NaCl(001), electron density differences, Mulliken population analysis, DOS and PDOS, and ELFs have been examined. The main conclusion is that the adsorption bond is dominated by electrostatics and a small charge transfer from Na to water, along with a weak hydrogen bonding interaction with the substrate Cl atoms. For each of these analysis tools the differences between LDA and PBE were small and so the analysis performed to date has not provided any clear specific reason why the LDA adsorption energy is so much larger than that obtained from PBE. Work with symmetry-adapted perturbation theory [229] is currently underway to address this issue.

Summary and Outlook

In this thesis, various electronic structure simulation methods such as density-functional theory and explicitly correlated methods, e.g., Møller-Plesset perturbation theory and coupled cluster have been applied to the several different aspects of surface process on NaCl(001).

First, the properties of bulk NaCl, NaCl(001), and stepped NaCl(001) surfaces have been examined with density-functional theory. The properties of bulk NaCl such as equilibrium lattice constant, bulk modulus, formation energy, and cohesive energy have been computed with the LDA, PBE, and PBE-WC *xc* functionals. The good agreement obtained for these properties with previous experimental and theoretical studies established firm foundations for the subsequent work on NaCl(001). Further, the new PBE-WC functional offers improved performance over both LDA and PBE in the description of key bulk properties such as the equilibrium lattice constant and bulk modulus. However, no clear improvement with PBE-WC over PBE was observed for the energetics properties of bulk NaCl, e.g., the formation energy, cohesive energy, and lattice energy.

When coming to NaCl(001), first the buckling and relaxation of atoms in the surface layer was predicted to be small and the bulk equilibrium interlayer distance has been recovered at the third layer from the surface which is also in good agreement with the corresponding experimental measurements. For the surface energy of NaCl(001), a fundamental property of any surface, the experimental values are old (from the 1960's and before) and differ considerably from each other. For the first time, the surface energy of NaCl(001) has been determined from first principles computations and the range of 9–15 meV/Å^2 was obtained from DFT GGA and LDA calculations. Also the new PBE-WC functional yield a similar surface energy to the PBE functional. In the absence of reliable experimental measurements it is difficult to judge which functional is the most reliable. Some speculations were made that LDA might actually be the most reliable functional of those tested, based on experience from quantum Monte Carlo on Mg(001) and comparisons between DFT and experiment for the surface energy of Pb. This is, however, a clear area where more work would be highly desirable, both from experiment and theory. For example, quantum Monte Carlo or quantum chemistry simulations aimed at establishing more precisely the surface energy of NaCl(001) would be highly desirable.

The step formation energies are crucial to the prediction of the surface morphology. From the current thesis, the step formation energy of monoatomic height steps on NaCl(001) has been predicted to be ∼42 meV/Å from DFT-PBE calculation which is, to my knowledge, the first *ab initio* estimate of the step formation energy

of NaCl(001). The interaction between neighboring steps on NaCl(001) has been predicted to be repulsive and small. Furthermore, the relative stabilities between nonpolar (100) terminated and polar (111) terminated steps have been compared under 1 atm and UHV pressures up to 1000 Kelvin.

One particular highlight of current thesis comes from the studies of the halide atom adsorption on alkali halide surfaces. To a big surprise, both DFT and MP2 indicate that the halogen atoms bond preferentially to halide substrate atoms on a series of alkali halide surfaces (NaF(001), NaCl(001), and NaBr(001)), rather than to the alkali atoms as might be anticipated. An analysis of the electronic structures in each system reveals that this novel adsorption mode is stabilized by the formation of a textbook two-center three-electron covalent bond. This discovery served as an example as to never stop to question some "conventional wisdom". Moreover, this finding has important implications to the initial epitaxial alkali halide crystal growth.

A large part of my PhD work has been dedicated to achieving high accuracy in terms of adsorption energies beyond what is available from current density-functional theory. Or more precisely, moving beyond the typically large range in adsorption energies from different DFT exchange-correlation functionals. To this end, the water adsorption on NaCl(001) was examined as a model system. Considerable efforts have been employed with MP2 and CCSD(T) together with the extrapolation to complete basis set limit and embedding cluster technique to arrive at a reliable estimate of the adsorption energy which is 487 and 517 meV for fixed or relaxed slab. Careful tests on the cluster size, basis set, and core-valence electrons correlation guarantee the high accuracy from our estimate which is close to the "chemical accuracy" to be obtained. This has lead to one of the most reliable theoretical estimates of an adsorption energy of a molecule on a solid surfaces made to date. Further, none of the *xc* functionals tested, those popular in treating adsorption at solid surfaces, such as LDA and PBE, and hybrid functionals (PBE0 and B3LYP) yielded results that were particularly close the quantum chemistry value (>100 meV difference). In particular the hybrid functionals show basically no change from their non-hybrid counterparts.

With regard to water adsorption, there are many clear areas for further study. For example, it would be very exciting to refine the adsorption energy estimate from quantum chemistry. As discussed in section 6.5 there remain error bars of ± 62 meV on the value obtained here. Getting these error bars and closing in on the exact value for the adsorption energy would be well worth doing. Of course, it would be good if an improved experimental measurement of the adsorption energy (such as from microcalorimetry) was to be obtained to provide a real stern test for the theoretical values. In addition it would be interesting to test other DFT *xc* functionals to identify which one was most reliable for water adsorption on NaCl, whilst at the same time predicting other relevant properties (e.g. surface energies, step formation energies) with high precision. More generally, having followed a roadmap to obtain high accuracy estimates of adsorption energies of molecules on insulators, it would be very interested to obtain other benchmark adsorption energies for some other adsorption systems. Indeed, in ongoing work water on LiH(001) is being examined.

In the final chapter, analysis on the electronic structures that lay behind the water adsorption system were performed. This has shed some light on the nature of the interaction between water on salt. The conclusion is that it is mainly electrostatic with some hydrogen bonding contribution. However, there is obviously much scope for understanding this interaction at a deeper level. In particular, it would be important and interesting to understand exactly why such different adsorption energies are obtained with the different *xc* functionals. As part of this work, Symmetry-Adapted Perturbation Theory (SAPT) is now being used.

Appendices

Appendix A Selected Convergence Tests

A.1 NaCl(001) and Defects on NaCl(001)

Some of the tests carried out in order to determine the numerical accuracy of the computational set-up employed for the calculations in chapter 3 and chapter 4 are reported here. Specifically, convergence tests on the dependence of the surface energy on the plane-wave cut-off (Figure A.1(a)) and $\boldsymbol{k}$ point mesh (Figure A.1(b)) used are presented as are convergence tests on the dependence of the ledge energy on the plane-wave cut-off (Figure A.1(c)) and $\boldsymbol{k}$ point mesh (Figure A.1(d)). In all calculations a fixed 4 layer NaCl slab was used and the Monkhorst-Pack $\boldsymbol{k}$ point meshes reported correspond to the sampling per 1×1 surface unit cell. It can be seen from Figure A.1 that our chosen cut-off energy (400 eV) and $\boldsymbol{k}$ point mesh (4×4) yield surface energies and ledge energies converged to within 0.2 meV/Å^2 and 0.5 meV/Å, respectively, of those obtained with a much higher cut-off (1200 eV) and much denser $\boldsymbol{k}$ point mesh (16×16×1).

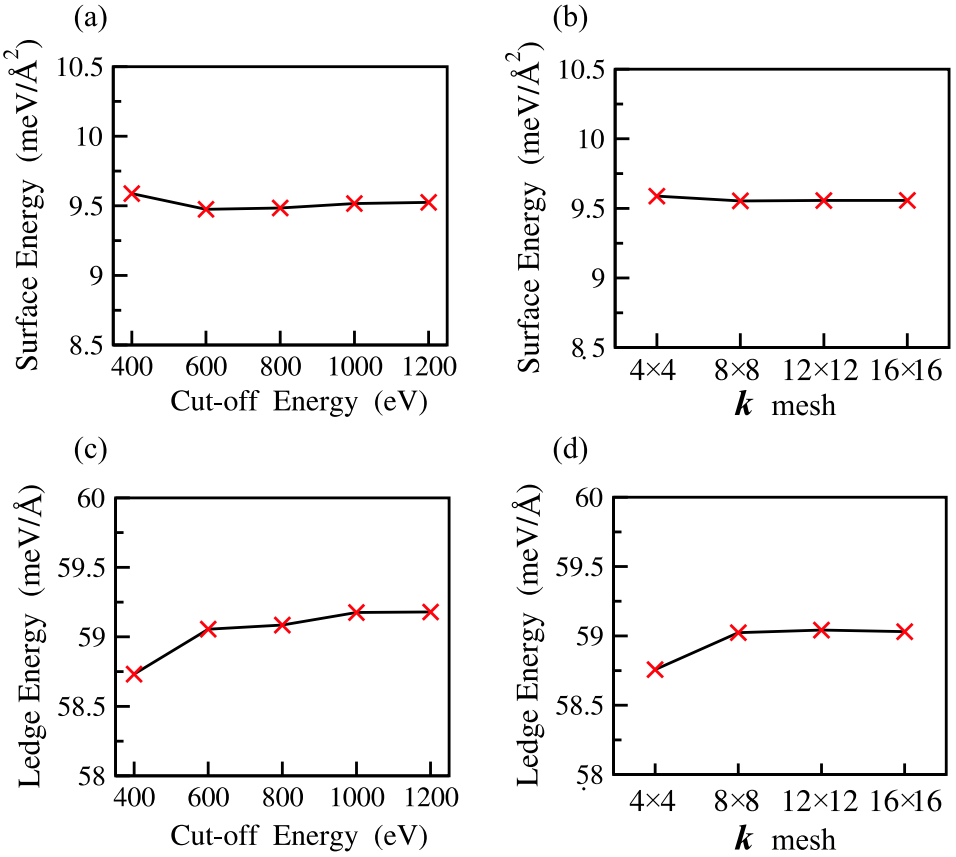

Figure A.1: (a)-(b) Variation of the computed PBE surface energy of a 4 layer NaCl(001) slab with plane-wave cut-off energy (a) and $\boldsymbol{k}$ point mesh (b). (c)-(d) As for (a) and (b) but now for the ledge energy.

A.2 Water on NaCl(001)

Results of some of the tests on the set-up of the periodic DFT calculations reported in chapter 6 are given here. All tests are carried out with the PBE functional and a 1×1 unit cell. Specifically, in Table A.1 results are reported for $\boldsymbol{k}$ point mesh, plane-wave cut-off, vacuum spacing between neighboring slabs in the supercell, and slab thickness. From the table it can be established for this small 1×1 unit cell, the computational setup with 4×4×1 $\boldsymbol{k}$ point mesh, 400 cut-off energy, 15 Å vacuum space, and 4 layer slab could guarantee an accuracy of ∼10 meV.

Table A.1: Selected convergence tests on the computed adsorption energy, E_{ads}, for the periodic DFT(PBE) calculations.

Setup		E_{ads} (meV/H_2O)
$\boldsymbol{k}$ point mesh	4×4×1 (8 $\boldsymbol{k}$)	358
	8×8×1 (32 $\boldsymbol{k}$)	359
cut-off energy (eV)	400	358
	600	362
vacuum space (Å)	15	402
	20	398
slab layer	2 layers	393
	4 layers	402
	6 layers	401

Appendix B Thermodynamic Relations of Non Stoichiometric Step

Here we briefly sketch the thermodynamic route that takes us from Eq. (4.1) to Eq. (4.3), which enables the ledge energy of stoichiometric and non-stoichiometric steps on NaCl(001) to be compared. As given in Eq. (4.1) the ledge energy is:

$$E_{\text{ledge}} = (E_{\text{slab}} - E_{\text{bulk}} - \gamma A)/2L$$

where E_{bulk} is the energy of the (stoichiometric) NaCl formula unit in bulk NaCl. The well-known problem is that one cannot define the energy of the atomic species in a compound like NaCl, and thus one cannot determine E_{ledge} for a non-stoichiometric system, i.e., one in which there are different numbers of Na and Cl atoms. However, by employing thermodynamics and considering Na and Cl as "subunits" of NaCl the problem can be quite effectively side-stepped.

To begin we consider the equilibrium condition for NaCl, which we express as

$$(E_{\text{Na(s)}} + \mu_{\text{Na}}) + \frac{1}{2}(E_{\text{Cl}_2\text{(g)}} + \mu_{\text{Cl}_2}) = E_f + E_{\text{NaCl(s)}} \tag{B.1}$$

where, as before, E_f is the formation energy of NaCl, and $E_{\text{Na(s)}}$, $E_{\text{Cl}_2\text{(g)}}$, and $E_{\text{NaCl(s)}}$ are the total energies of Na atoms in bulk Na, gas phase Cl_2 molecules, and bulk NaCl, respectively. Setting the total energies to zero yields a formation energy for NaCl that is now given by the chemical potentials of chlorine molecules, μ_{Cl_2}, and Na atoms, μ_{Na} :

$$\mu_{\text{Na}} + \frac{1}{2}\mu_{\text{Cl}_2} = E_f \tag{B.2}$$

If we choose the chemical potential of Cl_2, μ_{Cl_2}, as the only independent variable, then its accessible range is obviously given by

$$E_f \leqslant \mu_{\text{Cl}_2} \leqslant 0 \tag{B.3}$$

where the lower limit, the "chlorine poor" limit, is the computed heat of formation of NaCl, which with the PBE functional is -3.63 eV (Table 3.1). By construction the other limit, the "chlorine rich" limit is given by, $E_{\text{Cl}_2}(g)$, the computed total energy of gas phase chlorine molecules. Combining Eq. (B.1) and (B.2) thus leads to the expression for the ledge energy given in Eq. (4.3),

$$E_{\text{ledge}} = \left\{ E_{\text{slab}} - N_{\text{Na}} \left[E_{\text{Na(s)}} + \left(E_f - \frac{1}{2}\mu_{\text{Cl}_2} \right) \right] - \frac{1}{2} N_{\text{Cl}} \left(E_{\text{Cl}_2}(g) + \mu_{\text{Cl}_2} \right) - \gamma A \right\} / 2L$$

where E_{ledge} now depends only on the chemical potential of Cl_2 molecules.

Further, treating the Cl_2 molecules as an ideal-gas reservoir allows us to extract the temperature and pressure dependence of the chlorine chemical potential, $\mu_{\text{Cl}}(T, p)$, which gives a crude temperature and pressure dependence for the relative

stabilities of the differently terminated steps on NaCl(001). Specifically, the chlorine chemical potential is given by

$$\begin{aligned}\mu_{\mathrm{Cl}}(T,p) =& \frac{1}{2} + \Delta\mu_{\mathrm{Cl}}(T,p) \\ =& \frac{1}{2}\left[E_{\mathrm{Cl_2(g)}} + \mu_{\mathrm{Cl_2}}(T,p^\circ) + k_B T \ln\left(\frac{p_{\mathrm{Cl_2}}}{p^\circ}\right)\right]\end{aligned} \tag{B.4}$$

Appendix C *Ab initio* Molecular Dynamics Simulations of a Cl Adatom

A Born-Oppenheimer *ab initio* molecular dynamics simulation was run in the canonical ensemble at 300 K for a total of 12.5 ps in order to gain insight into the dynamical properties of this adsorption system. Throughout the entire lifetime of this short simulation the Cl adatom remains at the Cl adsorption site, with the dynamical behavior of this system resembling an embedded Cl^-_2 molecule rather than a single Cl adatom.

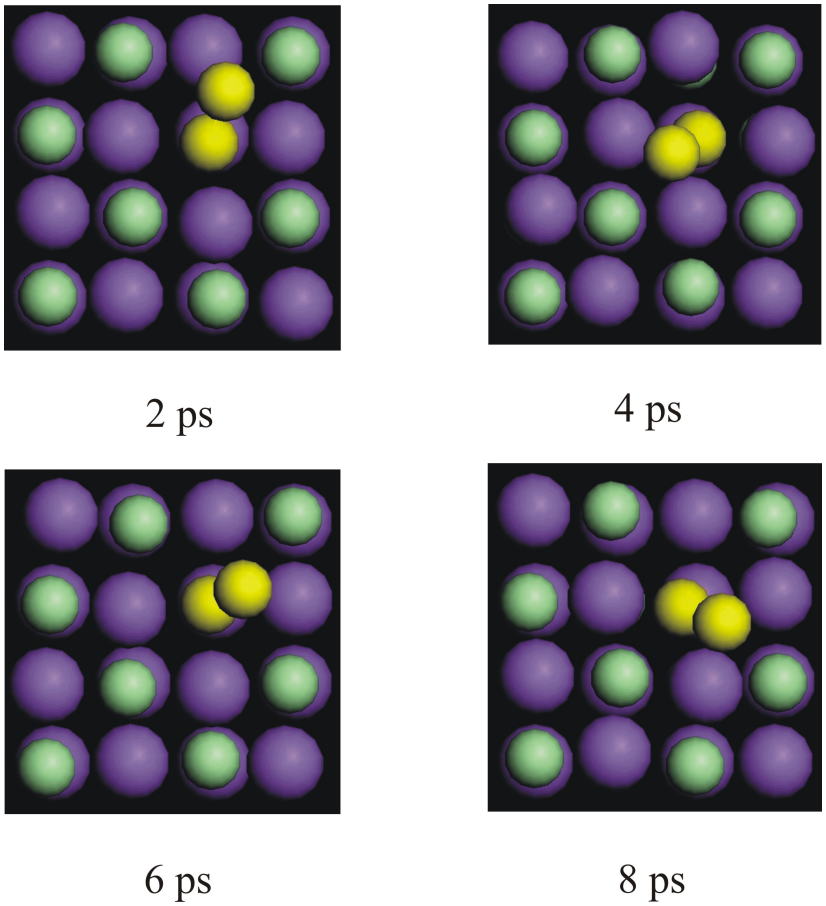

Figure C.1: Four snapshots taken at 2, 4, 6, and 8 ps from the *ab initio* molecular dynamics simulation of the Cl adatom on NaCl(001). The yellow atoms are the Cl adatom and the Cl atom of the surface.

Appendix D Electron Density Differences

Electron density difference plots for the different embedding schemes discussed in chapter 6 are shown in the following figures. The electron density difference between the naked cluster and the cluster embedded in PCs are shown in Figure D.1 and the electron density difference between the cluster embedded in PCs and in PCs+ECPs is shown in Figure D.2, respectively. With both embedding schemes the density at the central Na adsorption site is not perturbed by the embedding.

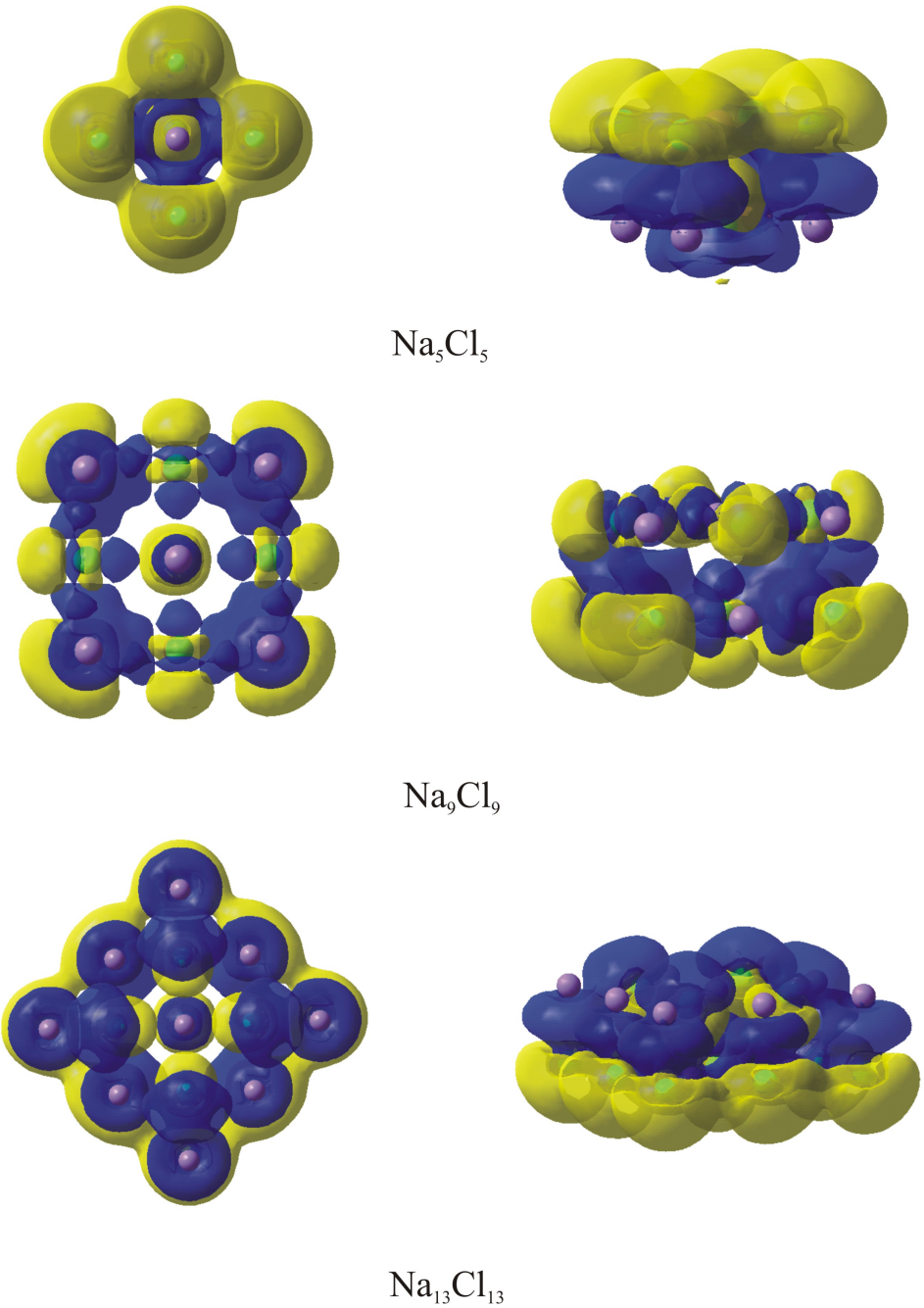

Figure D.1: Isosurface of the electron density difference ($\Delta\rho$) between the density (ρ_{naked}) of the naked clusters and the density (ρ_{PCs}) of the clusters embedded in PCs . $\Delta\rho = \rho_{\text{naked}} - \rho_{\text{PCs}}$. Blue is positive and yellow is negative. The isovalue is 0.0004 a.u.

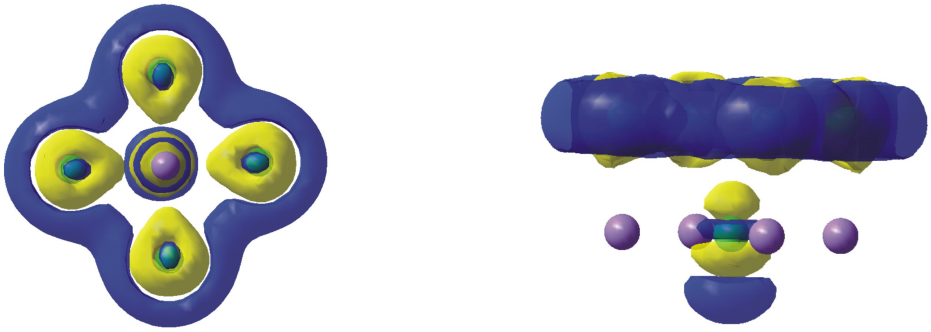

Na_5Cl_5

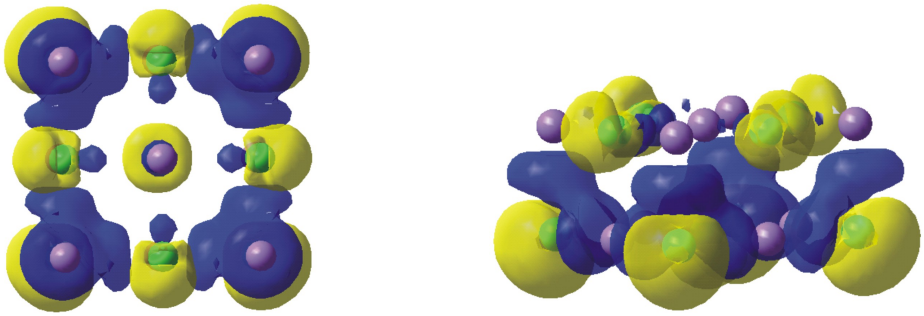

Na_9Cl_9

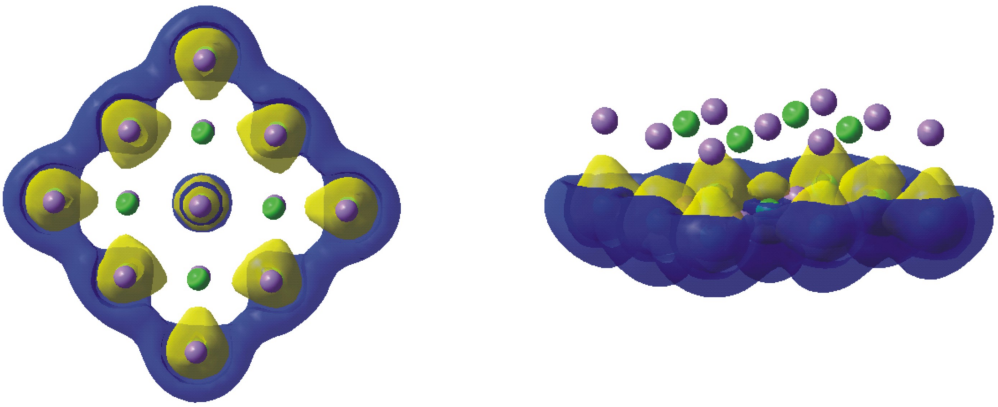

$Na_{13}Cl_{13}$

Figure D.2: Isosurface of the electron density difference ($\Delta\rho$) between the density (ρ_{PCs}) of the clusters embedded in the point charges (PCs) and the density ($\rho_{\mathrm{PCs+ECPs}}$) of the clusters embedded in the combination of PCs and effective core potentials (ECPs). $\Delta\rho = \rho_{\mathrm{PCs}} - \rho_{\mathrm{PCs+ECPs}}$. Blue is positive and yellow is negative. The isovalue is 0.0004 a.u.

Acknowledgements

At the end, the sincere thanks from the bottom of my heart go to those people whose help are indispensable to the finish of the thesis. First of all, Prof. Mattias Scheffler give me the opportunity to carry out my PhD work in such excellent environment in theory department. His continuous four years support is essential to everything I have achieved in my PhD time. My PhD project was done with Dr. Angelos Michaelides. As his first PhD student ever, he teach me almost everything from the basics of density-functional theory to the writing of the scientific paper. His supervision is unmatchable and I am with great luck to be his first PhD student which will be treasured forever. I would like thank Prof. Eckehard Schöll at Technischen Universität Berlin for his valuable help and guidance.

The colleagues in theory department at Fritz-Haber-Institut gave me various different help during last four years. In particularly, Dr. Sami Amira shared his physics knowledge and western culture with me at lunch table and in office. Dr. Javier Carrasco introduce the embedding technique to me and the conversation with him is always beneficial. I appreciated the ICE group members, Dr. Limin Liu, XiaoLiang Hu, Biswajit Santra, Ding Pan, and Jie Ma, for their numerous help. I thank my office mate Björn Hülsen for the beautiful memory in the same office for three years. My Chinese friends in theory department, QingMiao Hu, Dengke Yu, YongSheng Zhang, Li Sheng, Wei Guo, Hong Jiang, XinZheng Li, and XinGuo Ren, make my life in Berlin sometimes just like in my hometown and the Friday afternoon ping-pong session brought me lots of funs. As a person who can not speak Deutsch, I can't imagine what my life will become in Berlin without help from Gabriele Tysper, Julia Pach, and Olaf Kostbahn. They are always glad to translate or make calls for me for my seemingly endless requests when Deutsch is only language works.

I am fortune to have a family which is always behind me regardless of whatever happened. I thank my beloved parents and my lovely sister. My wife, XiaoYing Sun, make great sacrifice for me in past two years. Thanks for her love and tolerance. This thesis is dedicated to her!

Curriculum Vitae

Personal Data

Name:	Bo Li	Sex:	male
Nationality:	P.R. China	Marital Status:	married
Place of Birth:	Harbin, China	Date of Birth:	07.07.1978

Education

2004–2008	Theory Department of Fritz-Haber-Insitut der Max-Planck-Gesellschaft, Germany, PhD.
2001–2004	Institute of Theoretical Chemistry, State Key Laboratory of Theoretical and Computational Chemistry, Jilin University, China, M.S.
1997–2001	Chemistry Department, HeilonJiang University, China, B.S.

Publications

1. "Textbook" Adsorption on "Nontextbook" Adsorption Sites: Halogen Atoms on Alkali Halide Surfaces, Bo Li, Angelos Michaelides, and Matthias Scheffler, Phys. Rev. Lett. **97**, 046802 (2006).

2. Density Functional Theory Study of Flat and Stepped NaCl(001), Bo Li, Angelos Michaelides, and Matthias Scheffler, Phys. Rev. B **76**, 075401 (2007).

3. How Strong is the Bond between Water and Salt?, Bo Li, Angelos Michaelides, and Matthias Scheffler, Surf. Sci. **602**, L135 (2008).

Bibliography

[1] D. Alfè, M. J. Gillan, and G. D. Price, Nature **405**, 172 (2000). 1

[2] M. J. Gillan, D. Alfè, J. Brodholt, L. Vocadlo, and G. D. Price, Rep. Prog. Phys. **69**, 2365 (2006). 1

[3] G. Kresse, A. Gil, and P. Sautet, Phys. Rev. B **68**, 073401 (2003). 2, 75

[4] P. J. Feibelman, B. Hammer, J. K. Nørskov, F. Wagner, M. Scheffler, R. Stumpf, R. Watwe, and J. Dumesic, J. Phys. Chem. B **105**, 4018 (2001). 2

[5] B. Hammer, L. B. Hansen, and J. K. Nørskov, Phys. Rev. B **59**, 7413 (1999). 2, 27, 34, 58, 60, 61

[6] F. Tran, R. Laskowski, P. Blaha, and K. Schwarz, Phys. Rev. B **75**, 115131 (2007). 2

[7] M. Fuentes-Cabrera, M. I. Baskes, A. V. Melechko, and M. L. Simpson, Phys. Rev. B **77**, 035405 (2008). 2

[8] J. P. Perdew and K. Schmidt, in *Density Functional Theory and Its Application to Materials*, edited by V. Van Doren (AIP Press, Melville, New York, 2001). 2, 26

[9] W. M. C. Foulkes, L. Mitas, R. J. Needs, and G. Rajagopal, Rev. Mod. Phys. **73**, 33 (2001). 2, 59

[10] S. R. Feldman, *Kirk-Othmer Encyclopedia of Chemical Technology* (Wiley, New York, 2005). 2

[11] N. W. Ashcroft and N. D. Mermin, *Solid State Physics* (Saunders College Publishing, Texas, 1985). 2, 29, 50

[12] C. Kittel, *Introduction to Solid State Physics*, 8 ed. (Wiley, New York, 2005). 2

[13] J. Repp, G. Meyer, F. E. Olsson, and M. Persson, Science **305**, 492 (2004). 2, 50

[14] F. E. Olsson, S. Paavilainen, M. Persson, J. Repp, and G. Meyer, Phys. Rev. Lett. **98**, 176803 (2007). 2

[15] M. Heyde, M. Sterrer, H.-P. Rust, and H.-J. Freund, Nanotechnology **17**, S101 (2006). 2

[16] M. H. Hakala, O. H. Pakarinen, and A. S. Foster, Phys. Rev. B **78**, 045418 (2008). 2

[17] Q. Dai, J. Hu, and M. Salmeron, J. Phys. Chem. B **101**, 1994 (1998). 3

[18] L. Pauling, J. Am. Chem. Soc. **53**, 3225 (1931). 3, 50

[19] L. W. Bruch, A. Glebov, J. P. Toennies, and H. Weiss, J. Chem. Phys. **103**, 5109 (1995). 3, 59, 62, 72

[20] Y. Yang, S. Meng, and E. G. Wang, Phys. Rev. B **74**, 245409 (2007). 3, 59, 62, 76

[21] P. Cabrera-Sanfelix, A. Arnau, G. R. Darling, and D. Sanchez-Portal, J. Chem. Phys. **126**, 214707 (2007). 3, 59, 62

[22] J. M. Park, J. H. Cho, and K. S. Kim, Phys. Rev. B. **69**, 233403 (2004). 3, 34, 59, 62

[23] H. Meyer, P. Entel, and J. Hafner, Surf. Sci. **177**, 488 (2001). 3, 34, 59, 62

[24] M. A. Henderson, Surf. Sci. Rep. **46**, 1 (2002). 3, 59

[25] Y. Yang and E. G. Wang, J. Comp. and Theo. Nanoscience **5**, 247 (2008). 3, 59

[26] S. Fölsch, A. Stock, and M. Henzler, Surf. Sci. **264**, 65 (1992). 3, 59, 72

[27] M. Born and R. Oppenheimer, Ann. Phys.(Leipzip) **84**, 457 (1927). 6

[28] J. Behler, B. Delley, S. Lorenz, K. Reuter, and M. Scheffler, Phys. Rev. Lett. **94**, 036104 (2005). 7

[29] J. Behler, K. Reuter, and M. Scheffler, Phys. Rev. B **77**, 115421 (2008). 7

[30] A. M. Wodtke, J. C. Tully, and D. J. Auerbach, Int. Rev. Phys. Chem. **23**, 513 (2004). 7

[31] A. C. Luntz, M. Persson, and G. O. Sitz, J. Chem. Phys. **124**, 091101 (2006). 7

[32] P. A. M. Dirac, Proc. R. Soc. A **123**, 714 (1929). 7

[33] D. P. Taylor, W. P. Hess, and M. I. McCarthy, J. Phys. Chem. B **101**, 7455 (1997). 9

[34] P. Baranek, G. Pinarello, C. Pisani, and R. Dovesi, Phys. Chem. Chem. Phys. **2**, 3893 (2000). 9

[35] S. Casassa, A. Ferrari, M. Busso, and C. Pisani, J. Phys. Chem. B **106**, 12978 (2002). 9

[36] P.-O. Löwdin, Adv. Chem. Phys. **2**, 207 (1959). 10

[37] B. Santra, A. Michaelides, and M. Scheffler, J. Chem. Phys. **127**, 184104 (2007). 11

[38] C. Møller and M. S. Plesset, Phys. Rev. **46**, 618 (1934). 13, 59, 60

[39] A. Szabo and N. S. Ostlund, *Modern Quantum Chemistry: Introduction to Advanced Electronic Structure Theory* (Dover Press, USA, 1982). 14

[40] A. P. Scott and L. Radom, J. Phys. Chem. **100**, 16502 (1996). 14

[41] P. R. Rablen, J. W. Lockman, and W. L. Jorgensen, J. Phys. Chem. A **102**, 3782 (1998). 14

[42] L. A. Curtiss, P. C. Redfern, K. Raghavachari, and J. A. Pople, J. Chem. Phys. **114**, 108 (2001). 14

[43] M. L. Leininger, W. D. Allen, H. F. Schaefer III, and C. D. Sherrill, J. Chem. Phys. **112**, 9213 (2000). 14

[44] J. Čížek, J. Chem. Phys. **45**, 4256 (1966). 14

[45] J. Čížek and J. Paldus, Int. J. Quan. Chem. **5**, 359 (1971). 14

[46] R. J. Bartlett and M. Musial, Rev. Mod. Phys. **79**, 291 (2007). 14, 59, 60

[47] T. Helgaker, P. Jorgensen, and J. Olsen, *Molecular Electronic Structure Theory* (Wiley, New York, 2000). 14

[48] C. D. Sherrill and H. F. Schaefer III, Adv. Quan. Chem. **34**, 143 (1999). 14

[49] J. D. Watts, J. Gauss, and R. J. Bartlett, J. Chem. Phys. **98**, 8718 (1993). 16

[50] S. Hirata, M. Nooijen, I. Grabowski, and R. J. Bartlett, J. Chem. Phys. **114**, 3919 (2001). 16

[51] W. Klopper, J. G. C. M. van Duijneveldt-van de Rijdt, and F. B. van Duijneveldt, Phys. Chem. Chem. Phys. **2**, 2227 (2000). 16

[52] E. M. Mas, R. Bukowski, K. Szalewicz, G. C. Groenenboom, P. E. S. Wormer, and A. van der Avoird, J. Chem. Phys. **113**, 6687 (2000). 16

[53] A. K. Rappe and E. R. Bernstein, J. Phys. Chem. A **104**, 6117 (2000). 16

[54] Q. Zhang, R. Bell, and T. N. Truong, J. Phys. Chem. **99**, 592 (1995). 16

[55] D. E. Woon and T. H. Dunning, J. Chem. Phys. **103**, 4572 (1995). 19, 60

[56] D. E. Woon and T. H. Dunning, J. Chem. Phys. **99**, 1914 (1993). 19, 21

[57] T. H. Dunning, J. Phys. Chem. A **104**, 9062 (2000). 19

[58] E. R. Davison and D. Feller, Chem. Rev. **86**, 881 (1986). 19

[59] F. B. van Duijneveldt, J. G. C. M. van Duijneveldt-van de Rijdt, and J. H. van Lenthe, Chem. Rev. **94**, 1873 (1994). 20

[60] S. F. Boys and F. Bernardi, Mol. Phys. **19**, 553 (1970). 20, 67

[61] D. G. Truhlar, Chem. Phys. Lett. **294**, 45 (1998). 20, 21

[62] D. Feller, J. Chem. Phys. **96**, 6104 (1992). 21

[63] J. M. L. Martin, Chem. Phys. Lett. **259**, 669 (1996). 21

[64] A. Halkier, T. Helgaker, P. Jørgenson, W. Klopper, H. Koch, J. Olson, and A. K. Wilson, Chem. Phys. Lett. **286**, 243 (1998). 21

[65] R. G. Parr, Ann. Rev. Phys. Chem. **34**, 631 (1983). 22

[66] T. Ziegler, Chem. Rev. **91**, 651 (1991). 22

[67] P. Geerlings, F. D. Proft, and W. Langenaeker, Chem. Rev. **103**, 1793 (2003). 22

[68] R. O. Jones and O. Gunnarsson, Rev. Mod. Phys. **61**, 689 (1989). 22

[69] R. G. Parr and W. Yang, *Density-Functional Theory of Atoms and Molecules* (Oxford University Press, New York, 1989). 22

[70] M. R. Dreizler and E. K. U. Gross, *Density Functional Theory : An Approach to the Quantum Many-Body Problem* (Springer, Berlin, 1990). 22

[71] L. H. Thomas, Proc. Camb. Phil. Soc. **23**, 542 (1927). 22

[72] E. Fermi, Rend. Accad. Lincei. **6**, 602 (1927). 22

[73] P. Hohenberg and W. Kohn, Phys. Rev. **136**, B864 (1964). 23, 58

[74] W. Kohn and L. J. Sham, Phys. Rev. **140**, A1133 (1965). 24, 58

[75] M. Gell-Mann and K. A. Brueckner, Phys. Rev. **106**, 364 (1957). 26

[76] D. M. Ceperley and B. J. Alder, Phys. Rev. Lett. **45**, 566 (1980). 26

[77] J. P. Perdew and A. Zunger, Phys. Rev. B **23**, 5048 (1981). 26, 34, 58, 60

[78] J. P. Perdew and Y. Wang, Phys. Rev. B **45**, 13244 (1992). 26

[79] S. J. Vosko, L. Wilk, and M. Nusair, Can. J. Phys. **58**, 1200 (1980). 26

[80] O. Gunnarsson and B. I. Lundqvist, Phys. Rev. B **13**, 4274 (1976). 26

[81] O. Gunnarsson, M. Jonson, and B. I. Lundqvist, Sol. Stat. Comm. **24**, 765 (1977). 26

[82] T. Ziegler, A. Rauk, and E. J. Baerends, Theor. Chim. Acta **43**, 261 (1977). 26

[83] K. Burke, J. P. Perdew, and M. Ernzerhof, J. Chem. Phys. **109**, 3760 (1998). 26

[84] J. P. Perdew, K. Burke, and Y. Wang, Phys. Rev. B **54**, 16533 (1992). 27, 58

[85] J. P. Perdew, K. Burke and M. Ernzerhof, Phys. Rev. Lett. **77**, 3865 (1996); **78**, 1396 (1197). 27, 34, 58, 60

[86] Y. Zhang and W. Yang, Phys. Rev. Lett. **80**, 890 (1998). 27, 34

[87] Z. Wu and R. E. Cohen, Phys. Rev. B **73**, 235116 (2006). 27, 34, 35, 36

[88] J. P. Perdew, A. Ruzsinszky, G. I. Csonka, O. A. Vydrov, G. E. Scuseria, L. A. Constantin, X. Zhou, and K. Burke, Phys. Rev. Lett. **100**, 136406 (2008). 27

[89] R. Armiento and A. E. Mattsson, Phys. Rev. B **72**, 085108 (2005). 27

[90] A. E. Mattsson, R. Armiento, J. Paier, G. Kresse, J. M. Wills, and T. R. Mattsson, J. Chem. Phys. **128**, 084714 (2008). 27

[91] J. M. Tao, J. P. Perdew, V. N. Staroverov, and G. E. Scuseria, Phys. Rev. Lett. **91**, 146401 (2003). 27

[92] A. D. Becke, J. Chem. Phys. **98**, 5648 (1993). 27, 75

[93] C. Lee, W. Yang, and R. G. Parr, Phys. Rev. B **37**, 785 (1988). 27, 75

[94] J. P. Perdew, M. Ernzerhof, and K. Burke, J. Chem. Phys. **105**, 9982 (1996). 28

[95] C. Adamo and V. Barone, J. Chem. Phys. **110**, 6185 (1999). 28, 75

[96] A. D. Becke, J. Chem. Phys. **98**, 1372 (1993). 28, 53

[97] V. N. Staroverov, G. E. Scuseria, J. M. Tao, and J. P. Perdew, Phys. Rev. B **69**, 075102 (2004). 28, 34, 40

[98] D. R. Hamann, M. Schlüter, and C. Chiang, Phys. Rev. Lett. **43**, 1494 (1979). 31

[99] D. Vanderbilt, Phys. Rev. B **48**, 7892 (1990). 31, 34, 51, 60

[100] N. Troullier and J. L. Martins, Phys. Rev. B **43**, 1993 (1991). 31

[101] G. P. Kerker, J. Phys. C **13**, L189 (1980). 31

[102] D. Vanderbilt, Phys. Rev. B **32**, 8412 (1985). 31

[103] M. C. Payne, M. P. Teter, D. C. Allan, T. A. Arias, and J. D. Joannopoulos, Rev. Mod. Phys. **64**, 1045 (1992). 31, 34

[104] M. Bochstedte, A. Kley, J. Neugebauer, and M. Scheffler, Comput. Phys. Comm. **107**, 187 (1997). 31, 34

[105] J. G. Roberts, S. Hoffer, M. A. V. Hove, and G. A. Somorjai, Surf. Sci. **437**, 75 (1999). 33, 37, 38

[106] J. Vogt and H. Weiss, Surf. Sci. **491**, 155 (2001). 33, 34, 37, 38

[107] V. E. Henrich and P. A. Cox, *The Surface Science of Metal Oxides* (Cambridge University Press, Cambridge, 1996). 33

[108] Y. Yang, S. Meng, and E. G. Wang, Phys. Rev. B. **74**, 245409 (2006). 34

[109] S. J. Clark, M. D. Segall, C. J. Pickard, P. J. Hasnip, M. I. J. Probert, K. Refson, and M. C. Payne, Zeitschrift für Krystallographie **220**, 567 (2005). 34, 51, 60

[110] S. G. Louie, S. Froyen, and M. L. Cohen, Phys. Rev. B **26**, 1738 (1982). 34, 60

[111] H. J. Monkhorst and J. D. Pack, Phys. Rev. B **13**, 5178 (1976). 34, 51

[112] G. Sandrone and D. A. Dixon, J. Phys. Chem. A **102**, 10310 (1998). 35, 36, 37

[113] M. Chall, B. Winkler, P. Blaha, and K. Schwarz, J. Phys. Chem. B **104**, 1191 (2000). 35, 36

[114] J. Paier, K. Hummer, G. Kresse, I. C. Gerber, and J. G. Ángyián, J. Chem. Phys. **124**, 154709 (2006). 35, 36

[115] T. J. Lewis, A. Lehoczky, and C. V. Briscoe, Phys. Rev. **161**, 877 (1967). 35, 36

[116] D. R. Lide (Ed.) and H. P. R. Frederikse (Ed.), *CRC Handbook of Chemistry and Physics* (CRC Pr., Boca Raton, Fla., 1995). 35, 36, 54

[117] W. C. Malcolm (Ed.), *JANAF Thermochemical Tables* (U.S. National Bureau of Standards, Woodbury, NY, 1998) 4 ed. 35, 36

[118] G. Makov and M. C. Payne, Phys. Rev. B **51**, 4014 (1995). 37

[119] J. P. Perdew, J. A. Chevary, S. H. Vosko, K. A. Jackson, M. R. Pederson, D. J. Singh, and C. Fiolhais, Phys. Rev. B **46**, 6671 (1992). 37

[120] P. W. Tasker, Phil. Mag. A **39**, 119 (1979). 38, 39

[121] F. M. Jaegar, Z. Anorg. Chem. **101**, 1 (1917). 38, 39

[122] S. G. Lipsett, F. M. G. Johnson, and O. Maass, J. Am. Chem. Soc. **49**, 1940 (1927). 38, 39

[123] G. C. Benson, H. P. Schreiber, and F. Vanzeggeren, Can. J. Chem. **34**, 1553 (1956). 38, 39

[124] G. C. Benson, J. Chem. Phys. **35**, 2113 (1961). 38, 39

[125] P. L. Gunshall and G. E. Gross, J. App. Phys. **36**, 2459 (1965). 38, 39

[126] P. A. Cox, F. W. H. Dean, and A. A. Williams, Vacuum **33**, 839 (1983). 38, 39

[127] T. Zykova-Timan, D. Ceresoli, U. Tartaglino, and E. Tosatti, Phys. Rev. Lett. **94**, 176105 (2005). 38, 39

[128] M. C. Desjonqures and D. Spanjaard, *Concepts in Surface Physics* (Springer, Amsterdam, 1998). 38

[129] V. K. Kumikov and K. B. Khokonov, J. Appl. Phys. **54**, 1346 (1983). 38

[130] J. L. F. Da Silva, C. Stampfl, and M. Scheffler, Surf. Sci. **600**, 703 (2006). 38

[131] D. K. Yu and M. Scheffler, Phys. Rev. B **70**, 155417 (2007). 38, 61

[132] D. Alfè and M. J. Gillan, J. Phys.: Condens. Matter **18**, L435 (2006). 38, 61

[133] N. O. Lipari and A. B. Kunz, Phys. Rev. B **3**, 491 (1971). 40

[134] G. K. Wertheim, J. E. Rowe, D. N. E. Buchanan, and P. H. Citrin, Phys. Rev. B **51**, 13675 (1995). 40

[135] J. C. Slater, *Quantum Theory of Molecules and Solids, 2: Symmetry and Energy Bands in Crystal* (McGraw-Hill, New York, 1976). 41

[136] P. K. de Boer and R. A. de Groot, Phys. Lett. A **256**, 227 (1999). 41

[137] C. Freysoldt, Ph.D. thesis, Freie Universität Berlin, 2007. 41

[138] J. D. Levine and P. Mark, Phys. Rev. **144**, 751 (1966). 41

[139] H. Jeong and E. D. Williams, Surf. Sci. Rep. **34**, 171 (1999). 44, 46

[140] G. Wulff, Z. Krist **34**, 449 (1901). 44

[141] D. K. Yu, H. P. Bonzel, and M. Scheffler, Phys. Rev. B **74**, 115408 (2006). 44

[142] H. P. Bonzel, D. K. Yu, and M. Scheffler, Appl. Phys. A **87**, 391 (2007). 44, 48

[143] D. K. Yu, H. P. Bonzel, and M. Scheffler, New J. Phys. **8**, 65 (2006). 44

[144] P. Feibelman, Phys. Rev. B **52**, 16845 (1995). 44

[145] Z. J. Tian and T. S. Rahman, Phys. Rev. B **47**, 9751 (1993). 44

[146] M. Giesen and G. S. Icking-Konert, Surf. Rev. Lett. **6**, 27 (1999). 44

[147] H. Tanaka, Y. Watanabe, and I. Sumita, Appl. Surf. Sci. **60**, 474 (1992). 44

[148] J. Wei, X. S. Wang, N. Bartelt, and E. Williams, Phys. Rev. Lett. **69**, 3885 (1992). 44

[149] J. Frohn, M. Giesen, M. Poensgen, J. F. Wolf, and H. Ibach, Phys. Rev. Lett. **67**, 3543 (1991). 45

[150] G. Z. Wang, J. F. Webb, and J. Zi, Surf. Sci. **601**, 1944 (2007). 45

[151] V. B. Shenoy and C. V. Ciobanu, Phys. Rev. B **67**, 081402 (2003). 46

[152] E. D. Williams, Surf. Sci. **299**, 502 (1994). 46

[153] C. Herring, Phys. Rev. **82**, 87 (1951). 48

[154] J. Kollar, L. Vitos, B. Johansson, and H. L. Skriver, Phys. Stat. Sol. **217**, 405 (2000). 49

[155] E. Feldbach, M. Kirm, A. Luchchik, C. Lushchik, and I. Martinson, J. Phys.: Condens. Matter **12**, 1991 (2000). 50

[156] F. E. Olsson and M. Persson, Surf. Sci. **540**, 172 (2003). 50

[157] H. C. Allen, J. M. Laux, R. Vogt, B. J. Finlayson-Pitts, and J. C. Hemminger, J. Phys. Chem. **100**, 6371 (1996). 50

[158] H. R. Prupacher and J. D. Klett, *Mircophysics of Clouds and Precipitation* (Kluwer, Dordrecht, 1997). 50

[159] M. J. Frisch, G. W. Trucks, H. B. Schlegel, G. E. Scuseria, M. A. Robb, J. R. Cheeseman, J. A. Montgomery, Jr., T. Vreven, K. N. Kudin, J. C. Burant, J. M. Millam, S. S. Iyengar, J. Tomasi, V. Barone, B. Mennucci, M. Cossi, G. Scalmani, N. Rega, G. A. Petersson, H. Nakatsuji, M. Hada, M. Ehara, K. Toyota, R. Fukuda, J. Hasegawa, M. Ishida, T. Nakajima, Y. Honda, O. Kitao, H. Nakai, M. Klene, X. Li, J. E. Knox, H. P. Hratchian, J. B. Cross, V. Bakken, C. Adamo, J. Jaramillo, R. Gomperts, R. E. Stratmann, O. Yazyev, A. J. Austin, R. Cammi, C. Pomelli, J. W. Ochterski, P. Y. Ayala, K. Morokuma, G. A. Voth, P. Salvador, J. J. Dannenberg, V. G. Zakrzewski, S. Dapprich, A. D. Daniels, M. C. Strain, O. Farkas, D. K. Malick, A. D. Rabuck, K. Raghavachari, J. B. Foresman, J. V. Ortiz, Q. Cui, A. G. Baboul, S. Clifford, J. Cioslowski, B. B. Stefanov, G. Liu, A. Liashenko, P. Piskorz, I. Komaromi, R. L. Martin, D. J. Fox, T. Keith,

M. A. Al-Laham, C. Y. Peng, A. Nanayakkara, M. Challacombe, P. M. W. Gill, B. Johnson, W. Chen, M. W. Wong, C. Gonzalez, and J. A. Pople, Gaussian 03, Revision C.02, Gaussian, Inc., Wallingford, CT, 2004. 51, 60

[160] B. Braïda, P. C. Hiberty, and A. Savin, J. Phys. Chem. A **102**, 7872 (1998). 53

[161] B. Braïda and P. C. Hiberty, J. Phys. Chem. A **104**, 4618 (2001). 53

[162] G. A. Somorjai, *Introduction to Surface Chemistry and Catalysis* (Wiley, New York, 1994). 58

[163] A. Stuck, C. E. Wartnaby, Y. Y. Yeo, J. T. Stuckless, N. Al-Sarraf, and D. A. King, Surf. Sci. **349**, 229 (1996). 58, 73

[164] L. W. Bruch, R. D. Diehl, and J. A. Venables, Rev. Mod. Phys. **79**, 1381 (2007). 58

[165] C. W. Bauschlicher and S. R. Langhoff, Science **254**, 394 (1991). 58

[166] L. A. Curtiss, K. Raghavachari, P. C. Redfern, and J. A. Pople, J. Chem. Phys. **106**, 1063 (1997). 58

[167] A. Stroppa, K. Termentzidis, J. Paier, G. Kresse, and J. Hafner, Phys. Rev. B **76**, 195440 (2007). 58, 59

[168] Q. M. Hu, K. Reuter, and M. Scheffler, Phys. Rev. Lett. **98**, 176103 (2007); **99**, 169903(E) (2007). 58, 59, 65, 75

[169] J. Sauer, Chem. Rev. **89**, 199 (1989). 58

[170] G. D. Barrera, D. Colognesi, P. C. H. Mitchell, and A. J. Ramirez-Cuesta, Chem. Phys. **317**, 119 (2005). 58

[171] B. Montanari and N. M. Harrison, Chem. Phys. Lett. **364**, 528 (2002). 58

[172] M. Dion, H. Rydberg, E. Schröder, D. C. Langreth, and B. I. Lundqvist, Phys. Rev. Lett. **92**, 264401 (2004). 59

[173] O. A. von Lilienfeld, I. Tavernelli, U. Roethlisberger, and D. Sebastiani, Phys. Rev. B **71**, 195119 (2005). 59

[174] T. Schwabe and S. Grimme, Phys. Chem. Chem. Phys. **9**, 3397 (2007). 59

[175] J. L. Whitten and H. Yang, Surf. Sci. Rep. **24**, 55 (1996). 59, 65

[176] P. V. Sushko, A. L. Shluger, and C. R. A. Catlow, Surf. Sci. **450**, 153 (2000). 59, 65

[177] C. Tuma and J. Sauer, Phys. Chem. Chem. Phys. **8**, 3955 (2006). 59, 65

[178] J. A. Mejías, A. M. Márquez, J. Sanz, M. Fern, J. M. Ricart, C. Sousa, and F. Illas, Surf. Sci. **327**, 59 (1995). 59, 65, 66

[179] N. Lopez, F. Illas, N. Rosch, and G. Pacchioni, J. Chem. Phys. **110**, 4873 (1999). 59

[180] G. Pacchioni, J. Ricart, and F. Illas, J. Am. Chem. Soc. **116**, 10152 (1994). 59, 65

[181] S. Humbel, S. Sieber, and K. Morokuma, J. Chem. Phys. **105**, 1959 (1996). 59

[182] U. Gutdeutsch, U. Birkenheuer, S. Krüger, and N. Rösch, J. Chem. Phys. **106**, 6020 (1997). 59, 65

[183] P. Huang and E. A. Carter, J. Chem. Phys. **125**, 084102 (2006). 59, 65

[184] M. A. Nygrena and L. G. M. Pettersson, J. Chem. Phys. **105**, 9339 (1996). 59, 65

[185] E. J. Bylaska, W. A. de Jong, K. Kowalski, T. P. Straatsma, M. Valiev, D. Wang, E. Apra, T. L. Windus, S. Hirata, M. T. Hackler, Y. Zhao, P.-D. Fan, R. J. Harrison, M. Dupuis, D. M. A. Smith, J. Nieplocha, V. Tipparaju, M. Krishnan, A. A. Auer, M. Nooijen, E. Brown, G. Cisneros, G. I. Fann, H. Fruchtl, J. Garza, K. Hirao, R. Kendall, J. A. Nichols, K. Tsemekhman, K. Wolinski, J. Anchell, D. Bernholdt, P. Borowski, T. Clark, D. Clerc, H. Dachsel, M. Deegan, K. Dyall, D. Elwood, E. Glendening, M. Gutowski, A. Hess, J. Jaffe, B. Johnson, J. Ju, R. Kobayashi, R. Kutteh, Z. Lin, R. Littlefield, X. Long, B. Meng, T. Nakajima, S. Niu, L. Pollack, M. Rosing, G. Sandrone, M. Stave, H. Taylor, G. Thomas, J. van Lenthe, A. Wong, and Z. Zhang, "NWChem, A Computational Chemistry Package for Parallel Computers, Version 4.7" (2005), Pacific Northwest National Laboratory, Richland, Washington 99352-0999, USA. 60

[186] R. Dovesi, V. R. Saunders, C. Roetti, R. Orlando, C. M. Zicovich-Wilson, F. Pascale, B. Civalleri, K. Doll, N. M. Harrison, I. J. Bush, P. D. Arco, and M. Llunell *CRYSTAL06 User's Manual*; Università di Torino, 2006. 60

[187] T. H. Dunning, J. Chem. Phys. **90**, 1007 (1989). 60

[188] C. Tuma, A. D. Boese, and N. C. Handy, Phys. Chem. Chem. Phys. **1**, 3939 (1999). 61

[189] X. L. Hu and A. Michaelides, Surf. Sci. **602**, 960 (2008). 61

[190] Y. Kanai, X. Wang, A. Selloni, and R. Car, J. Chem. Phys. **125**, 234104 (2006). 61

[191] B. Hammer, Surf. Sci. **459**, 323 (2000). 61

[192] M. Gajdos, A. Eichler, and J. Hafner, J. Phys.: Condens. Matter **16**, 1141 (2004). 61

[193] N. W. Winter, R. M. Pitzer, and D. K. Temple, J. Chem. Phys. **87**, 2945 (1987). 65

[194] P. J. Hay and W. R. Wadt, J. Chem. Phys. **82**, 270 (1985). 66

[195] W. Kohn, Int. J. Quan. Chem. **56**, 229 (1995). 67

[196] F. Jensen, Theor. Chem. Acc. **113**, 267 (2005). 67

[197] A. J. C. Varandas, J. Chem. Phys. **126**, 244105 (2007). 67

[198] V. A. Rassolov, J. A. Pople, P. C. Redfern, and L. A. Curtiss, Chem. Phys. Lett. **350**, 573 (2001). 68

[199] A. Schulz, B. J. Smith, and L. Radom, J. Phys. Chem. A **103**, 7522 (1999). 68

[200] M. A. Iron, M. Oren, and J. M. L. Martin, Mol. Phys. **101**, 1345 (2003). 68

[201] C. W. J. Bauschlicher, S. R. Langhoff, H. Partridge, and J. E. Rice, J. Chem. Phys. **95**, 5142 (1991). 68

[202] D. Feller, E. D. Glendening, D. E. Woon, and M. W. Feyereisen, J. Chem. Phys. **103**, 3526 (1995). 68

[203] P. Jurečka and P. Hobza, Chem. Phys. Lett. **365**, 89 (2002). 68, 71

[204] D. G. Truhlar, Chem. Phys. Lett. **294**, 45 (1998). 70

[205] A. Halkier, T. Helgaker, P. Jørgensen, W. Klopper, and J. Olsen, Chem. Phys. Lett. **302**, 437 (1999). 70

[206] D. W. Schwenke, J. Chem. Phys. **122**, 014107 (2005). 70

[207] P. L. Fast, M. L. Sánchez, and D. G. Truhalr, J. Chem. Phys. **111**, 2921 (1999). 70

[208] S. B. Huh and J. S. Lee, J. Chem. Phys. **118**, 2035 (2003). 70

[209] J. Pittner and P. Hobza, Chem. Phys. Lett. **390**, 496 (2004). 71

[210] J. Heidberg and W. Häser, J. Electron. Spectrosc. Relat. Phenom. **54**, 971 (1990). 72

[211] H. Shindo, M. Ohashi, O. Tateishi, and A. Seo, J. Chem. Soc. Faraday Trans. **93**, 1169 (1992). 73

[212] S. Ghosal, J. C. Hemminger, H. Bluhm, B. S. Mun, E. L. D. Hebenstreit, G. Ketteler, D. F. Ogletree, F. G. Requejo, and M. Salmeron, Science **307**, 563 (2005). 73

[213] J. M. Perezjorda and A. D. Becke, Chem. Phys. Lett. **233**, 134 (1995). 73

[214] J. C. Boettger, Phys. Rev. B **55**, 11202 (1997). 73

[215] D. C. Patton and M. R. Pederson, Int. J. Quan. Chem. **69**, 619 (1998). 73

[216] X. Xu and W. A. Goddard, J. Phys. Chem. A **108**, 2305 (2004). 73

[217] S. Parthiban, G. de Oliveira, and J. Martin, J. Phys. Chem. A **105**, 895 (2001). 75

[218] L. A. Curtiss, K. Raghavachari, P. C. Redfern, and J. A. Pople, J. Chem. Phys. **106**, 1063 (1997). 75

[219] E. Ruiz, D. R. Salahub, and A. Vela, J. Phys. Chem. **100**, 12265 (1996). 75

[220] A. D. Becke, J. Chem. Phys. **98**, 5648 (1993). 75

[221] M. Marsman, J. Paier, A. Stroppa, and G. Kresse, J. Phys.: Condens. Matter **20**, 064201 (2008). 75

[222] A. E. Mattsson, R. Armiento, J. Paier, G. Kresse, J. M. Wills, and T. R. Mattsson, J. Chem. Phys. **128**, 084714 (2008). 75

[223] T. Todorova, A. Seitsonen, J. Hutter, I. F. W. Kuo, and C. Mundy, J. Phys. Chem. B **110**, 3685 (2006). 75

[224] O. Engkvist and A. J. Stone, J. Chem. Phys. **110**, 12089 (1999). 76

[225] A. Savin, A. D. Becke, J. Flad, R. Nesper, H. Preuss, and H. G. von Schnering, Angew. Chem. Int. Ed. **30**, 409 (1991). 76, 80

[226] CPMD V3.11.1 Copyright IBM Corp 1990-2008, Copyright MPI für Festkörperforschung Stuttgart 1997-2001. 76

[227] A. Michaelides, Faraday Discuss. **136**, 287 (2007). 80

[228] A. D. Becke and K. E. Edgecombe, J. Chem. Phys. **92**, 5397 (1990). 80

[229] B. Jeziorski, R. Moszynski, and K. Szalewicz, Chem. Rev. **94**, 1887 (1994). 83